Laboratory and Field Measurements of Frazil Ice Characteristics

by

Vincent John McFarlane

A thesis submitted in partial fulfillment of the requirements for the degree of

Doctor of Philosophy

in

WATER RESOURCES ENGINEERING

Department of Civil and Environmental Engineering
University of Alberta

ABSTRACT

Measurements of frazil ice characteristics in both laboratory and field environments have each been hindered by different challenges to date. In the laboratory, the resolution of the digital imaging systems used to photograph suspended particles has limited the size of the smallest frazil ice crystals that could be observed. In field settings there has not been a practical method by which to directly measure in-situ frazil ice particles due to the difficulty of capturing clear, underwater photographs in harsh winter conditions. As a result, most field studies to date have been carried out using acoustic devices to detect suspended particles. However, these measurements require direct observations for calibration and validation. This study was designed to overcome the challenges faced by previous studies in order to measure complete size distributions of frazil ice particles throughout the supercooling process at various turbulence intensities and in various rivers.

A series of laboratory experiments were conducted in which frazil ice particles were produced at three different turbulence intensities. The water temperature was measured and high-resolution, cross-polarised digital images of suspended frazil crystals as small as 22 μm were captured throughout each experiment. An image processing algorithm was written to analyse the frazil ice images and calculate the moving average mean and standard deviation of the particle diameter, and the number of suspended particles throughout the supercooling process. The mean particle diameter was calculated to be 0.94, 0.66, and 0.59 mm with standard deviations of 0.73, 0.51, and 0.45 mm at turbulent kinetic energy (TKE) dissipation rates of 23.9, 85.5, and 336 cm^2/s^3, respectively. The mean particle size was observed to reach a maximum shortly after the maximum degree of supercooling was reached, then decrease and remain at a constant value during the

residual supercooling phase. A lognormal distribution was a good fit to the particle size distribution at all stages of the supercooling process.

A digital imaging system, called the FrazilCam, was designed and constructed for use in field environments. The FrazilCam was successfully deployed in the Kananaskis, Peace, and North Saskatchewan Rivers in Alberta. Images captured using the FrazilCam in the first deployment season in 2014-15 were analysed and it was discovered that suspended sediment particles with diameters on the order of 0.1 mm were visible in the images and indistinguishable from ice. This issue was overcome by training support vector machine (SVM) algorithms to identify the differences between sediment and ice particles in each river. The SVM algorithms were able to classify sediment particles with 98% accuracy and remove them from the frazil ice size distributions. Using the SVM algorithms, data from the 2014-15, 2015-16, and 2016-17 freeze-up seasons were analysed. The mean particle diameter was found to range from 0.63 to 1.32 mm during the principal supercooling phase, and from 0.32 to 0.93 mm during the residual supercooling phase. Additionally, the number concentration of suspended frazil crystals varied from 1.48×10^4 to 1.81×10^6 particles/m^3. Assuming a constant particle aspect ratio of 37, the volume concentration was estimated to range from 1.0 to 18×10^{-6} m^3/m^3. Time-series data collected using the FrazilCam indicated that the mean particle diameter and concentration remain approximately constant throughout the residual supercooling phase, and a lognormal distribution was confirmed to describe all of the size distributions calculated under steady flow conditions. A unique supercooling event was recorded during one of the FrazilCam deployments in which the maximum degree of supercooling was −0.145°C. On this occasion ice predominantly grew as shard-like crystals on submerged objects including the bed material rather than suspended disc-shaped frazil crystals.

PREFACE

Chapter 2 of this thesis has been published as McFarlane, V., Loewen, M., Hicks, F., 2015. Measurements of the evolution of frazil ice particle size distributions. Cold Reg. Sci. Technol. 120, 45–55. I was responsible for data collection and analysis, writing the image processing algorithm, and writing the manuscript. I worked collaboratively with Dr. Loewen and Dr. Hicks on the design of the experimental apparatus. Dr. Loewen and Dr. Hicks were both supervisory authors and were involved with concept formation and manuscript composition and editing.

Chapter 3 of this thesis has been published as McFarlane, V., Loewen, M., Hicks, F., 2017. Measurements of the size distribution of frazil ice particles in three Alberta rivers. Cold Reg. Sci. Technol. 142, 100–117. I was responsible for data collection and analysis and writing the manuscript. I worked collaboratively with Dr. Loewen on the design of the field apparatus and coordination of field work trips, and he also assisted with data collection. Dr. Loewen and Dr. Hicks were both supervisory authors and were involved with concept formation and manuscript composition and editing.

Chapter 4 of this thesis has been submitted for publication as McFarlane, V., Loewen, M., Hicks, F., 2018. Field measurements of suspended frazil ice. Part I: A support vector machine learning algorithm to identify frazil ice particles. I was responsible for data collection and analysis, training the support vector machine learning algorithm, modifying the image processing algorithm, and writing the manuscript. Dr. Loewen was the supervisory author and I worked collaboratively with him on experimental design and formulating ideas. Dr. Loewen and Dr. Hicks were both involved with manuscript composition and editing.

Chapter 5 of this thesis has been submitted for publication as McFarlane, V., Loewen, M., Hicks, F., 2018. Field measurements of suspended frazil ice. Part II: Observations and analyses of frazil ice properties during the principal and residual supercooling phases. I was responsible for data collection and analysis and writing the manuscript. Dr. Loewen was the supervisory author and I worked collaboratively with him on experimental design and formulating ideas, and he assisted with field data collection. Dr. Loewen and Dr. Hicks were both involved with concept formation and manuscript composition and editing.

ACKNOWLEDGMENTS

I would like to thank my supervisors, Dr. Mark Loewen and Dr. Faye Hicks, for all of the help and guidance that they have provided over the past eight years. I would certainly not be here if they had not introduced me to the wonderful world of river ice during my undergraduate degree and continued to provide me with opportunities to research, teach, and, most importantly, learn throughout my graduate studies. I would also like to thank Dr. Yuntong (Amy) She for her guidance as a member of my supervisory committee, Dr. Shawn Clark and Dr. Paul Myers for serving on the examining committee, and Dr. Evan Davies for chairing the exam.

Great thanks are also owed to Perry Fedun for his exceptional assistance with all things technical throughout my studies. From building, troubleshooting, and fixing experimental apparatus to delivering replacement parts to the riverbank in the middle of a snowstorm on a cold, winter morning, Perry always comes through. This research truly would not have been possible without his help.

Thank you to my friends and colleagues Hayden Kalke, Chris Schneck, and Jeff Kemp for assisting me with field work at all hours of the day and night. Wading in the river at 2:00 AM in −30°C temperatures is far safer and more enjoyable with friends around and I owe them a great debt for putting their own work on hold to help me out.

I would also like to thank all of my friends, family, and especially my partner, Laura, for their love, support, and understanding throughout this journey. Through the most challenging and stressful times it made an incredible difference knowing that I had them to lean on.

This research was supported by the Natural Sciences and Engineering Research Council of Canada (NSERC), which is gratefully acknowledged.

TABLE OF CONTENTS

LIST OF TABLES

LIST OF FIGURES

1 INTRODUCTION

1.1 BACKGROUND

Frazil ice particles form early in the freeze-up process in the turbulent, supercooled flows of northern rivers. These particles are typically discoid in shape (Figure 1-1) and have been observed to range from ~0.02 to 5 mm in diameter in laboratory settings (e.g. Clark and Doering, 2008, 2006; Daly and Colbeck, 1986; Doering and Morris, 2003; McFarlane, 2014). While in the 'active' state (i.e. when the water remains supercooled), frazil particles will rapidly freeze together to form frazil flocs (Figure 1-2). Once the flocs are large enough for the buoyant force to overcome the fluid turbulence they will rise to the surface and form larger accumulations. The portion of these accumulations that protrudes above the water surface and is exposed to the cold air will then freeze, forming ice floes called frazil pans (Figure 1-3). As the surface concentration of frazil pans approaches 100%, bridging will typically occur across the channel width and an ice cover will begin to form in the upstream direction as more pans accumulate.

In addition to forming flocs, active frazil particles will also readily freeze to the bed or any other submerged structures (e.g. river water intakes) forming accumulations of anchor ice, as shown in Figure 1-4 (Daly, 2013). Anchor ice accumulations may then continue to grow through additional frazil ice accretion and the in-situ growth of individual crystals (Kempema and Ettema, 2011; Qu and Doering, 2007). These accumulations have been estimated to cover up to 70% of the river bed on the Peace River in Alberta (Jasek, 2016), drastically altering the river geomorphology and reducing flow area (Figure 1-5). Additionally, the release of anchor ice has been observed to contribute to sediment transport through 'rafting' (e.g. Kalke et al., 2017; Kempema and Ettema, 2011) and the formation of anchor ice waves, or 'AI waves', which have been observed to cause flow

increases of up to 22% on the Peace River, Alberta (Jasek, 2016). The formation of anchor ice on water intakes can cause large head losses or, in extreme circumstances, completely block the flow (Richard and Morse, 2008).

Due to the challenges posed by carrying out field work in harsh winter conditions and the difficulties in predicting when frazil and anchor ice formation events will occur, very little quantitative data have been collected in rivers to study these processes. Instead, the majority of past studies have focused on laboratory measurements. While these studies have provided valuable information about the size distribution, concentration, and overall characteristics of frazil particles, and the formation and evolution of anchor ice under varying conditions, field data are needed to truly understand these processes. Recently, acoustic devices have shown promise in detecting frazil ice production during supercooling events and estimating particle concentrations and size distributions (Ghobrial et al., 2013a, 2013b; Marko et al., 2015; Marko and Jasek, 2010a, 2010b). However, calibration of these acoustic instruments with laboratory data requires a number of assumptions for use in the field (e.g. that frazil particles have similar shapes, sizes, and concentrations in the field) and direct field measurements of frazil properties in rivers are required to validate or revise these assumptions (Ghobrial et al., 2013b).

1.2 Literature Review

The study of frazil ice properties has been an area of interest for many years and a number of studies into the formation, shape, growth rate, size, aspect ratio, and concentration have been performed. The first quantitative information on frazil ice particle sizes in real streams was provided by Osterkamp and Gosink (1983) who successfully photographed in-situ frazil ice particles in the Chatanika River, Alaska. Osterkamp and Gosink (1983) noted that the photographed particles ranged in size from 0.1 to 1 mm in diameter and

made the qualitative observation that the size distribution remained relatively constant, although there was a significant change in the number concentration of suspended particles from approximately 10^4 to 10^7 particles/m^3 throughout the four-hour camera deployment.

A much larger number of previous investigations have been carried out in laboratory settings, and the impact of turbulence intensity, degree of supercooling, and the stage in the supercooling process on frazil ice properties has been examined. Many laboratory experiments have focused specifically on the size distribution of frazil ice particles. Daly and Colbeck (1986) produced and photographed frazil ice particles in a 36.6 m long flume and determined that the particle diameters were well described by a lognormal distribution with a mean diameter typically above ~0.1 mm. The crystals measured by Daly and Colbeck (1986) ranged in size from approximately 35 μm to 0.5 mm, number concentrations ranged from 1.7×10^5 to 9.8×10^5 particles/m^3, and diameter to thickness, or 'aspect' ratios, were found to range from approximately 6.4 to 9.6. Further laboratory studies by other researchers have also found that a lognormal distribution describes the size distribution of frazil particles quite well, including a large amount of work conducted in a counter-rotating flume at the University of Manitoba (Clark and Doering, 2008, 2006, 2004, 2009; Doering and Morris, 2003; Ye et al., 2004). While there has been general agreement in terms of the shape of the size distribution, the mean particle size has varied widely between experiments from the 0.1 mm range observed by Daly and Colbeck (1986) to a maximum of nearly 2 mm by Clark and Doering (2006). However, some measurements were made earlier in the supercooling process which may have limited the size to which the particles could have grown (e.g. Daly and Colbeck, 1986). In other studies, the smallest observable particle size was limited by the resolution of the digital

images acquired (Clark and Doering, 2008, 2006, 2004, 2009; Doering and Morris, 2003; Ye et al., 2004).

Several other investigations have focused on how the size distribution changes as a function of time during the supercooling process. A typical supercooling event can be broken down into two phases: principal supercooling phase, which begins when the temperature first cools below zero degrees Celsius and ends when a stable, slightly supercooled temperature is reached; and the residual supercooling phase, during which the water temperature remains at the stable, slightly supercooled temperature (Figure 1-6). A large variation has been observed in the number concentration and mean particle size of frazil throughout principal supercooling, with the number of particles rapidly increasing around the time the minimum temperature is reached and the mean particle size beginning to decrease at the same time (e.g. Clark and Doering, 2008, 2006, 2009; Doering and Morris, 2003; Ye et al., 2004). However, the influence of other flow variables such as turbulence intensity is much less certain. Ye et al. (2004) observed an increase in mean particle size with increasing Reynolds number and Clark and Doering (2008) noted an increase in mean diameter with increasing values of the dissipation rate of turbulent kinetic energy up to ~900 cm^2/s^3, with the mean diameter decreasing once the dissipation rate increased beyond this point. However, Ettema et al. (1984) found that the mean size of observable frazil 'platelets' (i.e. flocs) decreased with increasing turbulence intensity.

Research on the theory behind the formation and growth of frazil ice crystals has been carried out by Osterkamp (1978) and Daly (1984), both of whom developed a set of equations describing the dynamics of frazil ice particles. Osterkamp (1978) suggested that a mass exchange process, whereby ice particles created elsewhere (e.g. snow, frost, etc.) enter the flow and form frazil particles, in combination with 'secondary nucleation',

wherein particles grow around miniscule fragments of ice that have broken free from 'parent' crystals, were the most likely mechanisms responsible for frazil ice nucleation. Daly (1984) concluded that secondary nucleation was the dominant formation process for frazil ice particles in supercooled flows and was responsible for the rapid increase in frazil production during a supercooling event; however, he agreed with Osterkamp (1978) that a mass exchange process was likely responsible for nucleation of the initial frazil crystals. Daly (1984) also determined that the limiting factor in the growth rate of frazil ice particles is the rate at which the latent heat released during crystallisation can be advected away from the crystal.

Despite the significant knowledge that has been gained from the theoretical work and laboratory studies that have taken place, the lack of field studies means that our understanding of how frazil ice behaves in field environments is quite limited. It is necessary to collect and analyse data about in-situ frazil ice particles to further increase our fundamental knowledge of the river ice formation process and enhance our ability to predict how freeze-up will unfold in rivers of various characteristics.

1.3 Study Objectives

The objectives of this study were focused on addressing the lack of knowledge regarding the size distribution and concentration of frazil ice particles in various settings. This investigation included a series of laboratory experiments to determine how frazil ice particles are affected by different variables in a controlled setting and a series of field experiments in three rivers with significantly different characteristics. This study had three specific objectives which are outlined below.

The first objective was to determine how the size distribution of frazil ice particles evolves throughout a supercooling event and under varying turbulence conditions in a controlled environment. This was achieved through a detailed laboratory study conducted in the cold room laboratory at the University of Alberta, described in Chapter 2. A high-resolution digital imaging system was used to capture photos of suspended frazil ice crystals produced at three different turbulence intensities in the frazil ice generation tank. Analysis of the images revealed how the particle size and concentration vary with time during the principal supercooling and residual supercooling phases.

The second objective was to develop a digital imaging system for measuring frazil particles in field environments. Chapter 3 presents detailed information about the development of a self-contained, fully submersible digital imaging system called the "FrazilCam" that uses the same photographic technique used in the laboratory. Using this system the first direct measurements of frazil ice particle sizes in real rivers were obtained in the winter of 2014-15. However, the images were affected by the presence of very small, suspended sediment particles in the flow. In order to more accurately separate the sediment and ice particles visible in the digital images during processing, the image-processing algorithm was modified to use a support vector machine learning algorithm (SVM). The process of training and validating the SVM algorithms for each river is described in Chapter 4, and the SVMs are used to reanalyse the data from Chapter 3.

The third objective was to investigate the properties of suspended frazil ice particles under varying meteorological and flow conditions in rivers. Field data that were collected during the winters of 2014-15, 2015-16, and 2016-17 are described in Chapter 5. Use of the SVMs made it possible to analyse these datasets with great detail and accuracy. These results

include the first ever direct measurements of frazil ice concentrations and the temporal evolution of frazil ice properties in rivers.

FIGURES

Figure 1-1: A digital image of frazil ice particles produced in the frazil ice tank in the University of Alberta cold room laboratory.

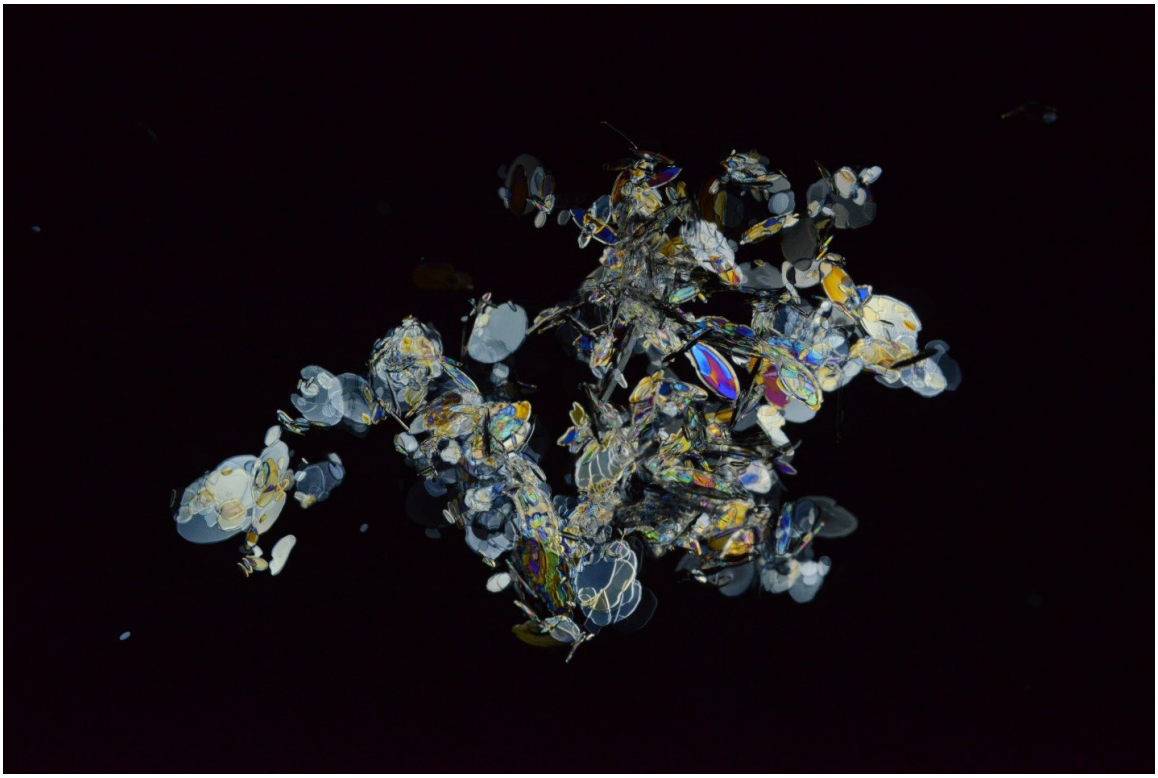

Figure 1-2: A digital image of a frazil ice floc produced in the frazil ice tank in the University of Alberta cold room laboratory.

Figure 1-3: Frazil pans on the Peace River, Alberta on December 17, 2014.

Figure 1-4: Anchor ice in the Kananaskis River, Alberta on November 26, 2012. (Photo courtesy of S. Emmer).

Figure 1-5: An anchor ice dam altering the bed characteristics and flow capacity on the King Creek in Kananaskis, Alberta on November 27, 2012.

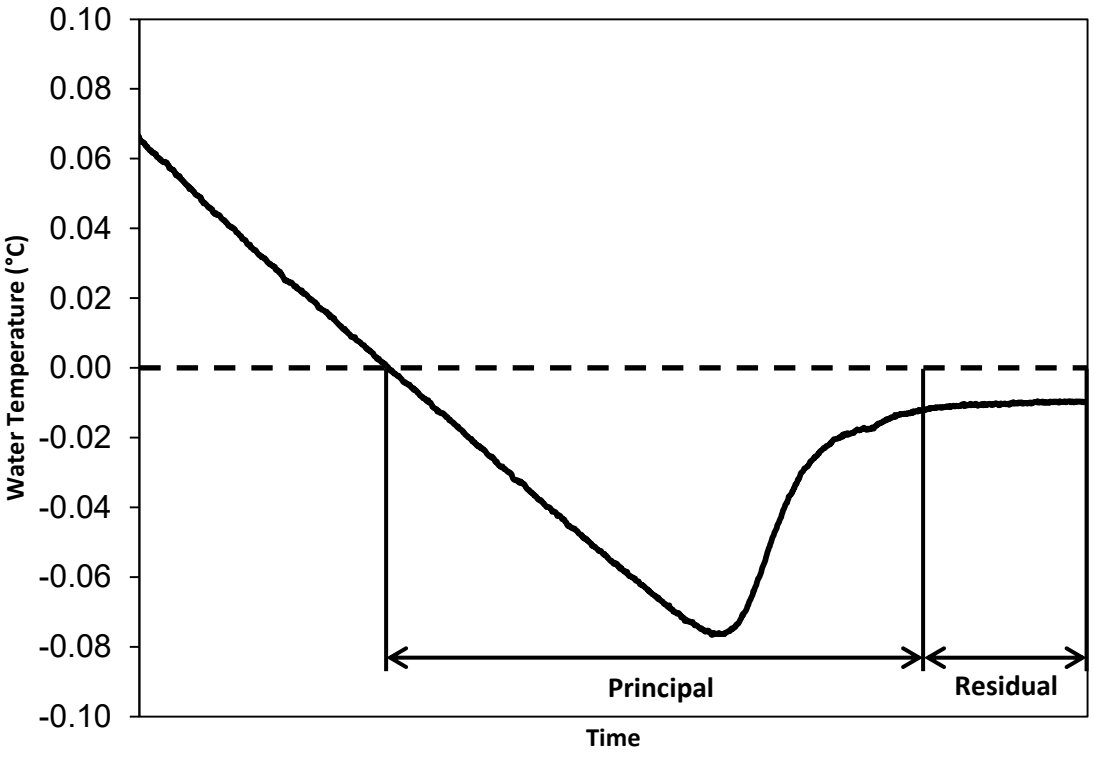

Figure 1-6: Illustration of a typical supercooling curve. The principal and residual supercooling phases are identified.

2 MEASUREMENTS OF THE EVOLUTION OF FRAZIL ICE PARTICLE SIZE DISTRIBUTIONS

2.1 INTRODUCTION

Frazil ice particles are formed in turbulent river flows when the water temperature has supercooled to a few one-hundredths of a degree below 0°C. Suspended frazil particles exhibit a highly adhesive behaviour in supercooled water. This 'active' frazil readily freezes onto other frazil particles (forming flocs), to the streambed (forming anchor ice), and to man-made structures, such as trash racks on water intakes. As a result, active frazil can cause a number of problems. Large accumulations formed on trash racks can, in extreme cases, entirely block the flow into water intakes (Richard and Morse, 2008). Anchor ice can drastically alter the river geomorphology by raising the bed level, reducing the effective flow area, and forming anchor ice dams, all of which severely impact fish habitat (e.g. Brown et al., 2011; Stickler et al., 2010). The hydraulic resistance of the riverbed is also affected by anchor ice formation; the bed roughness initially increases as anchor ice accumulations begin to form, then decreases to a minimum value as the spaces between the substrate and ice fill in and the anchor ice smooths over (Kerr et al., 2002).

The supercooling process that initiates frazil ice production is well understood and has been documented thoroughly in previous studies (e.g. Carstens, 1966; Clark and Doering, 2009; Osterkamp, 1978; Tsang and Hanley, 1985). During a typical supercooling event, assuming the heat loss from the water surface to the air above is constant, the water temperature initially decreases at a nearly constant rate. Shortly after the water temperature drops below 0°C, frazil ice crystals begin to form and release latent heat into the flow. As more and more crystals are produced, the amount of latent heat released becomes increasingly significant, decreasing the cooling rate until the maximum degree of

supercooling is reached, and the water temperature then begins to increase (Daly, 2013). Eventually a point in time is reached where the amount of heat lost to the cool air and the amount of heat gained from ice formation are in equilibrium, and the water temperature levels off at a 'residual' supercooled temperature. The period of time between when the water first drops below 0°C and when the residual temperature is reached is called the period of 'principal supercooling' (Ye et al., 2004). During this time period the size distribution of suspended frazil particles is constantly evolving due to the processes of particle formation, growth, and flocculation (Ye et al., 2004). The earliest particles are generally formed from small ice nuclei (e.g. snow flakes, frost, fragments of border or skim ice), which then increase in diameter (Daly, 2013). These larger particles collide either with each other or the riverbed and banks causing small ice nuclei to break free and form new, small crystals in a process known as 'secondary nucleation' (Daly, 2013). Active frazil ice particles are removed from suspension when they collide and freeze together forming frazil flocs which rise to the surface once they are large enough to overcome the turbulence in the flow (Daly, 2013).

Much of what is known about the characteristics of frazil ice has been determined from laboratory experiments. This is due to the difficulties presented by the small size, non-spherical shape, and optical properties of frazil ice, as well as the challenges of performing winter field work on rivers (Daly, 1994). Some photographs of suspended frazil ice particles in natural streams have been reported (Dubé et al., 2014; Osterkamp and Gosink, 1983), and the use of acoustic devices has proven to be a promising method for estimating concentrations and size distributions of particles in the field (e.g. Ghobrial et al., 2013b; Jasek et al., 2011; Marko et al., 2015; Morse and Richard, 2009; Richard et al., 2011), but quantitative field measurements of frazil ice properties remain very scarce.

The purpose of this study was to investigate how the size distribution of suspended frazil particles evolves throughout a supercooling event, and to explore the effects of increasing turbulence intensity on this process. A series of laboratory experiments was performed in a frazil ice tank at various turbulence intensities to examine this, and particle sizes were measured from high-resolution digital images. The use of high-resolution digital cameras allowed for the inclusion of very small particles in calculating the size distribution.

2.2 Literature Review

Individual frazil particles measured in laboratory environments are predominately disc-shaped and have been observed to have diameters in the range of 23 μm to 5 mm in the past, with size distributions in most cases well described by a lognormal distribution (e.g. Clark and Doering, 2008, 2006; Daly and Colbeck, 1986; Doering and Morris, 2003; Ghobrial et al., 2012; Gosink and Osterkamp, 1983; McFarlane, 2014; Ye et al., 2004). However, the minimums, maximums, means, and standard deviations of the particle diameters have been different in all of these studies. There are many possible factors that have contributed to these differences. Daly and Colbeck (1986), for example, observed particles ranging in diameter from about 35 μm to 0.5 mm using a 35 mm camera-microscope system and reported mean diameters "generally above 0.1 mm." Daly and Colbeck (1986) also reported particle concentrations ranging from 0.17 to 0.982 particles/cm^3. However, their frazil particles were produced in a 36.6 m long flume and consequently the particles may not have had sufficient time to grow to larger diameters before the water was recirculated and the existing particles were melted out. Alternatively, the counter-rotating flume used by researchers at the University of Manitoba (e.g. Clark and Doering, 2009, 2008, 2006; Doering and Morris, 2003; Ye and Doering, 2004; Ye et al., 2004) allowed frazil particles to continue to seed, develop, and flocculate over the course of an experiment, enabling larger particles to develop and be observed. As a result

larger mean particle sizes were observed in these studies (e.g. 0.79 to 1.58 mm by Clark and Doering (2008)). However, these measurements were limited by the resolution of the digital cameras used, which resulted in a minimum observable particle size of ~0.2 mm.

The differences between the measured particle sizes in past experimental studies may also be due to the influence of flow characteristics such as turbulence intensity on the development of frazil ice particles. Understanding these influences may be instrumental in improving our understanding of how frazil particles behave in natural river flows, which are much less predictable than laboratory environments. A few studies have measured the impact of different turbulence parameters on frazil size. Ettema et al. (1984) produced frazil ice particles in a mixing jar and used an oscillating grid to vary the turbulence intensity. In this way, flows were produced with values of the turbulence exchange coefficient ranging from approximately 6 to 19 cm^2/s and an overall trend of decreasing frazil 'platelet' (i.e. floc) size with increasing turbulence intensity was observed.

Ye et al. (2004) produced frazil ice particles in a counter-rotating flume at various air temperatures and water velocities and studied the impact of these variables on the supercooling process and mean particle size. In these experiments, Ye et al. (2004) observed that the frazil particles increased in number and mean diameter during the period of principal supercooling, and that the mean diameter reached a stable value (termed D_{50sp}) once the principal supercooling period had ended, while the number of observed particles dropped off. Ye et al. (2004) also compared the values of D_{50sp} to the Reynolds number of the flow, and found that the mean frazil diameter at the end of the principal supercooling period increased with an increasing Reynolds number.

Clark and Doering (2008) carried out a study specifically focusing on the effects of turbulence intensity on frazil ice particles in the same counter-rotating flume. By fitting

the flume with bed plates of varying roughness they were able to vary the dissipation rate of turbulent kinetic energy per unit mass in the flow, ε, from about 113 to 1496 cm^2/s^3. After calculating the size distributions of the observed particles for each of these flows, Clark and Doering (2008) observed that both the mean and standard deviation of the particle diameters first increased with increasing values of ε up to about 900 cm^2/s^3, and then decreased. For both the mean and standard deviations these relationships were well described by parabolic functions. Similar to Ye et al. (2004), they also observed that the number of clear, disc-shaped particles in the flow increased during the period of principal supercooling and decreased thereafter.

The results obtained by Clark and Doering (2008) and Ye et al. (2004) support the theoretical analysis presented by Daly (2013, 1994, 1984) who suggested that the limiting factor in the growth rate of a frazil particle's diameter is the rate at which the latent heat released by crystallisation can be advected away from the crystal by the flow. This means that, as the turbulence intensity increases, the frazil particles in the flow would be able to grow more quickly and, presumably, to a larger crystal diameter. However, increased turbulence intensity could also cause an increase in the number of crystal collisions, and it was hypothesised by Clark and Doering (2008) that there might be a point at which increasing turbulence intensity actually results in eddies that are strong enough to overcome the weak mechanical strength of frazil crystals. This would result in particle fracture and thereby physically limit the average particle size. Both of these processes would result in increased secondary nucleation. Daly (2013) noted that this would lead in a relatively large number of small frazil crystals being produced at high turbulence levels, and this could explain the decrease in mean particle size that Clark and Doering (2008) observed for dissipation rates greater than about 900 cm^2/s^3.

2.3 Experimental Set-up

Experiments were performed in the University of Alberta's Civil Engineering Cold Room Facility using a frazil ice production tank (illustrated in Figure 2-1) with base dimensions of 0.8 by 1.2 m and filled to a depth of 1.3 m with filtered tap water. During experiments, turbulence in the tank was generated by four variable speed propellers powered by NEMA 34 DC variable speed electric motors (278 W, 1.514 N-m of torque, max speed 1750 rpm) and mounted on the bottom of the tank. The frazil ice particles were illuminated using two arrays of Larson Electronics 24-bulb, three-watt light-emitting diode (LED) lights that were mounted against the back glass wall of the tank and diffused by translucent plastic sheeting. Directly opposite the lights, two Cavision 10 cm square glass polarising filters were mounted in the tank flush to the front glass wall. These polarisers were mounted parallel to each other and spaced 2.2 cm apart, with one of them rotated 90° with respect to the other, to cross-polarise the light passing through them. This achieved the effect of producing a black background in the captured images where only the ice particles passing between them, that had refracted the incident light, were visible. A Sea-Bird SBE 39 temperature recorder (accuracy ±0.002°C) was used to record the water temperature throughout the experiments and was connected to a computer located outside the cold room to allow for real-time monitoring of the supercooling process. The temperature recorder was placed in an approximately symmetrical location and at a comparable depth to the polarisers. This was to avoid interfering with the flow through the measuring volume while still providing a representative temperature to where the frazil particle images were captured.

The camera used for the experiments was a Nikon D800 digital single-lens reflex (DSLR) equipped with a Kenko 25 mm Uniplus Tube DG extension ring and an AF Micro-Nikkor 60 mm f/2.8D lens. The Nikon D800 has a 36 megapixel resolution and, when used with

the macro lens and extension tube, the average pixel size in the images was ~5.6 μm, allowing very small particles to be resolved in the images. This resulted in an average measuring volume of 24.6×10^{-6} m^3 in the experiments. During a series of preliminary experiments, the aperture, shutter speed, and ISO settings of the camera were tested, and settings of f/25, 1/2000s, and ISO 6400 were determined to offer the best balance of depth of field and brightness with minimal background noise.

Velocity time series measurements were recorded in the tank using a Nortek Vectrino acoustic Doppler velocimeter (ADV) mounted on a frame above the tank that allowed it to be positioned to record a vertical profile anywhere in the tank. The ADV could be positioned at depths ranging from the bottom of the tank up to a depth of about 240 mm below the water surface, due to the limited clearance above the tank in the cold room.

2.4 Experimental Procedure

At the start of each experiment the four propellers located at the bottom of the tank were set to the desired speed (125, 225, or 325 rpm), verified using a laser tachometer. The temperature recorder mounted in the tank was programmed to begin recording the water temperature and the air temperature in the cold room was reduced from 2°C to -10°C over approximately two to three minutes. Images were then captured of a clear plastic ruler positioned at the front, back, and mid-point between the polarisers, both to focus the camera and to provide a scale for processing the frazil images. When the water temperature reached 0°C, the camera was manually activated to record images at a rate of 1 Hz for a duration of 999 seconds. Once the camera had finished capturing images, the propellers were switched off and the temperature in the cold room was raised to 2°C to allow the ice to melt prior to the next experiment.

Measurements of the turbulent velocities were made using the Vectrino ADV in separate experiments while the water temperature was held constant at approximately 2°C. At each of the three propeller speeds, ADV measurements were made at nine depths at the three locations shown in Figure 2-1; at the centre of the tank, near the front glass wall where the polarisers were placed when collecting images, and directly above one of the propellers. These locations were selected to provide a representative sample of the turbulence characteristics throughout the tank. At the propeller speeds of 125 and 225 rpm velocity measurements were taken at a sampling frequency of 50 Hz for a duration of five minutes and, for the speed of 325 rpm, a frequency of 100 Hz was used for the same duration.

2.5 Data Analysis

2.5.1 ADV Data

The ADV data were analysed using a Matlab program. The first step in the analysis was the application of the despiking algorithm developed by Islam and Zhu (2013) to the raw ADV data files. This despiking method was selected because it has been demonstrated to be effective at removing spikes from data contaminated by up to 70% spikes (Islam and Zhu 2013). This method was applicable because up to 32.5% spikes were observed in the velocity time series data from the frazil ice tank. Next, the de-spiked time series data were corrected for Doppler noise using the method developed by Romagnoli et al. (2012) and decomposed into mean and turbulent velocity components. The decomposed data were then used to compute a variety of turbulence characteristics at each measurement point in the tank. In particular, frequency spectra computed from the de-spiked time series were plotted and the minimum and maximum frequencies for the range of frequencies within the inertial subrange were determined (i.e. frequencies where a slope of -5/3 occurred). This region of the frequency spectrum was then used to calculate the turbulent kinetic energy dissipation rate per unit mass at each location for each propeller speed (Tennekes

and Lumley, 1972). Taylor's 'frozen turbulence' hypothesis was used in calculating the dissipation rates from the frequency spectra, which requires the assumption that the turbulent structures do not change appreciably in the time it takes for them to be advected past the point of measurement (Stiansen and Sundby, 2001). The equation used was:

$$\varepsilon = 2\pi \left(\frac{P_i f^{5/3}}{A U_i^{2/3}} \right)^{3/2} \quad [1]$$

where ε is the dissipation rate of turbulent kinetic energy per unit mass (m^2/s^3); P_i is the power spectral density in direction i (m^2/s); f is the frequency (Hz); A is a constant taken to equal 0.49 (Pope, 2000); and U_i is the convective velocity in direction i (m/s). Stiansen and Sundby (2001) provide a detailed discussion and comparison of this, and other, methods for calculating the dissipation rate from the frequency spectra. A block width of 512 with a 50% overlap was used in calculating the frequency spectra, giving a normalised random error of ±13% for the 125 and 225 rpm propeller speeds (50 Hz sampling rate) and ±9% for the 325 rpm propeller speed (100 Hz sampling rate). A typical frequency spectrum fitted with the -5/3 slope is shown plotted in Figure 2-2.

In Figure 2-3 the dissipation rate, ε, is plotted versus the water depth at the measurement location directly above the one propeller, and can be seen to increase up to a depth of 825 mm for the w-component and 925 mm for the u- and v-components. The 1025 mm measurement, which was taken approximately 85 mm above the propeller, was the smallest by a significant amount in all cases. These small values are likely caused by the presence of very high shear close to the propeller that results in unreliable ADV velocity measurements (McLelland and Nicholas, 2000). Therefore, the dissipation rate estimates at the 1025 mm depth were omitted when depth-averaging the dissipation rates above the propeller and, to be consistent, at the other two vertical profile locations as well. The

depth-averaged values of the dissipation rate computed from the three velocity components at each location, and for all propeller speeds, are presented in Table 2-1.

Examination of the depth averaged values in Table 2-1 and the data plotted in Figure 2-3 shows that the dissipation rates estimated from the u and v velocity components were comparable, while the w-component value tended to be about an order of magnitude smaller. The reason for this discrepancy was investigated but no satisfactory explanation was found. The data in Table 2-1 also show that, as expected, the dissipation rate varies spatially in the tank and is highest directly over the propellers. Tank-averaged estimates of ε were calculated using the values computed from the u and v-components, which were then averaged spatially over the three measurements locations. This results in values of 23.9, 85.5, and 336 cm^2/s^3 for propeller speeds of 125, 225, and 325 rpm, respectively. Note that if the dissipation estimates computed from the w-component are included when calculating tank-averaged values this reduces the magnitude by only ~30%, and such a reduction would not alter any of the conclusions drawn from this study.

Determining how comparable the rates of dissipation in the tank are to those observed in natural rivers would be quite useful. However, an extensive literature search did not find any dissipation rates measured in rivers for comparison. As an alternative, estimates of the dissipation rates in a number of natural rivers in the Alberta were calculated using the average channel slopes, velocities, depths, and widths reported by Kellerhals et al. (1972) using the following equations:

$$u_* = \sqrt{gR_hS} \qquad [2]$$

$$\varepsilon = \frac{u_*^3}{\kappa R_h}\left[\ln\left(\frac{u_* R_h}{\nu}\right) - 1\right] \qquad [3]$$

where u_* is the shear velocity (m/s); R_h is the hydraulic radius (m), calculated based on the average channel depth and width; g is the acceleration due to gravity, taken to equal 9.81 m/s^2; κ is von Karman's constant, taken to be 0.4; and ν is the kinematic viscosity of water, taken to equal 1.8×10^{-6} m^2/s for water at 0°C (Clark and Doering, 2008). Kellerhals et al. (1972) reported 359 depth, width, slope, and velocity values for 54 different rivers, and using equations [2] and [3] dissipation rates were predicted to range from 4.2 to 14,968 cm^2/s^3, with an average of 1,164 cm^2/s^3. A total of 210 of these 359 estimates (58%) fell within the same range as the u and v-component depth-averaged dissipation rates obtained in this study (Table 2-1), indicating that the strength of the turbulent mixing in the tank was comparable to that in natural streams.

2.5.2 FRAZIL IMAGES

A typical cross-polarised digital image of frazil ice particles is shown in Figure 2-4. The digital images were processed using a MATLAB algorithm that was written to identify and compute the size of each individual frazil particle. The algorithm first loaded a 'raw' image and then subtracted a background image (i.e. an image captured prior to the formation of any ice in the tank) from it, to remove any of the imperfections visible in all of the images (e.g. spots on the lens, scratches on the glass, etc.). Second, the resulting image was converted into high-threshold and low-threshold binary images. The two binary images were then compared to each other using an iterative dilation and erosion procedure, until the extent of each individual particle had been determined. Next, the area and perimeter of each particle in the final binary image was compared to the area and perimeter of a fitted ellipse, since most frazil particles are expected to be disc-shaped. If the area and perimeter of the particle were similar enough to those of the fitted ellipse, then the particle was identified as a frazil ice particle and included in the data set used to calculate the properties of the size distribution. Approximately 75% of the particles identified were

confirmed to be disc shaped using this test, and by manually checking nearly 1000 particles it was determined that the particles were correctly identified as being disc shaped or not, more than 93% of the time. This test not only ensured that irregularly shaped individual particles were excluded; it also rejected any frazil flocs that appeared in the images. Finally, the diameter of each confirmed frazil particle was calculated and the properties of the resultant size distribution for the entire image series, including the mean, median, and standard deviation, were computed. As mentioned in section 2, a lognormal distribution has been observed to fit the size distribution of frazil particles in the past. With this in mind, a lognormal distribution with the same mean and standard deviation as the measured data was calculated for each experiment and plotted along with the observed size distribution for comparison. An example size distribution for a single experiment is shown in Figure 2-5 along with the computed lognormal distribution.

After computing the particle sizes for each individual experiment it was desirable to combine the data from each experiment (i.e. ensemble average) at each propeller speed in order to observe how the particle characteristics evolved with time. There were 10 experiments processed for the 125 rpm propeller speed, five for 225 rpm, and 12 for 325 rpm. The repeatability of the experiments at each propeller speed was assessed by comparing supercooling curves that were synchronised to the time at which the temperature reached 0°C. A plot showing the superimposed supercooling curves for the 12 experiments conducted at 325 rpm is presented in Figure 2-6. This plot shows that the rate of cooling (i.e. the slope of the curves from 0 to about 400 seconds) and the residual supercooling temperatures did not vary significantly (e.g. the cooling rate varied from 0.012 to 0.015 °C/minute over the 12 experiments). This demonstrates that the cold room temperatures were being varied in a controlled manner and that the supercooling process was repeatable. However, significant variations were observed in the minimum

temperature, which varied from −0.093°C to −0.072°C, and in the duration of the principal supercooling period, which varied from approximately 12 to 15 minutes. These variations may have been caused by variations in the seeding rate; that is, the rate at which ice crystals were introduced into the supercooled water from the air in the cold room. Model simulations by Hammar and Shen (1995) have shown that varying the seeding rate will produce variations in the supercooling curve very similar to those observed in Figure 2-6 (see their Figure 3). The most likely source of seed particles is the frost that forms in the cold room refrigeration system when warm air is cooled. These ice crystals enter the cold room via two large cold air vents mounted in the ceiling and the rate at which they seed the supercooled water in the tank would be expected to vary from one experiment to the next due to a variety factors. Despite the variations in the supercooling curves that were observed, the experiments were judged to be sufficiently repeatable that the data could be ensemble averaged at each of the three propeller speeds.

2.6 Results and Discussion

2.6.1 Evolution of Size Distribution

In order to observe how the particle properties changed throughout the supercooling process, the experiments for each propeller speed were synchronised using the time at which the minimum temperature was reached. The supercooling curve was then ensemble-averaged across all of the experiments and a 5 point median filter was applied to remove random noise (Pratt, 2007). In Figure 2-7, the time series of the 35 s moving mean, standard deviation, and number of observed particles are plotted for the 325 rpm experiments. By recording these three parameters, it is possible to plot a theoretical distribution at any point in time that approximates the size distribution of the observed frazil particles. Note that the mean and standard deviation plots begin later than the plot

of the number of particles because these two parameters were only calculated when a minimum of ten particles were available for averaging.

First, examining the number of observed particles (Figure 2-7a), it is clear that the number of particles increased quite rapidly at a fairly constant rate until just after the maximum supercooling had been reached, achieving an ensemble averaged peak number concentration of 1.8 particles/cm^3 in the sampling volume of 24.6 cm^3. This is logical, as the rapid increase in the number of frazil particles suspended in the water results in a large release of latent heat due to crystallisation, causing the water temperature to increase. The higher concentration of frazil particles also leads to an increased likelihood of particle collisions which has two potential effects: 1) increasing the number of small particles produced due to particle fracture and secondary nucleation, and 2) increasing the size and/or number of frazil flocs. As more and more particles flocculate and rise to the surface, the number of individual particles in suspension begins to decrease, and this can be seen as the number of particles decreases steadily when the water reaches the residual supercooling temperature. This is the same trend that was observed by both Ye et al. (2004) and Clark and Doering (2009, 2008, 2006).

In Figure 2-7b it is seen that the moving average particle diameter follows a similar trend as the number of suspended particles. Although the peak is not quite as pronounced, the mean particle size is relatively small when there are few particles in suspension (~0.35 mm at 480 s), slowly increases to a maximum as more and more particles are produced (~0.7 mm at 700 s), begins to decrease as the maximum number of particles is approached, and levels off to a relatively constant size once the number of particles begins to decrease (~0.6 mm at 930 s). The decrease in mean particle size is caused by some combination of an increase in the number of smaller particles and a decrease in the number of larger

particles. However, considering that at the time that the mean approaches an equilibrium value, the number of particles suspended in the water is decreasing, it seems likely that the number of large particles is decreasing faster than the number of small particles is increasing. This would imply that the larger frazil particles are more prone to flocculation, or fracture, than smaller ones due to an increased probability of larger particles colliding. A similar trend is observed in the standard deviation time series in Figure 2-7c, which begins at ~0.1 mm at 480 s and peaks at ~0.4 mm at 620 s, although the decrease occurs approximately 80 seconds earlier than that of the mean, and it continued to climb slowly for the remainder of the experiment.

Clark and Doering (2008) plotted the mean and standard deviation of their data in a similar manner, and the trend of an increase to a peak followed by a slow decrease to an equilibrium value is visible in some of their plots. However, their data were collected in bursts separated by 45 seconds and therefore it is possible that some of the temporal changes in the mean and standard deviation were not captured. This possibility was acknowledged by Clark and Doering (2008) when they noted that it was difficult to accurately resolve the variation of the mean and standard deviation owing to the small number of measurements recorded in the early stages of each experiment.

For comparison, the same time series plots are shown for the five 225 rpm experiments in Figure 2-8. The trend for all three subplots is similar for the 325 and 225 rpm experiments with the main difference being that the number of particles does not increase nearly as rapidly in the 225 rpm case and doesn't reach as high of a value (e.g. ~44 particles per experiment in Figure 2-7a but only ~24 particles per experiment in Figure 2-8a). This resulted in a peak concentration of 1.0 particles/cm^3 on average in the 225 rpm case. Based on visual observations made during the experiments and confirmed by the images taken

at each propeller speed, it is likely that the main reason for this is the amount of flocculation that occurred. While less time passed before flocculation was observed in the 325 rpm case, large flocs routinely became frozen to the polarisers during the 225 rpm experiments and had to be knocked loose. This was not a problem that was regularly encountered during either the 125 or 325 rpm experiments. Based on this information it appears that the turbulence characteristics of the 225 rpm case offered ideal conditions for allowing particles to flocculate and remain in suspension. The 325 rpm case produced the most particles and resulted in a large amount of flocculation, but the currents in the tank were strong enough to draw those flocs not buoyant enough to reach the surface down to the bottom, where they were shredded by the propellers, resulting in a large number of individual particles remaining in suspension. In the 125 rpm case, fewer particles were observed at any given time during an experiment, with a maximum concentration of 0.29 particles/cm^3 on average, which led to a decreased chance of flocculation occurring. Those flocs that did form were able to overcome the weaker currents in the tank and float up to the surface, resulting in few flocs appearing in the images or freezing onto the polarisers, but removing individual particles from suspension. It is of note that the peak concentrations observed in this study, which ranged from 0.29 to 1.8 particles/cm^3, are comparable to the concentrations of 0.17 to 0.982 particles/cm^3 reported by Daly and Colbeck (1986).

The growth rate and maximum achievable size of frazil ice particles has also been shown to be influenced by the concentration of particles in the flow and the level of supercooling (Forest, 1986; Forest and Sharma, 1992). As more and more frazil ice particles are produced, the concentration of dissolved solids in the supercooled water increases due to the rejection of these impurities from the frazil crystals, thereby reducing the freezing point of the water (Forest, 1986). Furthermore, the degree of supercooling of the water is

reduced due to the latent heat released by ice formation, as already discussed. Forest (1986) and Forest and Sharma (1992) demonstrated that these two factors combine to slow down and eventually halt the growth of individual frazil particles even though the water surrounding them remains supercooled to a certain degree. This could be the reason the average particle diameter approaches a near-constant value once the residual supercooling temperature has been reached in Figure 2-7b and Figure 2-8b.

To better understand how the shape of the size distribution evolves and observe whether or not a lognormal distribution is an appropriate approximation at all stages of a supercooling event, the time series were broken up into three time intervals based on the peak number of particles observed in the ensemble averaged data, following Clark and Doering (2006). Three intervals were defined based on the time at which number particles first reached 10% of the maximum, 90% of the maximum on either side of the peak, and when 30% of the maximum was observed on the subsequent decline, referred to as t_{10}, t_{90a}, $t_{90b,}$ and t_{30}, respectively. The 'production' interval included all particles observed between t_{10} and t_{90a}, the 'peak' interval included all particles observed between t_{90a} and t_{90b}, and the 'flocculation' interval included all particles observed between t_{90b} and t_{30}. The size distributions in these three intervals and the distribution over the entire duration are plotted in Figure 2-9 and Figure 2-10 for the 325 and 125 rpm experiments, respectively. The distributions for the 225 rpm case, though not shown, were very similar. The mean diameter, standard deviation, and total number of frazil particles observed in each interval are listed in Table 2-2 for the three propeller speeds. In all plotted intervals the distribution shapes were very similar although the mean and standard deviation vary slightly, which can be seen clearly in Table 2-2. Also apparent in Figure 2-9 is that the distributions seem to deviate from the ideal lognormal distribution and plateau at a diameter of approximately 2 mm. This was observed in all of the distributions at each

propeller speed, and was most pronounced for the 125 rpm experiments where a secondary peak was visible between 2 and 3 mm. The reason for this is unknown; however, the lognormal curve does still represent the shape of the distributions reasonably well, and appears to be a suitable approximation for the size distribution of frazil ice particles at any point in the supercooling process.

2.6.2 Effect of Turbulence

Across the 27 total experiments that were analysed, particles ranging in size from about 22 μm to 5.5 mm in diameter were observed. Only the 'pre-flocculation' images were used in calculating the size distributions for the suspended frazil particles to be compared to the turbulent kinetic energy dissipation rate. The images to be used in analyzing the effect of turbulence were determined for each experiment by noting the image in which small flocs (i.e. accumulations of 4 or more particles) appeared regularly. For the 325 rpm experiments this meant that ~350 images from each experiment were included in calculating the size distribution; for the 225 rpm experiments ~450 images were used; and for the 125 rpm experiments all 800 of the processed images were included. The means and standard deviations of the particle diameters obtained for each propeller speed after ensemble averaging, and the total number of detected frazil discs, are listed in Table 2-3.

It is clear from Table 2-3 that the mean particle size prior to flocculation decreased with increasing propeller speed, and therefore with increasing turbulence intensity. In Figure 2-11 the mean particle diameter prior to flocculation is plotted versus the mean depth-averaged dissipation rate (i.e. average of all three vertical profiles) as well as the maximum and minimum depth-averaged values for each propeller speed. At all three propeller speeds the minimum depth-averaged dissipation rate was observed near the glass and the maximum was observed directly over the propeller.

A power series regression was fitted to each relationship plotted in Figure 2-11 and described the decrease in mean particle size very well, with an R^2 value greater than 0.94 in all three cases. This trend is contrary to the results obtained by Clark and Doering (2008) and Ye et al. (2004). Specifically, Ye et al. (2004) found an increase in particle diameter with increasing Reynolds number, and Clark and Doering (2008) observed a parabolic relationship between the mean diameter and the dissipation rate, with the diameter increasing up to ~900 cm^2/s^3 and decreasing thereafter. All of the depth averaged dissipation rates for this study fall below the value of ~900 cm^2/s^3 that Clark and Doering (2008) found to be the turning point between particle size increase and decrease. However, contrary to those results, the results of this study indicate a decrease of mean particle size with an increasing turbulent kinetic energy dissipation rate in this range. This discrepancy could be the result of several factors. One possibility is the limitation to the size of observable particles imposed by the imaging system. In the case of Ye et al. (2004) the image resolution was 0.25 to 0.30 mm/pixel, meaning no particles smaller than ~1.25 mm in diameter could be measured. For Clark and Doering (2006) the resolution was 0.055 mm/pixel, allowing for particles as small as 0.165 mm to be observed. Similarly, Clark and Doering (2008) reported a resolution of ~0.056 mm/pixel and a minimum particle size of ~0.2 mm. As mentioned previously, the resolution in the present study was ~0.0056 mm/pixel and the smallest observed particle was 0.022 mm in diameter. The absence of these small particles, which have previously been observed by Daly and Colbeck (1986), would drive up the overall average of the calculated size distributions in all cases but this would probably not be enough to reverse the trend.

A more likely possibility is that the size distribution is affected by the method in which turbulence is generated. It is possible that the propellers used to generate turbulence in this study caused larger particles to fracture more easily, either due to the increased

turbulence near the propellers or through direct contact with the propellers themselves. This fracturing would cause many more small particles to form through secondary nucleation, reducing the overall average particle size. In comparison, the shear flow produced in the counter-rotating flume used by Clark and Doering (2008) and Ye et al. (2004) is much more similar to the process that produces turbulence in a natural river flow and could be a more accurate representation of the variations in frazil size that changing turbulence intensity produces. However, the only way to be certain is to perform similar measurements of both particle size and turbulence intensity in natural streams.

2.7 Summary and Conclusions

A series of experiments was conducted in which frazil ice particles were generated at different turbulence intensities and photographed under cross-polarised light in a laboratory frazil ice tank. The evolution of the frazil particle size distribution characteristics and numbers of suspended particles were studied throughout the supercooling process. It was found that the number of frazil particles initially increased quite rapidly and then decreased at a slower rate for the remainder of the experiment, as fewer particles were produced and existing particles were lost to flocculation or rose to the water surface. The mean particle size showed a similar trend although a near-equilibrium mean particle diameter was ultimately reached, at approximately the same time as the number of suspended particles peaked. This leads to the conclusion that larger particles may be more prone to form frazil flocs or fracture into smaller particles, thereby reducing the overall mean of the individual suspended particles. In addition, the growth of the remaining particles is halted due to a combination of an increased concentration of dissolved solids in the water, which depresses the freezing point, and an increase in water temperature. A lognormal distribution was found to offer a reasonable fit to the particle size distribution at all stages of the experiment. However, a secondary peak was observed

at particle diameters of approximately 2 to 3 mm, which was very pronounced at the lower propeller speeds and the cause of this is unknown.

At each of the propeller speeds used to generate turbulence in the tank, ADV measurements were used to estimate a representative estimate of the overall turbulent kinetic energy dissipation rate. The mean particle sizes were 0.94, 0.75, and 0.66 mm and the corresponding values of the turbulent kinetic energy dissipation rate were 23.9, 85.5, and 336 cm^2/s^3, at propeller speeds of 125, 225, and 325 rpm, respectively. This trend of decreasing particle size with increasing dissipation rate is contrary to the results obtained in two previous studies. Therefore, a priority for future research should be to directly measure the frazil particle size and turbulence intensity in natural streams to determine how varying turbulence levels impact the particle size distribution.

FIGURES

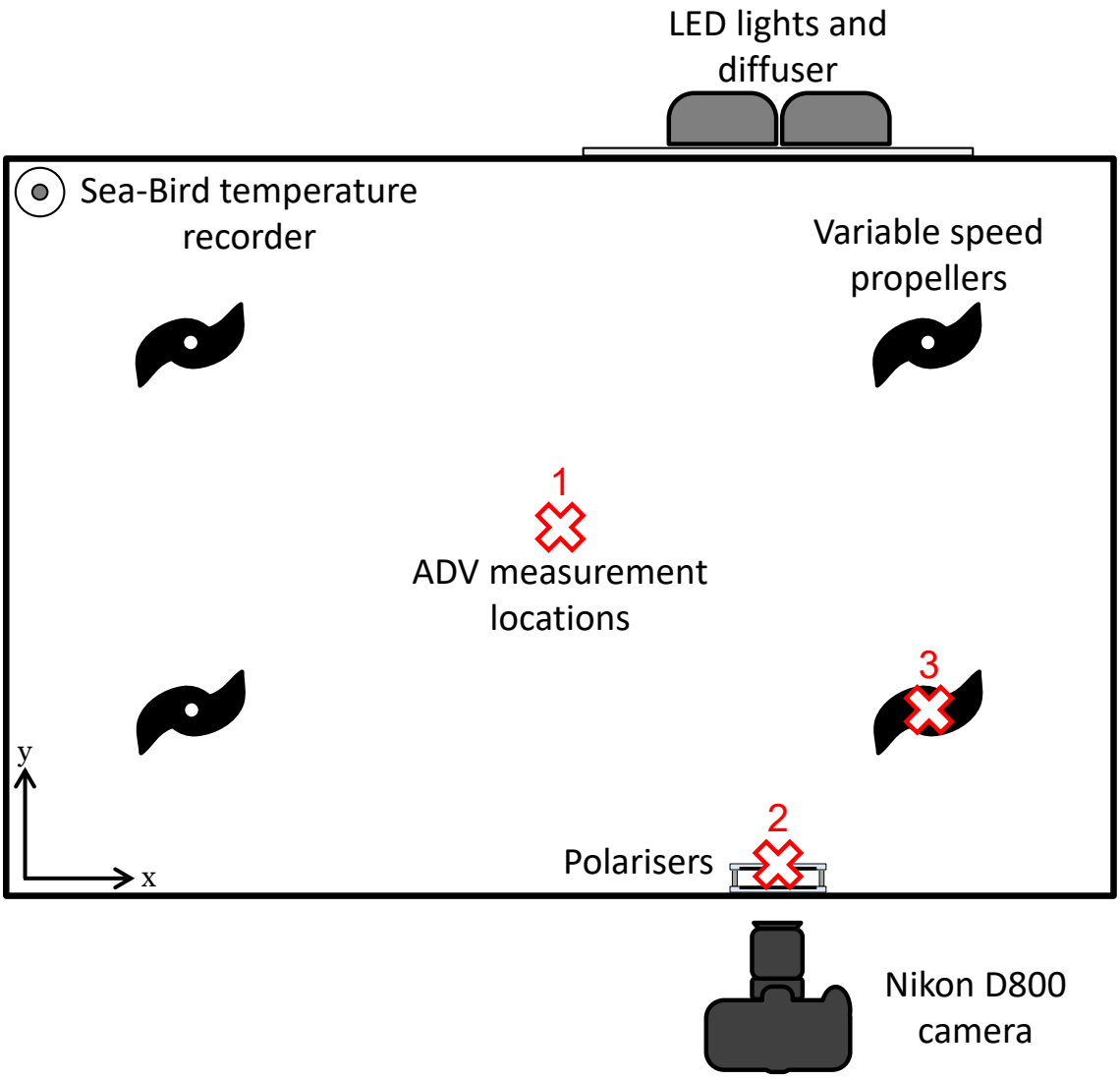

Figure 2-1: Plan view of the frazil ice tank showing the locations of the camera, LED lights, polarisers, four propellers, and the three locations where the ADV measurements were made (marked by the red X's). The coordinate system for the ADV measurements is defined such that the positive x and y-directions are towards the right and back of the tank, respectively, and the positive z-direction is towards the water surface.

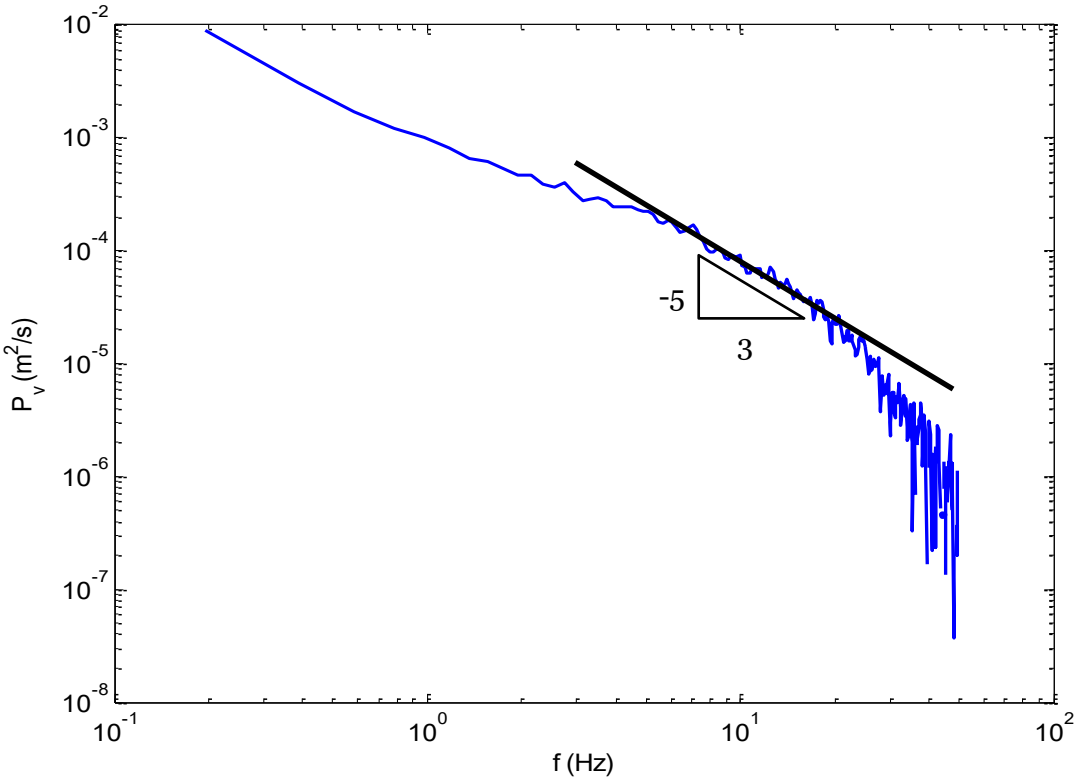

Figure 2-2: Power spectra calculated for the 325 rpm propeller speed in the centre of the tank at a depth of 625 mm. P_v is the value of the power spectral density (m^2/s) in the y-direction and f is the frequency (Hz). A line with a slope of -5/3 is shown over the region determined to be the inertial subrange, used to calculate the dissipation rate of the turbulent kinetic energy.

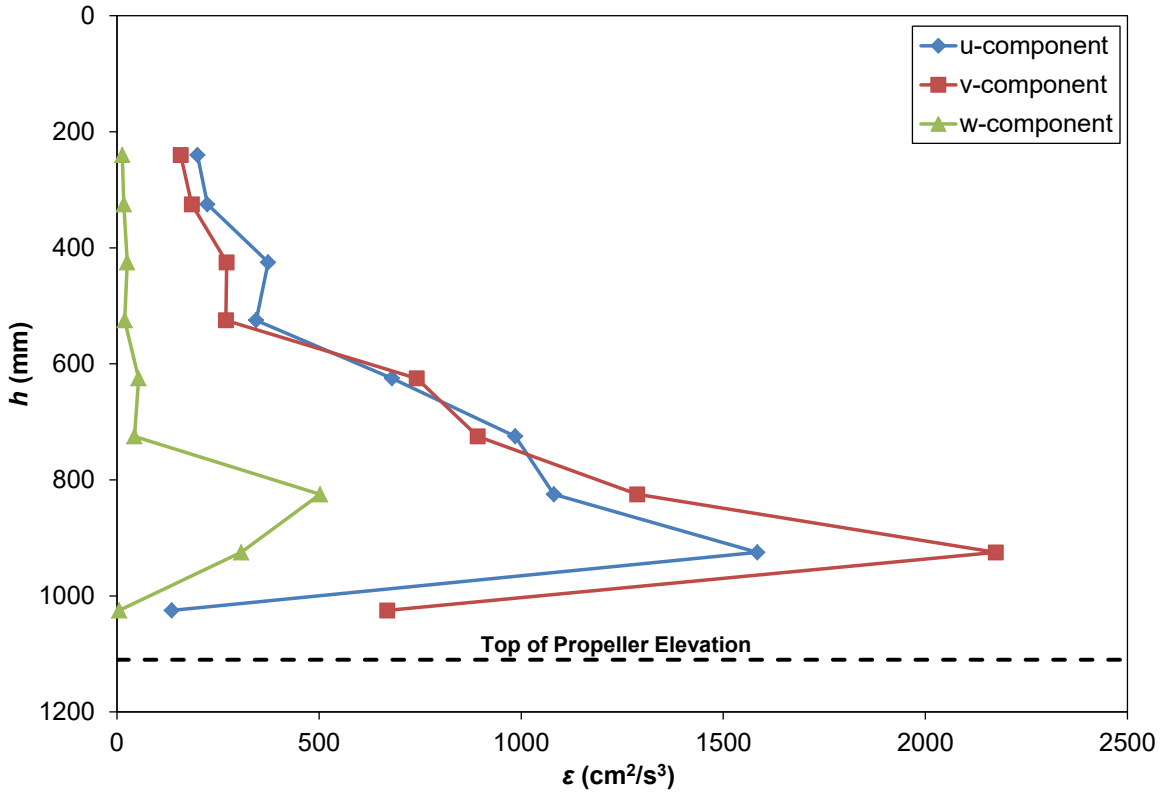

Figure 2-3: Turbulent kinetic energy dissipation rate (ε) throughout the water depth (h), measured above the propeller for a speed of 325 rpm. The u, v, and w-components represent the x, y, and z-directions, respectively.

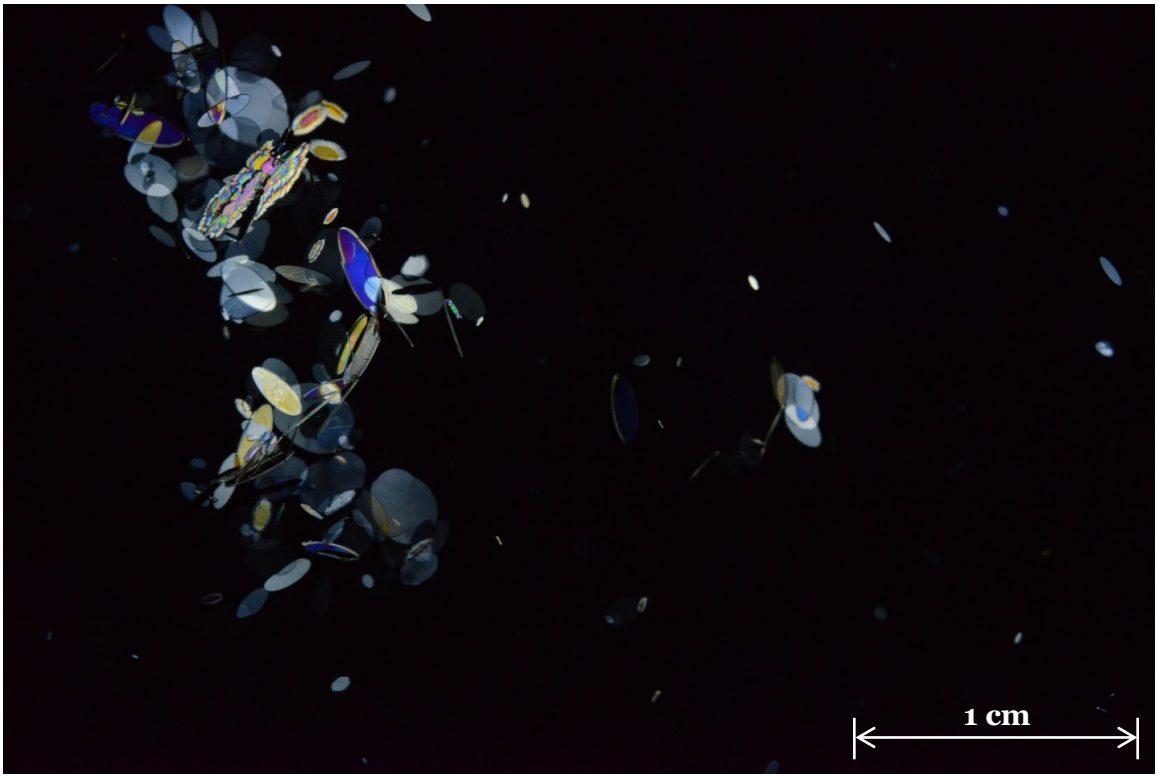

Figure 2-4: A sample unprocessed image, captured during one of the 225 rpm experiments, showing individual particles and a small frazil floc. The spacing between the polarisers was 2.2 cm.

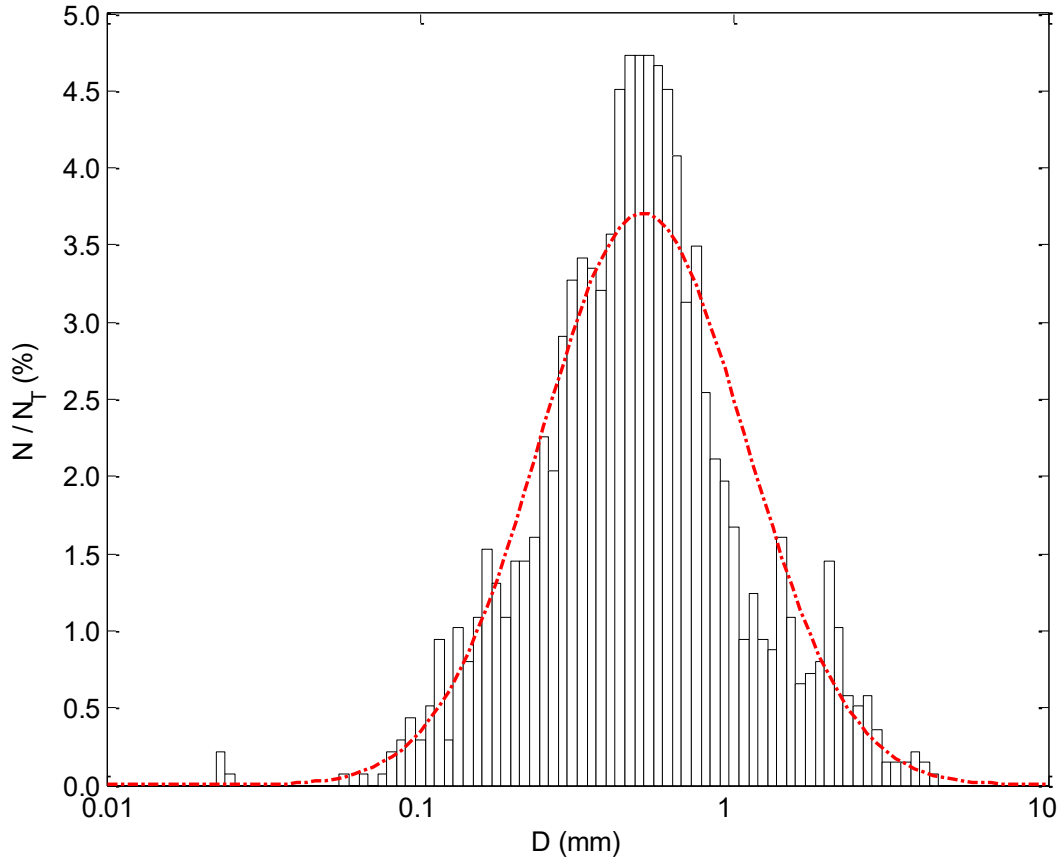

Figure 2-5: Size distribution for particles observed prior to flocculation for an experiment carried out at a propeller speed of 325 rpm. N is the number of particles in each bin, N_T is the total number of particles, and D is the diameter. The dot-dash line is the corresponding ideal lognormal distribution.

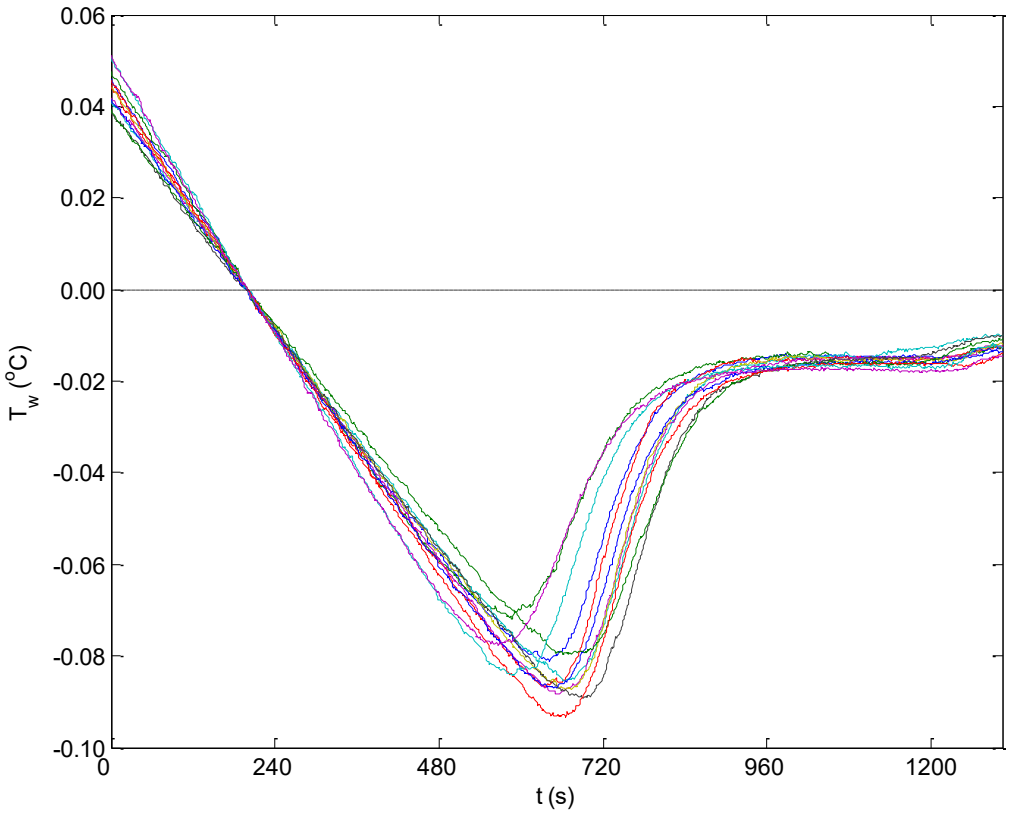

Figure 2-6: Superimposed supercooling curves showing the water temperature, T_w, as a function of time, t, for the 325 rpm experiments.

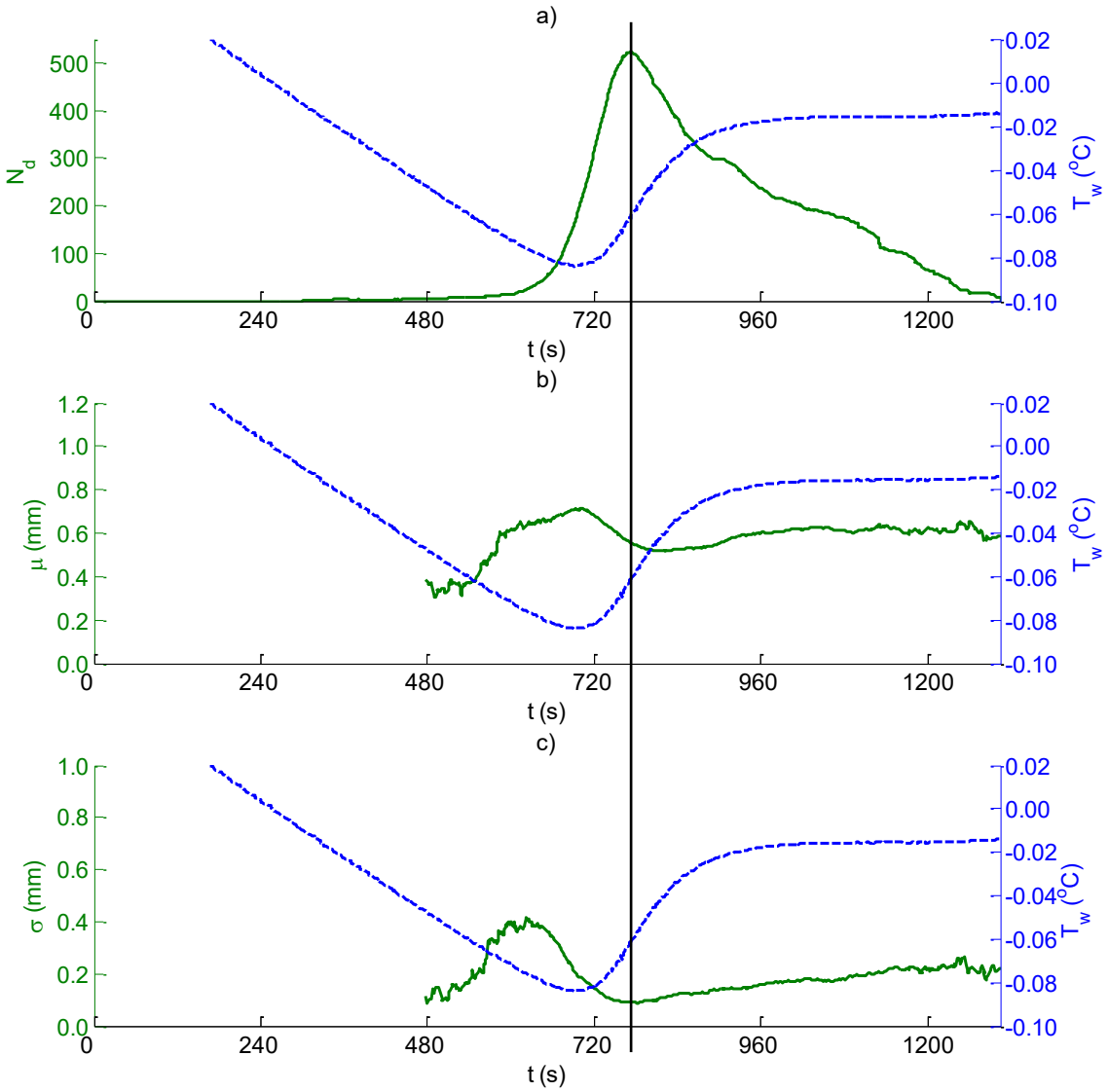

Figure 2-7: Time series of the 35 second moving average particle properties for the twelve 325 rpm experiments plotted along with the ensemble averaged supercooling curve, T_w (dashed line). a) N_d, the average number of particles observed in the 35 second window and summed over the 12 experiments, b) the mean particle diameter, μ, and c) the standard deviation, σ. The black vertical line indicates the time at which the maximum number of particles were observed.

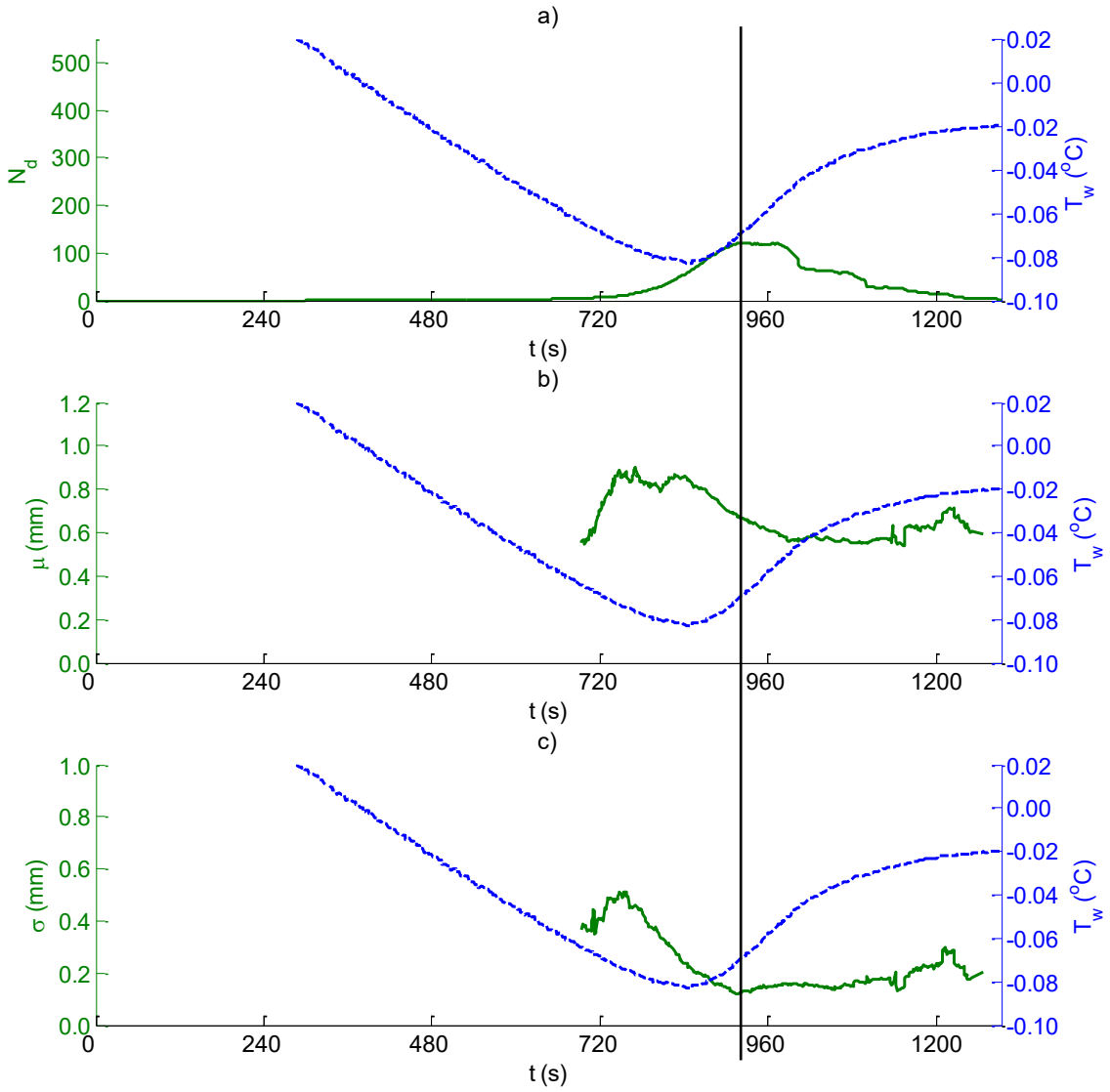

Figure 2-8: Time series of the 35 second moving average particle properties for the five 225 rpm experiments plotted along with the ensemble averaged supercooling curve, T_w (dashed line). a) N_d, the average number of particles observed in the 35 second window and summed over the 5 experiments, b) the mean particle diameter, μ, and c) the standard deviation, σ. The black vertical line indicates the time at which the maximum number of particles were observed.

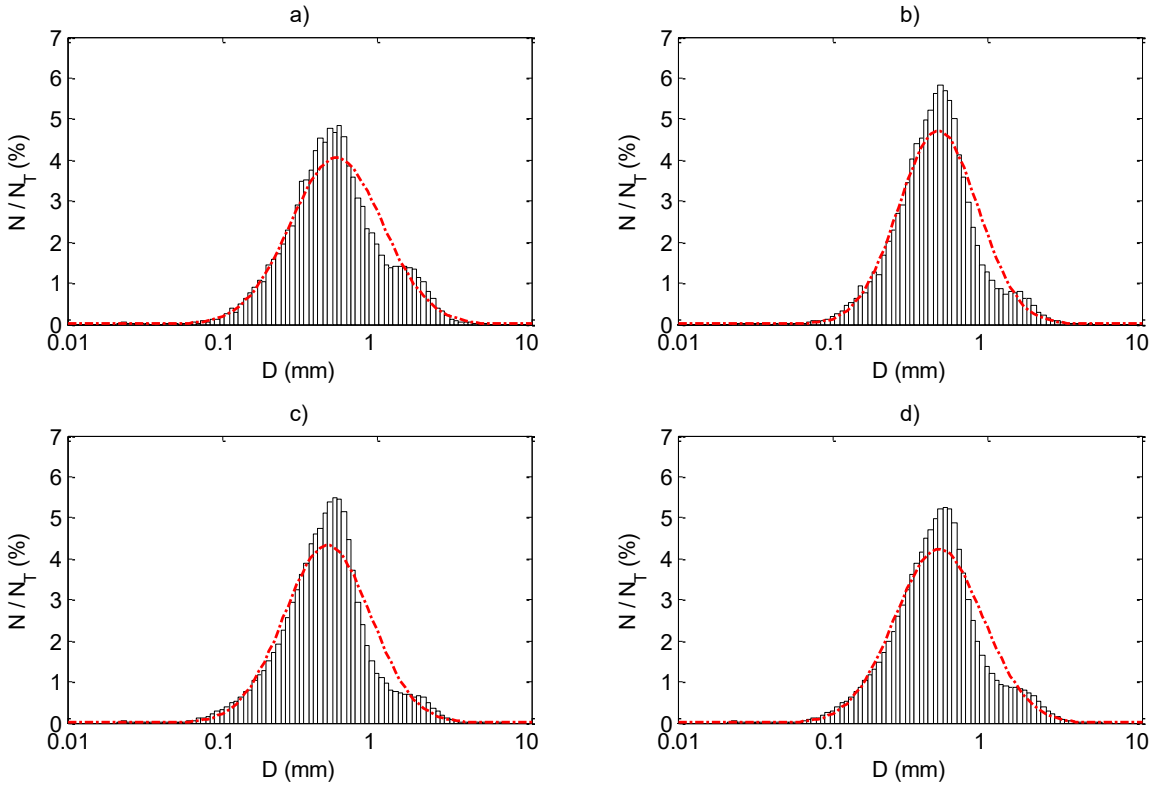

Figure 2-9: Ensemble size distributions at the 325 rpm propeller speed for a) the production range (i.e. from t_{10} to t_{90a}), b) the peak range (i.e. between t_{90a} and t_{90b}), c) the flocculation range (i.e. between t_{90b} and t_{30}) and d) the entire data series. N is the number of particles in each bin, N_T is the total number of particles, and D is the diameter. The dot-dash lines are the corresponding lognormal distributions.

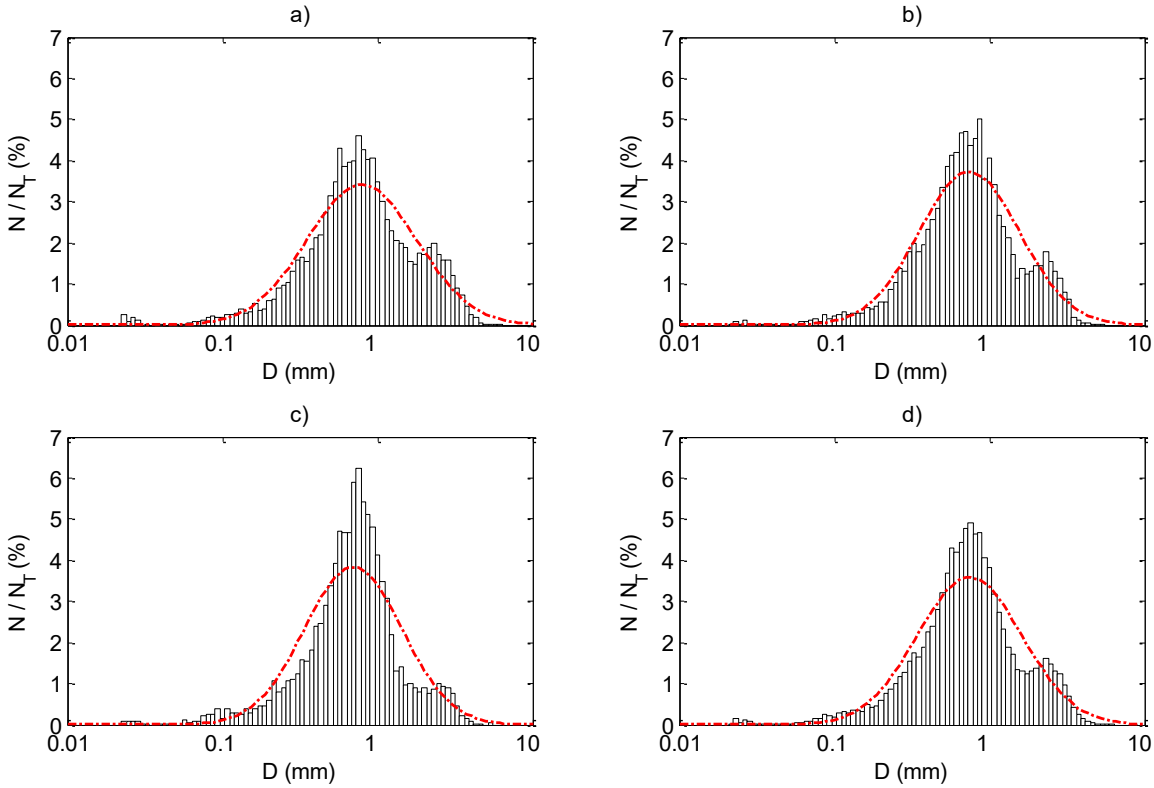

Figure 2-10: Ensemble size distributions at the 125 rpm propeller speed for a) the production range (i.e. from t_{10} to t_{90a}), b) the peak range (i.e. between t_{90a} and t_{90b}), c) the flocculation range (i.e. between t_{90b} and t_{30}) and d) the entire data series. N is the number of particles in each bin, N_T is the total number of particles, and D is the diameter. The dot-dash lines are the corresponding lognormal distributions.

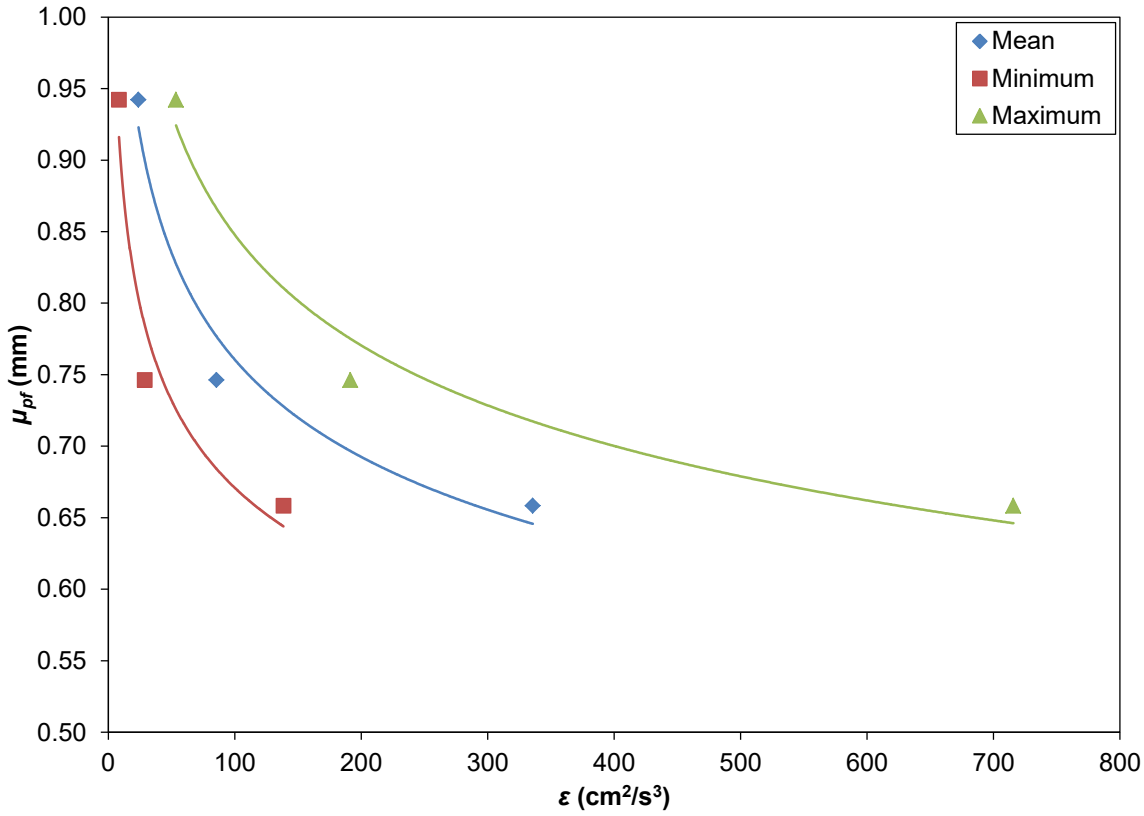

Figure 2-11: Mean pre-flocculation particle diameter, μ_{pf}, plotted as a function of the depth-averaged turbulent kinetic energy dissipation rate, ε.

TABLES

Table 2-1: Depth averaged values of the turbulent kinetic energy dissipation rate per unit mass, ε (cm^2/s^3) for each velocity component, propeller speed, and vertical profile location.

Velocity Component	125 RPM			225 RPM			325 RPM		
	Centre	Glass	Propeller	Centre	Glass	Propeller	Centre	Glass	Propeller
u	11.4	10.1	66.6	41.9	30.7	174.2	167.3	159.2	684.1
v	8.1	6.7	40.3	30.9	26.8	208.6	138.2	117.8	747.4
w	0.7	0.6	3.1	2.6	2.3	18.0	10.7	8.6	122.6
u-v average	9.7	8.4	53.5	36.4	28.8	191.4	152.7	138.5	715.7

Table 2-2: Size distribution properties for the particle diameter at all three propeller speeds in the three intervals.

Segment	125 RPM			225 RPM			325 RPM		
	Mean (mm)	Standard Deviation (mm)	Number of Particles	Mean (mm)	Standard Deviation (mm)	Number of Particles	Mean (mm)	Standard Deviation (mm)	Number of Particles
Production	1.03	0.81	9,638	0.80	0.64	6,878	0.67	0.52	21,346
Peak	0.92	0.69	8,304	0.64	0.47	10,795	0.56	0.38	27,551
Flocculation	0.85	0.63	6,146	0.58	0.40	7,480	0.57	0.43	79,457
Total	0.94	0.73	25,572	0.66	0.51	29,283	0.59	0.45	146,073

Table 2-3: Properties of the combined experimental data sets for each propeller speed, prior to particle flocculation.

Propeller Speed (rpm)	Tank Averaged ε (cm^2/s^3)	Number of Experiments	Number of Particles	Standard Deviation (mm)	Mean (mm)
125	23.9	10	25,572	0.73	0.94
225	85.5	5	4,143	0.71	0.75
325	335.6	12	19,374	0.54	0.66

ACKNOWLEDGEMENTS

This research was supported by the Natural Sciences and Engineering Research Council of Canada (NSERC), which is gratefully acknowledged. We thank Perry Fedun and Chris Krath for providing technical assistance, Christine Hereygers and Drs. David Sego and Derek Martin for facilitating access to the Cold Room Facility, and Dr. Ali Habibzadeh for assistance processing the ADV data.

REFERENCES

Brown, R.S., Hubert, W.A., Daly, S.F., 2011. A Primer on Winter, Ice, and Fish: What Fisheries Biologists Should Know about Winter Ice Processes and Stream-Dwelling Fish. Fisheries 36, 8–26. doi:10.1577/03632415.2011.10389052

Carstens, T., 1966. Experiments with supercooling and ice formation in flowing water. Geofys. Publ. 26, 1–18.

Clark, S., Doering, J., 2006. Laboratory Experiments on Frazil-Size Characteristics in a Counterrotating Flume. J. Hydraul. Eng. 132, 94–101. doi:10.1061/(ASCE)0733-9429(2006)132:1(94)

Clark, S., Doering, J., 2008. Experimental investigation of the effects of turbulence intensity on frazil ice characteristics. Can. J. Civ. Eng. 35, 67–79. doi:10.1139/L07-086

Clark, S.P., Doering, J.C., 2009. Frazil flocculation and secondary nucleation in a counter-rotating flume. Cold Reg. Sci. Technol. 55, 221–229. doi:10.1016/j.coldregions.2008.04.002

Daly, S.F., 1984. Frazil ice dynamics. Hanover, N. H.

Daly, S.F., 1994. Report on frazil ice. Cold Regions Research & Engineering Laboratory, Hanover, N. H.

Daly, S.F., 2013. Frazil Ice, in: Beltaos, S. (Ed.), River Ice Formation. Committee on River Ice Processes and the Environment, CGU-HS, Edmonton, Alberta, pp. 107–134.

Daly, S.F., Colbeck, S.C., 1986. Frazil ice measurements in CRREL's flume facility, in:

Proceedings of the IAHR Ice Symposium 1986. International Association for Hydraulic Research, Iowa City, Iowa, USA, pp. 427–438.

Doering, J.C., Morris, M.P., 2003. A digital image processing system to characterize frazil ice. Can. J. Civ. Eng. 30, 1.

Dubé, M., Turcotte, B., Morse, B., 2014. Inner structure of anchor ice and ice dams in steep channels. Cold Reg. Sci. Technol. 106-107, 194–206. doi:10.1016/j.coldregions.2014.06.013

Ettema, R., Karim, M.F., Kennedy, J.F., 1984. Laboratory experiments on frazil ice growth in supercooled water. Cold Reg. Sci. Technol. 10, 43–58. doi:10.1016/0165-232X(84)90032-6

Forest, T.W., 1986. Thermodynamic Stability of Frazil Ice Crystals, in: Proceedings of the Fifth International Offshore Mechanics and Arctic Engineering (OMAE) Symposium. The American Society of Mechanical Engineers, Tokyo, Japan, pp. 266–270.

Forest, T.W., Sharma, R., 1992. Growth Rates of Frazil Ice Discs, in: Proceedings of the 11th International Symposium on Ice. International Association for Hydraulic Research, Banff, Alberta, pp. 723–734.

Ghobrial, T.R., Loewen, M.R., Hicks, F., 2012. Laboratory calibration of upward looking sonars for measuring suspended frazil ice concentration. Cold Reg. Sci. Technol. 70, 19–31. doi:10.1016/j.coldregions.2011.08.010

Ghobrial, T.R., Loewen, M.R., Hicks, F.E., 2013. Characterizing suspended frazil ice in rivers using upward looking sonars. Cold Reg. Sci. Technol. 86, 113–126. doi:10.1016/j.coldregions.2012.10.002

Gosink, J.P., Osterkamp, T.E., 1983. Measurements and Analyses of Velocity Profiles and Frazil Ice-Crystal Rise Velocities during periods of Frazil-Ice Formation in Rivers. Ann. Glaciol. 79–84.

Hammar, L., Shen, H.T., 1995. Frazil Evolution in Channels. J. Hydraul. Res. 33, 291–306. doi:10.1080/00221689509498572

Islam, M.R., Zhu, D.Z., 2013. Kernel Density-Based Algorithm for Despiking ADV Data. J. Hydraul. Eng. 139, 785–793. doi:10.1061/(ASCE)HY.1943-7900-0000734

Jasek, M., Ghobrial, T., Loewen, M., Hicks, F., 2011. Comparison of CRISSP modeled and SWIPS measured ice concentrations on the Peace River, in: Proceedings of the 16th

Workshop on River Ice. CGU HS Committee on River Ice Processes and the Environment, Winnipeg, Manitoba, p. 25.

Kellerhals, R., Neill, C.R., Bray, D.I., 1972. Hydraulic and Geomorphic Characteristics of Rivers in Alberta. Alberta Cooperative Research Program in Highway and River Engineering, Edmonton, Alberta.

Kerr, D.J., Shen, H.T., Daly, S.F., 2002. Evolution and hydraulic resistance of anchor ice on gravel bed. Cold Reg. Sci. Technol. 35, 101–114. https://doi.org/10.1016/S0165-232X(02)00043-5

McFarlane, V.J., 2014. Laboratory Studies of Suspended Frazil Ice Particles. University of Alberta.

McLelland, S.J., Nicholas, A.P., 2000. A new method for evaluating errors in high-frequency ADV measurements. Hydrol. Process. 14, 351–366. doi:10.1002/(SICI)1099-1085(20000215)14:2<351::AID-HYP963>3.0.CO;2-K

Morse, B., Richard, M., 2009. A field study of suspended frazil ice particles. Cold Reg. Sci. Technol. 55, 86–102. doi:10.1016/j.coldregions.2008.03.004

Osterkamp, T.E., 1978. Frazil Ice Formation: A Review. J. Hydraul. Div. 104, 1239–1255.

Osterkamp, T.E., Gosink, J.P., 1983. Frazil ice formation and ice cover development in interior Alaska streams. Cold Reg. Sci. Technol. 8, 43–56.

Pope, S.B., 2000. Turbulent Flows. Cambridge University Press, Cambridge, U.K.

Pratt, W.K., 2007. Digital Image Processing, 4th Editio. ed. John Wiley & Sons, Hoboken, NJ.

Richard, M., Morse, B., 2008. Multiple frazil ice blockages at a water intake in the St. Lawrence River. Cold Reg. Sci. Technol. 53, 131–149. doi:10.1016/j.coldregions.2007.10.003

Richard, M., Morse, B., Daly, S.F., Emond, J., 2011. Quantifying suspended frazil ice using multi-frequency underwater acoustic devices. River Res. Appl. 27, 1106–1117. doi:10.1002/rra.1446

Romagnoli, M., García, C.M., Lopardo, R.A., 2012. Signal Postprocessing Technique and Uncertainty Analysis of ADV Turbulence Measurements on Free Hydraulic Jumps. J. Hydraul. Eng. 138, 353–357. doi:10.1061/(ASCE)HY.1943-7900.0000507

Stiansen, J.E., Sundby, S., 2001. Improved methods for generating and estimating turbulence in tanks suitable for fish larvae experiments. Sci. Mar. 65, 151–167. doi:10.3989/scimar.2001.65n2151

Stickler, M., Alfredsen, K.T., Linnansaari, T., Fjeldstad, H., 2010. The influence of dynamic ice formation on hydraulic heterogeneity in steep streams. River Res. Appl. 26, 1187–1197. doi:10.1002/rra.1331

Tennekes, H., Lumley, J.L., 1972. A first course in turbulence. MIT Press, Cambridge, Mass.

Tsang, G., Hanley, T.O., 1985. Frazil formation in water of different salinities and supercoolings. J. Glaciol. 31, 74–85.

Ye, S.Q., Doering, J., 2004. Simulation of the Supercooling Process and Frazil Evolution in Turbulent Flows. Can. J. Civ. Eng. 31, 915–926. doi:10.1139/L04-055

Ye, S.Q., Doering, J., Shen, H.T., 2004. A laboratory study of frazil evolution in a counter-rotating flume. Can. J. Civ. Eng. 31, 899–914.

3 MEASUREMENTS OF THE SIZE DISTRIBUTION OF FRAZIL ICE PARTICLES IN THREE ALBERTA RIVERS

3.1 INTRODUCTION

The size distribution of frazil ice particles in streams and rivers has been a subject of interest in river ice engineering for many years. Frazil ice formation in the turbulent flows of supercooled rivers can cause serious problems by obstructing water intakes for both water supply and hydroelectric facilities, and large frazil accumulations in the channel can lead to the formation of freeze-up ice jams and cause significant flooding (Daly, 2013). It is necessary to understand the physical properties of frazil ice particles to further the development of computer models to forecast river freeze-up and to mitigate the potential effects of a severe frazil ice event under various river conditions. However, the measurement of frazil ice particles in the field has proven to be a difficult undertaking.

Many previous studies, performed in laboratory environments, have investigated the size distribution of the disc-shaped frazil particles under various flow conditions (e.g. Clark and Doering, 2008, 2004; Daly and Colbeck, 1986; McFarlane et al., 2015). Daly and Colbeck (1986) found that a lognormal distribution fit the measured particle size distribution quite well, which has been confirmed by a number of subsequent laboratory investigations. Additionally, studies by Ettema et al. (1984), Ye et al. (2004), Clark and Doering (2008), and McFarlane et al. (2015) have demonstrated that variables, including turbulence intensity, affect the size distribution by altering the mean and standard deviation of the particle diameters, concentration of suspended particles, and the way in which the size distribution evolves throughout the supercooling process. Ettema et al. (1984) concluded that the production rate and concentration of frazil particles increased as a function of the maximum degree of supercooling and turbulence intensity, while the

particle size increased with increasing supercooling but decreased with increasing turbulence intensity. Ye et al. (2004), Clark and Doering (2008), and McFarlane et al. (2015) observed that the number of particles in suspension increased throughout the principal supercooling period (i.e. the time between initial supercooling and when the residual supercooling temperature was reached). Ye et al. (2004) also noted that the mean particle diameter grew during the principal supercooling period, before levelling off at a stable value, and that the final mean diameter decreased with increasing Reynolds number. Clark and Doering (2008) observed that the mean and standard deviation of the particle size distribution increased as the dissipation rate of turbulent kinetic energy increased up to a value of ~900 cm^2/s^3 and then began to decrease. The trend of increasing mean diameter during the principal supercooling phase, before levelling off at a stable value, was also evident in some of the data presented by Clark and Doering (2008). McFarlane et al. (2015) observed that the mean diameter increased steadily until the maximum degree of supercooling was achieved, at which point the mean diameter slowly decreased for the remainder of the supercooling event. It was hypothesised that the cause of the decrease in mean diameter was the rapid production of many new, small frazil particles combined with the fracture and/or flocculation of some of the larger particles in the flow. The dissipation rate of turbulent kinetic energy was also measured by McFarlane et al. (2015) and the mean particle diameter was found to decrease from 0.94 to 0.66 mm with increasing dissipation rates from 23.9 to 336 cm^2/s^3, contrary to the observations of Clark and Doering (2008), who observed an increase in mean particle diameter with increasing dissipation rates in this range.

These laboratory studies suggest that rivers with varying flow characteristics might produce frazil particles with significantly different size distributions. Measurements of frazil particles in a variety of rivers and at various stages of the supercooling process are

needed to verify this hypothesis. Underwater photographs of frazil ice particles in rivers have only been reported in a few cases (Dubé et al., 2014; Kempema and Ettema, 2016; Osterkamp and Gosink, 1983). Of these studies, Osterkamp and Gosink (1983) were the only ones to report any information about the frazil ice particle size distribution. They photographed frazil ice particles in the Chatanika River, Alaska and observed particles ranging in diameter from 0.1 to 1 mm, but did not provide a detailed description of their methodology. During the four hours that their camera was deployed they observed that the size distribution remained nearly constant while the suspended particle concentration varied significantly. However, the challenges of accurately measuring such small particles in the field have prevented any other direct, quantitative size distribution data from being collected.

Recently attempts to estimate frazil ice particle sizes in rivers have been made using upward-looking sonars. For example, mean particle diameters of 0.12 to 0.36 mm have been estimated in the St. Lawrence River (Richard et al., 2011), 0.26 to 0.41 mm in the North Saskatchewan River (Ghobrial et al., 2013b), and median diameters between 0.6 and 1.6 mm in the Peace River (Marko et al., 2015). However, these instruments do not make direct measurements of the individual ice particles, but rather make use of acoustic scattering models to convert the acoustic signals into estimates of the suspended particle size and concentration. This method requires that many assumptions be made regarding the properties (e.g. size, shape) of frazil particles in the field, and direct field measurements are required to validate these assumptions (Ghobrial et al., 2013b).

In order to study how frazil particles vary between different rivers and throughout the supercooling process in the field in more detail, two specially designed field camera systems were deployed at various stages of the supercooling process on three Alberta rivers

during the winter of 2014-15. Measurements were made during both the principal and residual supercooling phases, and the captured images were processed to accurately determine the size distribution of the suspended frazil ice particles.

3.2 SITE DESCRIPTION

The three Alberta rivers investigated in this study were the North Saskatchewan River at Edmonton, the Peace River near Fairview, and the Kananaskis River. These three regulated rivers were selected due to their differences in scale and flow conditions. A summary of the river characteristics is provided in Table 3-1 and the location of each study site is shown in Figure 3-1.

The freeze-up process at each of the study sites is quite different due to the presence of dams upstream. On the North Saskatchewan River the nearest dam is the Brazeau Dam located on one of its tributaries, the Brazeau River, approximately 230 km upstream of the Quesnell Bridge site. Further upstream on the North Saskatchewan River itself is the Bighorn Dam, ~420 km upstream of the Quesnell Bridge site. The hydropeaking effects of these dams combine to cause a daily water level fluctuation of ~0.3 to ~0.4 m on the North Saskatchewan River at Edmonton. Freeze-up unfolds in a fairly predictable manner each year on the North Saskatchewan River despite the hydropeaking operation of these dams. Frazil ice typically first occurs in mid-November followed by the formation of an intact ice cover in late November or early December.

On the Peace River, both the W.A.C. Bennett Dam (~309 km upstream) and the Peace Canyon Dam (~288 km upstream) operated by BC Hydro are upstream of the water intake for the town of Fairview. The release of warm water from the two dams throughout the winter causes freeze-up to progress slowly in the upstream direction. As the zero-degree

isotherm moves upstream past a site, supercooling and frazil ice formation begin. This frazil ice formation leads to the formation of frazil pans, which eventually become part of the ice front downstream, and anchor ice, which may also contribute to the ice front upon release from the riverbed. The region that lies between the zero-degree isotherm and the ice front remains supercooled and presents an opportunity to study suspended frazil ice particles. The ice front typically does not arrive at Fairview water intake until mid-January and therefore frazil ice formation can be studied at this location up until that time.

The Kananaskis River is also regulated, but due to maintenance work on the dam at the time of this study, regular hydropeaking operations were not occurring. Instead, the spillway was operating and the flow varied between ~11 and 15 m^3/s during the course of the deployments (Government of Alberta, 2017). At these discharges, high velocities prevent a stable ice cover from forming in much of the 47 km reach from the Pocaterra Dam powerhouse to Barrier Lake. Without an ice cover to insulate the water in the channel, frazil-generating supercooling events occur regularly on the Kananaskis River as long as the air temperature is cold enough. This presents many opportunities to study frazil ice formation.

3.3 Experimental Equipment and Methods

3.3.1 FrazilCam Development

To capture high-resolution photographs of suspended frazil particles in the field, two imaging systems, named 'FrazilCams', were designed, built, and tested (Figure 3-2). The FrazilCams were designed to imitate the laboratory setup developed by McFarlane et al. (2014). Each system consisted of a 36-megapixel Nikon D800 digital single-lens reflex (DSLR) camera equipped with a Micro-Nikkor 60 mm f/2.8D lens and enclosed in an underwater housing. Two Cavision polarising filters, each 7 cm × 7 cm square, were

rotated 90° with respect to one another and mounted 2.2 cm apart to allow the passage of frazil particles in between. A Nikon SB-910 Speedlight, contained in a Subal SN-910 underwater housing, was directed through the polarising filters and into the lens of the camera, and a 5 mm thick piece of white acrylic was mounted between the flash and the polarisers to diffuse the light. In order to prevent frazil ice from passing between the camera lens and the polarising filters and thereby obstructing the images, a PVC cowling was installed that enclosed this area but still allowed it to fill with water. A brass fitting in the top of the PVC enclosure also allowed for the injection of hot water to melt any ice that may have become trapped. The only difference between the two FrazilCam systems was the make of the housing used to enclose the camera: an Aquatica AD800 underwater housing was used for one system and an Ikelite D800 housing was used for the other. All of the equipment was mounted on a MiniTec aluminum bar which was surrounded by a PVC frame. The frames were designed to allow the FrazilCams to sit near the riverbed with a low centre of gravity to reduce the risk of the cameras tipping over during deployment, but were made tall enough to function as a roll-cage if the unit were to tip over. Each frame also had the capacity to hold up to eight, ten-pound weights to help anchor the FrazilCams to the river bed.

The appropriate camera settings, including ISO, aperture, and focus were determined for each FrazilCam by taking test photographs of a clear plastic ruler while the FrazilCam was submerged in a tank of cold tap water. This also provided scale images to be used when processing the field data. The camera was positioned at an appropriate distance from the polarising lenses so as to maximise the field of view within the polarising filters, which ranged from 4.1 × 6.2 cm to 4.5 × 6.7 cm. This resulted in pixel sizes of 8.4 μm and 9.1 μm for the two FrazilCams, with an image resolution of 4912 × 7360 pixels. To reduce image blurring and effectively ‘freeze’ the image, the Nikon Speedlight was operated at its lowest

power setting which produced a flash duration of approximately 1/38,500 s, which was a sufficiently short exposure time. The duration of the flash pulse was verified through repeated measurements with a Thorlabs DET02AFC silicon biased photodetector.

3.3.2 INSTRUMENTATION

In addition to photographing the frazil particles it was also of interest to measure the water depth, velocity, and temperature at the deployment locations. During all deployments, the water temperature was measured using an RBR SoloT (accuracy ±0.002°C) temperature recorder that was attached to the FrazilCam frame and sampling at a frequency of 1 Hz. In the North Saskatchewan and Kananaskis Rivers the depth averaged water velocity was measured using a SonTek Flow Tracker handheld acoustic Doppler velocimeter (ADV) sampling at 1 Hz for 240 s, and the water depth was measured using the depth markings on the wading rod. In the Peace River the water depth and velocity were visually estimated as the Flow Tracker was not available at the time the FrazilCam was deployed. A Garmin handheld GPS was used to record the coordinates of each site.

On the Kananaskis River additional RBR SoloT temperature recorders were deployed, continuously sampling at a frequency of 1 Hz from February 27 to March 2, 2015 at three different locations along the river: the two FrazilCam deployment locations, as well as at the Fortress Bridge crossing further upstream, approximately 13 km downstream of the Pocaterra Dam. This was done to monitor the water temperature and to allow the evolution of a supercooling event along the river to be observed. The time at which the FrazilCam images were captured could then be compared with the continuous water temperature data to determine at which stage in the supercooling event the frazil particles were photographed.

3.4 Data Processing

All of the captured image data were processed in two stages. First, the images were analysed using a MATLAB algorithm that was developed to identify and determine the diameter of individual disc-shaped particles, described in detail by McFarlane et al. (2014). This algorithm has been manually verified to correctly identify 93% of disc-shaped frazil particles with a diameter of 3 pixels or larger (McFarlane et al., 2014).

Second, the processed data were adjusted for the presence of small, suspended sediment particles by subtracting a randomly generated lognormal distribution with the same mean and standard deviation as the observed sediment. One of the challenges of making field measurements of frazil ice size distributions using the FrazilCam is that suspended sediment particles may also appear in the images. As a result the raw size distributions computed from the captured images may be a combination of frazil ice and sediment particle sizes. Although sediment particles are less transparent than ice particles, it is still possible for them to refract the incident light and appear in the cross-polarised images if the particle is thin enough. This follows from the fact that analysing thin-sections of minerals (~30 μm thick) under cross-polarised light for identification purposes is a common technique in mineralogy (Verma, 2010). Therefore, in order to obtain accurate frazil ice particle size distributions, the raw size distributions need to be adjusted; that is, the contribution of the sediment particles to the final frazil ice size distribution should be minimised. This became apparent when a size distribution of particles with a peak at ~0.1 mm was observed even when water temperatures were above zero degrees and no ice was present. The possibility was considered that this size distribution was caused by background noise in the images rather than sediment, but this does not appear to be the case as no such distribution was observed when images were captured of filtered tap water in the laboratory. Fortunately, ice-free images (i.e. prior to the onset of supercooling) were

collected under similar flow conditions at all of the sites except for Emily Murphy Park on the North Saskatchewan River and Fairview on the Peace River. These ice-free images were processed to determine the size distribution of the sediment particles in the flow that were thin enough to be visible when viewed under cross-polarisation. Figure 3-3 shows the size distribution of the sediment particles at the Village Bridge site, and upon comparison to the size distribution calculated for the same site when ice was present, shown in Figure 3-4, it can be seen that the sediment particle size distribution peaks at approximately the same diameter as the secondary peak in Figure 3-4. Based on these data, it was determined that the raw size distributions would need to be adjusted to eliminate the effect of sediment particles if the size distribution appeared bimodal with one of the peaks centred at a diameter of approximately 0.1 mm.

The simplest solution would be to subtract the measured sediment size distribution from the raw size distribution. However, because the number of sediment particles per image was typically larger than the total number of ice and sediment particles in the raw images this method was not applicable. There are a number of plausible explanations for this, including: variations in suspended sediment concentrations between the times when the ice-free images and raw images were gathered due to changing flow conditions, different FrazilCam deployment locations, or the flocculation of sediment particles together with ice particles. During the deployments in the Kananaskis River the water was noticeably shallower at the time that the sediment data were obtained, and the flow rate reported by Alberta Environment and Parks had decreased to approximately 11 m^3/s from 14 m^3/s the day before (Government of Alberta, 2017). As a result, the cameras had to be deployed in slightly different locations where the flow was deep enough (~15 m downstream of the original deployment site at Opal and ~10 m upstream of the original deployment site at the Village Bridge). However, for the North Saskatchewan River deployments at the

Quesnell Bridge and Government House Park sites the flow rate remained approximately constant. Perhaps the most likely explanation for the smaller number of total particles is that there was a significant reduction in the suspended sediment concentration once frazil ice began to form. The scavenging or mechanical trapping of suspended sediment by frazil flocs has been observed previously in several fresh and saltwater laboratory flume experiments. Reimnitz et al. (1993) observed that freshwater frazil flocs collected more sediment than saltwater flocs, and measurements by Kempema et al. (1986) showed that frazil ice formation reduced the suspended sediment concentration in freshwater by as much as 50% relative to the concentration measured prior to frazil formation.

Therefore, since direct subtraction of the sediment particles was not possible, an alternative method was developed to subtract a scaled representative suspended sediment size distribution from the corresponding raw size distribution. In the case of the Village Bridge site, for example, the suspended sediment particles were found to have a mean diameter of 0.11 mm with a standard deviation of 0.05 mm. To subtract an appropriate number of particles from the measured raw size distribution, a lognormal size distribution with the same mean and standard deviation as the measured sediment particle size distribution was randomly generated using a MATLAB algorithm and plotted on top of the raw size distribution, as shown in Figure 3-5. The number of particles in this randomly generated distribution was then varied until the random distribution was visually determined to overlap the raw size distribution as closely as possible. The randomly generated distribution was then subtracted from the raw size distribution to obtain an estimate of the frazil ice particle size distribution. In order to obtain a better estimate of the resulting size distribution the process of randomly generating and subtracting a representative sediment size distribution was repeated 1,000 times (using the same number of particles each time) and the resulting frazil ice size distributions were averaged.

This resulted in the frazil ice particle size distribution for which the mean and standard deviation of the frazil diameter could be calculated. The frazil ice particle size distribution for the Village Bridge site is shown in Figure 3-6, which has a mean 0.34 mm.

It was also of interest to calculate the percentage of particles that were disc-shaped in order to determine if this is in fact the predominate shape for frazil ice particles in rivers, as has been observed in the lab (McFarlane et al., 2015). This percentage was calculated by using the number of particles that remained before and after the fitted ellipse criteria was applied in the MATLAB algorithm to filter out the non-disc particles. However, since the size distributions were not adjusted to minimise the influence of sediment particles until after the fitted ellipse criteria was applied, the raw size distributions were used to calculate the disc-shaped particle percentage. To minimise the influence of sediment in the raw size distributions, all particles smaller than the mean plus two standard deviations of the sediment particle size distribution used to adjust that site were ignored when calculating this percentage. The mean plus two standard deviations was chosen as an appropriate cut-off because approximately 98% of the data should be contained below this point in a lognormally distributed data set. It should be noted that by removing smaller particles from the size distribution prior to calculating the disc-shaped percentage the results may become biased towards a lower disc-shaped percentage. This is because many of the large non-disc 'particles' may have in fact been accumulations of many particles in the form of flocs or small pieces of released anchor ice. Therefore, since the algorithm identifies flocs as a single non-disc-shaped particle, the result is a larger number of non-disc particles being recorded by the algorithm. This, together with the reduced number of small, disc-shaped particles due to eliminating all particles smaller than a certain diameter, may cause the percentage of disc-shaped particles to be underestimated. These results are presented later, in section 3.6.1.

3.5 FIELD DEPLOYMENTS

Between November 2014 and March 2015, the two FrazilCam systems were deployed in the North Saskatchewan, Peace, and Kananaskis Rivers. These rivers vary significantly from each other in terms of size, depth, velocity, and bed material, and, as a result, the deployment strategy varied somewhat between sites. However, in order to safely wade into the river and deploy the FrazilCam systems, locations were sought with depth-averaged water velocities between approximately 0.25 and 0.75 m/s, and depths in the range of 0.5 to 1.0 m. The mean air temperature, minimum water temperature, water depth, and depth-averaged velocity during the FrazilCam deployments are given in Table 3-2. Images of the FrazilCam during two of the deployments are shown in Figure 3-7.

Before each deployment, the FrazilCam was set up to ensure that clear, focused images were captured over the desired time period. This involved cleaning the polarising filters using glass cleaner and a microfiber cloth, verifying the correct spacing was set between the camera and the polarisers, and focusing the camera lens. Fresh batteries were installed in both the camera and the flash to ensure there was enough battery life to last the entire deployment. All of the submerged cable connections and the seals in the waterproof housings were lubricated with silicone O-ring lubricant to create a tight seal and to avoid having any water leak into the housings that would damage the equipment. The camera was then programmed to acquire images at a specified frequency over the desired time period. This varied depending on the water temperature at the beginning of the deployment. If the water temperature was above zero degrees indicating that a supercooling event had not yet started, the camera was programmed to capture images at a lower frequency. This was done to increase the sampling duration so that images would be captured throughout the supercooling event. However, if supercooling was already underway at the beginning of the deployment, the camera was programmed to capture

images at a higher frequency to record the maximum amount of data as quickly as possible before the event ended. The camera settings and the number of images captured during each deployment are given in Table 3-3.

Once the FrazilCam was set up as described above, the system was ready to be deployed. The procedure varied slightly from one deployment to the next, but through some trial and error the following final procedure was developed. First, while the FrazilCam was still on the river bank, hot fresh water was injected into the PVC enclosure around the camera lens and polarising filters. This was done to prevent ice crystals from forming on the near face of the polarising lens or from becoming trapped inside the PVC enclosure (i.e. inside the cowling), which would obstruct the images. The FrazilCam was then carefully lowered into the water near the bank and more hot water was injected into the PVC enclosure to melt any ice crystals that may have flowed into the enclosure. Next, each face of the submerged polarising lenses was carefully rinsed with hot saline water to melt any ice that may have formed on the polarisers as they entered the water. The FrazilCam was then carried carefully to the deployment location, placed perpendicular to the flow to allow the particles to pass between the polarising filters, and left in place until image capture had concluded.

3.5.1 North Saskatchewan River

The first deployments took place in the North Saskatchewan River at Edmonton from November 9 to 11, 2014. As this was one of the first deployment attempts, the FrazilCam was not yet in its final configuration and was mounted with a higher centre of gravity and weighed down with cinder blocks. One FrazilCam was deployed near the right bank beneath the Quesnell Bridge and the second was deployed ~5.9 km downstream near the left bank at Government House Park (see Figure 3-1b). These two locations were chosen due to ease of access and because they offered suitable flow depths and velocities. The

cameras were deployed on the afternoon of November 9 and programmed to begin capturing images at 5:00 AM on November 10 because supercooling was expected to occur between 5:00 and 7:30 that morning. Unfortunately, supercooling temperatures were not observed in that time interval (although the images captured would prove useful later on for suspended sediment analysis), so the camera memory cards and batteries were replaced with unused ones and the cameras were redeployed. The cameras at the Quesnell Bridge and Government House Park were programmed to begin capturing images at 9:45 and 10:30 AM, respectively, on November 10, with both cameras capturing a burst of nine images at a frequency of 1 Hz every 90 seconds. Supercooling was finally observed at 14:34 at the Government House Park site and at 15:08 at the Quesnell Bridge site on November 10, and there was significant border ice growth and a high concentration of frazil pans in the stream when the cameras were collected in the morning of November 11. The FrazilCam deployed underneath the Quesnell Bridge had been knocked on its side by the time it was recovered the next morning and this was likely caused by a large frazil pan colliding with it at some point in the night. Additionally, a large frazil floc had become trapped between the polarisers and obstructed many of the images. The second FrazilCam, deployed at Government House Park, became completely surrounded by frazil slush that had accumulated underneath a large growth of border ice and accumulation of frazil pans. This resulted in the PVC enclosure around the camera lens completely filling with slush, obscuring many of the images. To avoid these issues in future deployments, the FrazilCams were repositioned lower in the PVC frames to move the centre of gravity closer to the bed to prevent tipping, and the PVC enclosure around the lens was modified to fit more tightly. This still allowed water to enter but prevented ice crystals from entering and obstructing the view.

Despite the issues encountered on November 10, some very useful data were obtained. The enclosure around the lens on the camera at Government House Park did not become filled with slush until 16:03, meaning that images had been captured throughout much of the principal supercooling period, which began at 14:34 and ended at 16:22, when the residual supercooling temperature was reached at that site. Similarly, at the Quesnell Bridge site, the frazil floc did not become trapped between the polarisers until 16:40, and over half of the field of view was still unobstructed until about 17:00. At this site, the principal supercooling period lasted from 15:08 to 17:35. As a result, images of frazil particles were captured during a significant portion of the principal supercooling period at both sites in the North Saskatchewan River.

Following these deployments, a warming trend was observed in the Edmonton area and river temperatures climbed above 0°C. Conditions were suitable for another deployment attempt on November 27, 2014 at 8:00 in the morning after the air temperature had once again reached lows of –10°C the previous two nights, and fell to –11°C in the morning. One FrazilCam was deployed at the Emily Murphy Park site and programmed to capture 8,991 images at a frequency of 1 Hz. The water temperature, depth, and velocity were measured to be –0.011°C, 0.72 m, and 0.52 m/s, respectively during the deployment. It was also snowing quite heavily throughout the entire deployment on November 27, meaning there were new seed particles constantly being introduced into the flow to initiate frazil formation. This resulted in the accumulation of anchor ice on a significant fraction of the river bed near the deployment site and a relatively high concentration of slushy frazil pans formed from frazil flocs, snow slush, and released anchor ice. These slushy pans periodically became trapped on the frame, camera housing, and between the polarisers, and were manually removed to prevent slush from filling the field of view or obstructing the flash. A typical raw image from this deployment is presented in Figure 3-8a and it can

be seen that the particles were predominantly disc-shaped. Slushy frazil ice pans and released anchor ice pans would occasionally collide with the FrazilCam frame producing images like the one displayed in Figure 3-8b. This indicates that the frazil ice particles contained in these pans evolve into complex shapes.

3.5.2 PEACE RIVER

The Peace River was the second river investigated, with one FrazilCam being deployed on December 19, 2014. A similar deployment strategy as in the North Saskatchewan River was followed, with the FrazilCam being placed on the bed near the water intake at Fairview, Alberta at 16:38 (see Figure 3-1c). The air temperature was −9°C throughout the deployment, the water temperature was −0.014°C, and the water depth and velocity were estimated visually to be ~0.75 m and ~0.5 m/s, respectively. It was not snowing during the deployment so the suspended ice concentration was not as high as in the North Saskatchewan. However, a surface ice concentration of ~35 % was observed and anchor ice was blanketing a significant portion of the bed, indicating active frazil production. A photo of the FrazilCam deployed in the Peace River is shown in Figure 3-7a.

The procedure for rinsing the polarisers with hot, saline water had not yet been developed at the time of the Peace River deployment. Additionally, the hot water used for rinsing had been in the thermos for ~9 hours to that point, and was no longer hot but simply warm. As a result, while lowering the FrazilCam into the river, some of the water inside the PVC enclosure leaked onto one of the polarising lenses where it promptly froze, forming crystals that obscured ~50 % of each image. This did not pose a serious problem when processing the images as the region blocked by these crystals was simply blacked out. An example image from this deployment is shown in Figure 3-9.

3.5.3 KANANASKIS RIVER

Both FrazilCams were deployed multiple times over the course of three days, from February 28 to March 2, 2015, at two different locations in the Kananaskis River. The two sites at which the FrazilCams were deployed were the Opal Day Use area in the Spray Valley Provincial Park, and the Kananaskis Village Bridge in the Evan-Thomas Provincial Recreation Area (see Figure 3-1d). These two sites are approximately 21 and 36 km downstream of the Pocaterra Dam, respectively.

The first deployment for both FrazilCams occurred at the Village Bridge site on the morning of February 28, 2015. The Aquatica unit was deployed near the left bank of the river ~10 m downstream of the bridge, in a water depth of 0.50 m and a water velocity of 0.61 m/s. The Ikelite unit was positioned ~10 m downstream of the bridge near the right bank where the depth was 0.39 m and the mean flow velocity was 0.66 m/s. Both cameras were programmed to capture 8,991 images at a frequency of 1 Hz. However, the FrazilCams were positioned in direct sunlight during this deployment and the camera shutter speed was set at 1/100 s. This meant that, even though the flash pulse duration was only 1/38,500 s, the direct sunlight was bright enough that the frazil ice particles in each image were partially exposed for the full 1/100 s while the shutter was open, resulting in blurred images. This problem was eliminated by using a faster shutter speed of 1/320 s and ensuring that the FrazilCams were positioned in the shade in future deployments.

The second Kananaskis River deployment occurred the following day, on the morning of March 1, 2015. For this deployment the two FrazilCams were located at different sites and both cameras were programmed to take 9 image bursts at a frequency of 1 Hz every 18 seconds. The Aquatica unit was deployed at the Village Bridge site, this time positioned ~60 m upstream of the bridge near the left bank. This location had a water depth of 0.63

m, a depth-averaged velocity of 0.63 m/s, and nearby trees to provide shade for the unit. A photo of the camera deployed in this location is shown in Figure 3-7b. This camera was programmed to begin capturing photos at 7:20 AM, and recorded a total of 5,845 images over the course of 3 hours and 15 minutes. The Ikelite unit was deployed at the Opal site, positioned near the right bank at the downstream end of a meander. This location had a depth of 0.6 m, a velocity of ~0.27 m/s, and nearby trees to provide shade. This camera was programmed to begin capturing photos at 8:05 AM and a total of 7,176 images were captured over 3 hours and 45 minutes. A sample FrazilCam image is shown in Figure 3-10.

For the third deployment the two FrazilCams were deployed at the same locations as during the second deployment, but this time they were deployed on the evening of March 1 and programmed to begin capturing photos in the early morning of March 2, 2015. The purpose of this change in procedure was to attempt to capture images throughout the entire duration of a supercooling event, rather than only at the residual temperature as was the case in the previous two deployments. However, the air temperature did not drop as low as was forecast for that night (the low temperature was –12°C during the deployments while the forecast was for –16°C) and supercooling was not observed at either site. Despite the disappointment of not capturing any images with ice particles in the early stages of a supercooling event, this turned out to be a fortunate occurrence as small amounts of sediment suspended in the flow were observed instead. These ice-free images were used to estimate the size distributions of the sediment particles visible in the frazil ice images.

3.6 RESULTS

3.6.1 RAW SIZE DISTRIBUTIONS

The raw size distributions containing ice and sediment particles from each site are shown in Figure 3-11, arranged in chronological order. Figure 3-11f shows the raw size distribution from the Opal site in the Kananaskis River. At this site, the influence of suspended sediment was very clear as the resulting size distribution was bimodal with a large peak at a diameter of ~0.12 mm and a smaller peak at ~0.6 mm. Similar features were observed in the size distributions from the Village Bridge site (Figure 3-11e), the Government House Park and Quesnell Bridge sites in the North Saskatchewan River (Figure 3-11a and b), and the Fairview site in the Peace River (Figure 3-11d). At the Emily Murphy Park site, as shown in Figure 3-11c, the raw data were well described by a lognormal distribution (mean = 0.32 mm, standard deviation = 0.26 mm), which suggests that suspended sediment was not a major factor during this deployment.

The properties of the raw size distributions for all sites are provided in Table 3-4. The fraction of particles observed to be disc-shaped varied from 61% to 87%, indicating that the majority of frazil ice particles observed in the field were disc-shaped. These results are consistent with the laboratory measurements of McFarlane et al. (2015) which found that 75% of the frazil ice particles were disc-shaped. This indicates that frazil ice particles in the field have the same preference for disc-shaped growth as those observed in laboratory. However, the mean particle size ranged from 0.16 to 0.48 mm, which was quite small relative to laboratory experiments, indicating that the suspended sediment particles had a significant impact on the size distribution data.

3.6.2 Estimating Frazil Ice Size Distributions

A comparison of the sediment and raw size distributions at the Government House Park, Quesnell Bridge, Village Bridge, and Opal sites is shown in Figure 3-12. At each of these sites it is apparent that the sediment size distribution lines up almost perfectly with one of the peaks in the bimodal raw size distributions. Note that all of the sediment size distributions were well described by a lognormal distribution, which is consistent with measurements made in many previous studies (e.g. Kondolf and Adhikari, 2000; Mazumder et al., 2005). Overall, the sediment size distributions had mean diameters that ranged from 0.11 to 0.13 mm and standard deviations that ranged from 0.050 to 0.10 mm. The properties of the sediment size distributions measured at each site are listed in Table 3-5. Sediment properties are not reported for the Emily Murphy Park and Fairview sites because ice was present for the entire duration of those deployments and, therefore, no sediment size distributions could be computed.

As described above, the sediment size distributions were used to compute the frazil ice particle size distributions from the raw size distributions at the four sites where ice-free images were collected. However, the raw size distribution computed for the Emily Murphy Park site and plotted in Figure 3-11c did not display any obvious signs of being affected by suspended sediment and therefore it did not need to be adjusted. This is likely due to the fact that it was snowing during this deployment, providing an abundance of seed particles for nucleation of frazil ice crystals. This resulted in a much higher number concentration of particles in the images (i.e. 102 particles per image) than there were in other deployments, the next highest being 31 particles per image at Opal. This is much larger than the number concentration of sediment particles observed at any site. At Government House Park, which was only ~1.2 km upstream of the Emily Murphy Park site, only 6 sediment particles per image were observed. Therefore, the influence of the sediment

particles on this distribution appears to be negligible because the sediment particles were vastly outnumbered by the ice particles.

The influence of sediment particles was not negligible at the Fairview site on the Peace River and a large peak was visible in the raw distribution at a diameter of ~0.1 mm with a secondary peak at ~0.4 mm (Figure 3-11d). However, there were no ice-free images captured at this site and therefore it was not possible to adjust for the impact of sediment on the raw size distribution. Therefore, the data from the Fairview site could not be used to draw any conclusions about the size distribution of frazil ice particles.

The frazil ice size distributions for the other five sites are plotted in Figure 3-13 and their properties are listed in Table 3-6. After adjusting for the influence of sediment particles the mean particle size increased at each site. A theoretical lognormal distribution is an accurate fit to the size distribution obtained at the Emily Murphy Park site (Figure 3-13c), and a good fit to the size distributions from the Quesnell Bridge and Village Bridge sites (Figure 3-13b and d, respectively). However, at the Government House Park (Figure 3-13a) and Opal sites (Figure 3-13e) there was a peak in the size distribution at a diameter of ~0.1 mm in addition to a peak at larger diameters of 0.6 – 0.8 mm. The peaks at small diameters are likely artefacts of the adjustment process caused by a poor signal to noise ratio (i.e. number of ice particles / number of sediment particles << 1) at these two sites. Despite these artefacts in the frazil ice size distributions, the theoretical lognormal distribution still appears to offer a reasonable fit to the data. The mean particle diameter of the frazil ice size distributions ranged from 0.32 to 1.20 mm with a standard deviation ranging from 0.26 to 0.88 mm.

3.7 DISCUSSION

The data presented in Table 3-6 and Figure 3-13 are the first quantitative measurements of frazil ice size distributions made in rivers and it is useful to compare these to previous measurements. A complete summary of the previous field and laboratory particle size measurements found through an extensive review of the literature is provided in Table 3-7. The data in Table 3-7 show that frazil ice particle sizes measured optically or visually in the field and laboratory are in general agreement. The field measurements range from 0.1 to 6 mm and the laboratory measurements from 0.022 to 5.5 mm. However, the size ranges measured acoustically in the field were slightly smaller, ranging from 0.26 to 3 mm. In this field study the mean frazil particle size varied from 0.32 to 1.2 mm. These measurements are consistent with data summarized in Table 3-7 in that they are within the ranges observed previously in both the laboratory and field, and cover a similar range to the acoustic measurements.

It is also useful to make a more detailed comparison to previous direct measurements that were made with comparable image quality. For example, Clark and Doering (2008) observed mean particle diameters ranging from 0.79 to 1.58 mm measured throughout complete supercooling events produced under varying turbulence intensities in a counter-rotating flume. Similarly, McFarlane et al. (2015) measured mean particle sizes ranging from 0.59 to 0.94 mm during complete supercooling events, while generating turbulence of varying intensity in a stirred tank using three different propeller speeds. The smallest measured mean particle diameters that can be found in the literature are those reported by Daly and Colbeck (1986), who found mean diameters ranging from 0.13 to 0.25 mm for the frazil particles produced in their recirculating flume. The flume used by Daly and Colbeck (1986) was 36.6 m long and this limited the time the frazil particles had to nucleate and grow to the transit time in the flume, which varied from approximately one

to four minutes. As a result, the largest diameter measured was only ~0.5 mm for these relatively young frazil ice particles, which is much smaller than the maximum diameter of ~5 mm measured in other laboratory studies (e.g. McFarlane et al., 2015). Therefore, Daly and Colbeck's (1986) measurements may be a much better indication of the mean frazil particle size that can be expected when conditions are favourable for the dominance of young particles.

At the Quesnell Bridge and Government House Park sites on the North Saskatchewan River and at the Opal site on the Kananaskis River the mean ranged from 0.61 mm to 1.2 mm, which overlaps with the more recent laboratory data which ranged from 0.59 mm to 1.58 mm (e.g. Clark and Doering, 2008; McFarlane et al., 2015). Smaller mean diameters were measured at the two other sites – 0.32 mm at Emily Murphy Park and 0.34 mm at the Village Bridge – which is much closer to the range of 0.12 to 0.25 mm observed by Daly and Colbeck (1986). In order to understand this discrepancy, three variables were examined: the weather conditions, the local turbulence characteristics of the flow, and the stage in the supercooling process at which the measurements were made. As mentioned above, it was snowing quite heavily at the time the Emily Murphy Park measurements were made. This means that there would have been an abundance of seed particles falling on the surface of the supercooled river, providing seed crystals for the formation of large numbers of new frazil particles. These new particles would likely be very small since they were formed locally and may not have had time to grow larger. Therefore, the mean particle diameter would be expected to be smaller, similar to the young frazil particles measured by Daly and Colbeck (1986).

To examine the effect that the fluid turbulence had on the mean particle diameter, the local Reynolds number, *Re*, was computed at each of the five sites where accurate depth and

velocity measurements had been made (as presented in Table 3-2). The mean frazil ice particle diameter computed after adjusting for the effects of suspended sediment was then plotted versus the local Reynolds number and fitted with a 2nd order polynomial trendline, shown in Figure 3-14. With a coefficient of determination of 0.85 the 2nd order polynomial is a reasonable fit to the data. The data in Figure 3-14 show that the mean particle diameter initially increased with increasing *Re* up to ~160,000 and then began to decrease. Although this trendline was derived using only five data points, it is notable in that it is very similar to the trend observed by Clark and Doering (2008), who plotted the mean frazil ice particle diameter as a function of turbulence intensity. While Reynolds number cannot be directly compared to turbulence intensity these results indicate that the effects of turbulence on frazil ice formation should not be overlooked, and highlight the importance of measuring turbulence properties in future studies.

The impact the stage of the supercooling process has on the growth, size distribution, and number concentration of frazil particles has been explored in laboratory studies (e.g. Clark and Doering, 2008, 2009; Ettema et al., 1984; McFarlane et al., 2015; Ye et al., 2004). McFarlane et al. (2015) found that the mean particle diameter was small (~0.5 mm or smaller) in the early stages as the first particles began to form; steadily increased to a maximum value (ranging from 0.56 to 0.92 mm) at approximately the same time as the maximum degree of supercooling was reached; and then decreased and levelled off at an approximately constant value during the residual supercooling stage. For this reason, the data collected in this study will be discussed in detail in two parts: first, the data collected during the residual supercooling stage, and second, the data collected during the principal supercooling period.

3.7.1 RESIDUAL SUPERCOOLING

The supercooling curve for the Village Bridge deployment on the morning of March 1, 2015 is plotted in Figure 3-15a and the period of time during which the FrazilCam was deployed is highlighted. It can be seen in this figure that the supercooling event began at approximately 23:45 on the night of February 28, reached the maximum degree of supercooling, a minimum temperature of –0.06°C, at approximately 24:00, and then the temperature increased and the residual supercooling phase began at 00:15 on the morning of March 1. However, the FrazilCam was not deployed at this location until 07:20, which was well into the residual supercooling phase, and in fact the water temperature increased from –0.007°C to –0.003°C by the time the deployment finished at 10:34. Therefore, one reason that a relatively small mean particle diameter of 0.34 mm was observed at this location may be because the majority of the larger particles had already flocculated or fractured. Another reason may be that with the smaller degree of supercooling the frazil ice particles were not able to grow quite as rapidly, as the temperature gradient between the frazil particles and the surrounding water is directly related to the rate of heat transfer (Daly, 1984). The FrazilCam deployment also began during the residual supercooling phase at Opal, for which the water temperature is shown in Figure 3-15b. However, the water temperature at Opal actually increased from –0.002 to +0.02°C during the FrazilCam deployment. This indicates that the water was no longer supercooled at the FrazilCam location, and the frazil ice particles that were captured must have been produced upstream in a region that remained supercooled. The mean particle size observed at Opal was also larger (0.61 mm) than that at the Village (0.34 mm) and fewer particles were observed over a comparable deployment duration (14,419 particles remaining on average after adjustment for sediment at Opal compared to 97,341 at Village). The reason for this is unknown; however, because the water temperatures

throughout most of the deployment at Opal were above zero, it is possible that the smaller particles had melted.

In the North Saskatchewan River, water temperatures were only measured during the FrazilCam deployments. The water temperature increased from –0.011°C to –0.009°C during the deployment at Emily Murphy Park, and as the maximum degree of supercooling is generally significantly greater than this, it seems most likely that these measurements were made during the residual supercooling phase as well. As already discussed, it was snowing at the time of the North Saskatchewan deployment at Emily Murphy Park and this would have introduced abundant seed particles into the flow that could then act as nucleation sites for the formation of frazil ice particles. This may also have contributed to the small mean particle size of 0.32 mm.

In addition to the stage in the supercooling process at which the frazil particles were measured, other differences between the laboratory and field environments should be considered. The most obvious difference between the two environments is the means by which the turbulent flow was generated. In the laboratory experiments by McFarlane et al. (2015), turbulence was generated in the frazil ice production tank using four variable speed propellers mounted on the bottom of the tank. This was shown to generate turbulent kinetic energy dissipation rates of comparable magnitude to those expected in rivers. However, this is certainly a much different method of generating turbulence than occurs in rivers and this could result in differences in the number and size of frazil particles generated. It is worth noting that the counter-rotating flume apparatus used by researchers at the University of Manitoba (Clark and Doering, 2008, 2006, 2009; Ye et al., 2004; Ye and Doering, 2004) and the recirculating flume used by Daly and Colbeck (1986) would be expected to produce a more similar turbulent flow to that observed in

rivers. Additionally, the frazil ice tank used at the University of Alberta and the counter-rotating flume at the University of Manitoba were both used to measure frazil ice particles produced in a constant volume of water as it cools. However, the flume used by Daly and Colbeck (1986) was constantly producing new particles in a recirculating flow, and these particles were photographed as they passed fixed points along the flume. The frame of reference in these experiments was similar to that in the FrazilCam field experiments; that is, in both cases the camera was deployed at a fixed point along the channel and frazil ice particles were photographed as they advected past.

Another difference between the laboratory and field experiments is the degree of supercooling and duration of the principal supercooling period. For the twelve experiments with the highest propeller speed presented by McFarlane et al. (2015), the maximum degree of supercooling varied from –0.093 to –0.072°C and the duration of the principal supercooling period ranged from approximately 12 to 15 minutes. This is significantly different to the supercooling events that were measured in the North Saskatchewan and Kananaskis Rivers for this study, where the maximum degree of supercooling ranged from –0.061°C to –0.026°C and the duration of the principal supercooling period varied from 60 to 142 minutes.

3.7.2 PRINCIPAL SUPERCOOLING

Data were collected during the principal supercooling period in the North Saskatchewan River on November 10, 2014, at two different sites approximately 6 km apart. A plot of the water temperature time series during the supercooling event on November 10, 2014 at Government House Park is shown in Figure 3-16a. A total of 559 images were captured prior to the field of view becoming obstructed by slush, and the time period during which the images were collected is indicated in Figure 3-16a. After adjusting the size distribution

to remove the effects of the sediment particles (see Figure 3-13a), a total of only 413 ice particles remained with a mean diameter of 1.20 mm. However, it is worth noting that a sample size of 413 particles after subtracting the sediment distribution is very small. In addition, some smaller frazil ice particles may have been eliminated when the raw size distribution was adjusted to remove sediment particles which would increase the estimated mean diameter.

The water temperature time series during the supercooling event that occurred on November 10, 2014 at Quesnell Bridge is plotted in Figure 3-16b. At this site, a total of 936 images were captured during the principal supercooling period and the time period when these images were captured is highlighted in Figure 3-16b. A total of 1,262 particles remained after adjusting the data by subtracting the suspended sediment distribution and the final frazil ice size distribution (see Figure 3-13b) had a mean diameter of 0.73 mm. This falls in the range of mean diameters from 0.59 to 0.94 mm that was observed by McFarlane et al. (2015) during the principal supercooling period in a laboratory setting, and falls just below the range observed by Clark and Doering (2008).

Both data sets collected during the principal supercooling period produced larger mean particle diameters than any of the data collected during the residual supercooling phase. This could be interpreted to mean that larger particles are observed earlier in the supercooling process and that the mean particle size decreases once the residual temperature has been reached, as has been observed in laboratory studies (Clark and Doering, 2008; McFarlane et al., 2015). Additionally, it is very important to note that the frazil ice particle size distributions, after adjusting for the presence of sediment particles, are very similar to lognormal distributions in all five cases shown in Figure 3-13. This is a significant observation in that it indicates that a lognormal distribution may be a suitable

approximation of the frazil ice size distribution at any stage in the supercooling process. Unfortunately, the data sets collected during the principal supercooling period could not be used to examine the variation in the mean particle size over time. This was because there were not enough particles available to draw any sort of statistically significant conclusions if the data sets were broken down into smaller subsets with respect to time.

3.7.3 FUTURE WORK

More accurate FrazilCam measurements of frazil ice particle size distributions in rivers with significant suspended sediment concentrations should be possible in the future if changes are made to the experimental methodology. First, every effort should be made to ensure that a sufficient number of FrazilCam images are captured at the site prior to the onset of supercooling in order to obtain an accurate estimate of the size distribution of sediment particles. These background sediment images should be captured immediately before supercooling begins so that the flow rate and depth are the same as when the frazil ice images are captured. Secondly, a small water sample should be collected during each deployment for lab analysis to determine if the suspended sediment concentration changed significantly between when the background and frazil ice images are captured. Thirdly, if it is not possible to capture enough background sediment images before frazil ice formation has started, a large water sample should be collected from the river at the same time as the FrazilCam is deployed. The water sample needs to be large enough that the FrazilCam can be completely immersed in it in the laboratory, and background sediment images can be captured while the water is energetically mixed to suspend the sediment. Continuous turbidity measurements should also be made at all times when the FrazilCam is deployed to monitor any temporal changes that may occur when both the background images and the frazil ice images are captured. These types of measurements

can be made with compact data loggers equipped with optical backscatter turbidity sensors.

3.8 CONCLUSIONS

A self-contained, fully-submersible digital imaging system named the FrazilCam has been developed and successfully deployed to capture high-resolution images of frazil ice particles in rivers. Images of frazil particles were captured in the North Saskatchewan, Peace, and Kananaskis Rivers in Alberta. In two of the six deployments, images were captured during the principal supercooling period, and in the other four deployments the water had reached the residual supercooling temperature. The images were processed to determine the diameter of the individual disc-shaped frazil ice particles and the properties of the resulting size distributions were calculated in each case. Suspended sediment was visible in the frazil ice images, but ice-free images were captured in most cases providing data that were used to calculate the suspended sediment size distributions, and the mean and standard deviation of the sediment particle diameters ranged from 0.11 to 0.13 mm and 0.05 to 0.1 mm, respectively. The frazil ice size distributions were adjusted for the effects of the sediment particles by subtracting a randomly generated distribution with the same mean and standard deviation as the sediment at that site.

For the data captured during the principal supercooling phase in the North Saskatchewan River the mean diameter was found to range from 0.73 to 1.20 mm. This was significantly larger than the mean diameter of 0.32 mm that was observed during the residual supercooling stage in the North Saskatchewan River. The trend of larger frazil ice particle diameters during the principal supercooling phase compared to during the residual supercooling phase is consistent with the laboratory observations of McFarlane et al. (2015) and Clark and Doering (2008). However, the mean diameters measured at the

residual temperatures were still quite small when compared to those observed in many laboratory studies. The main reason for the small mean of 0.32 mm in the North Saskatchewan River is believed to be the abundance of natural seed particles due to snowfall at the time the observations were made, providing nuclei for the formation of very small, fresh frazil ice particles. The five frazil ice size distributions (see Figure 3-13) were well described by a lognormal distribution, which has long been observed to be a good approximation for the frazil ice particle size distributions produced in the lab. It was also observed that between 61% and 87% of the observed particles were disc-shaped, indicating that frazil ice particles in the field exhibit the same preference for disc-shaped growth as has been observed in the laboratory.

FIGURES

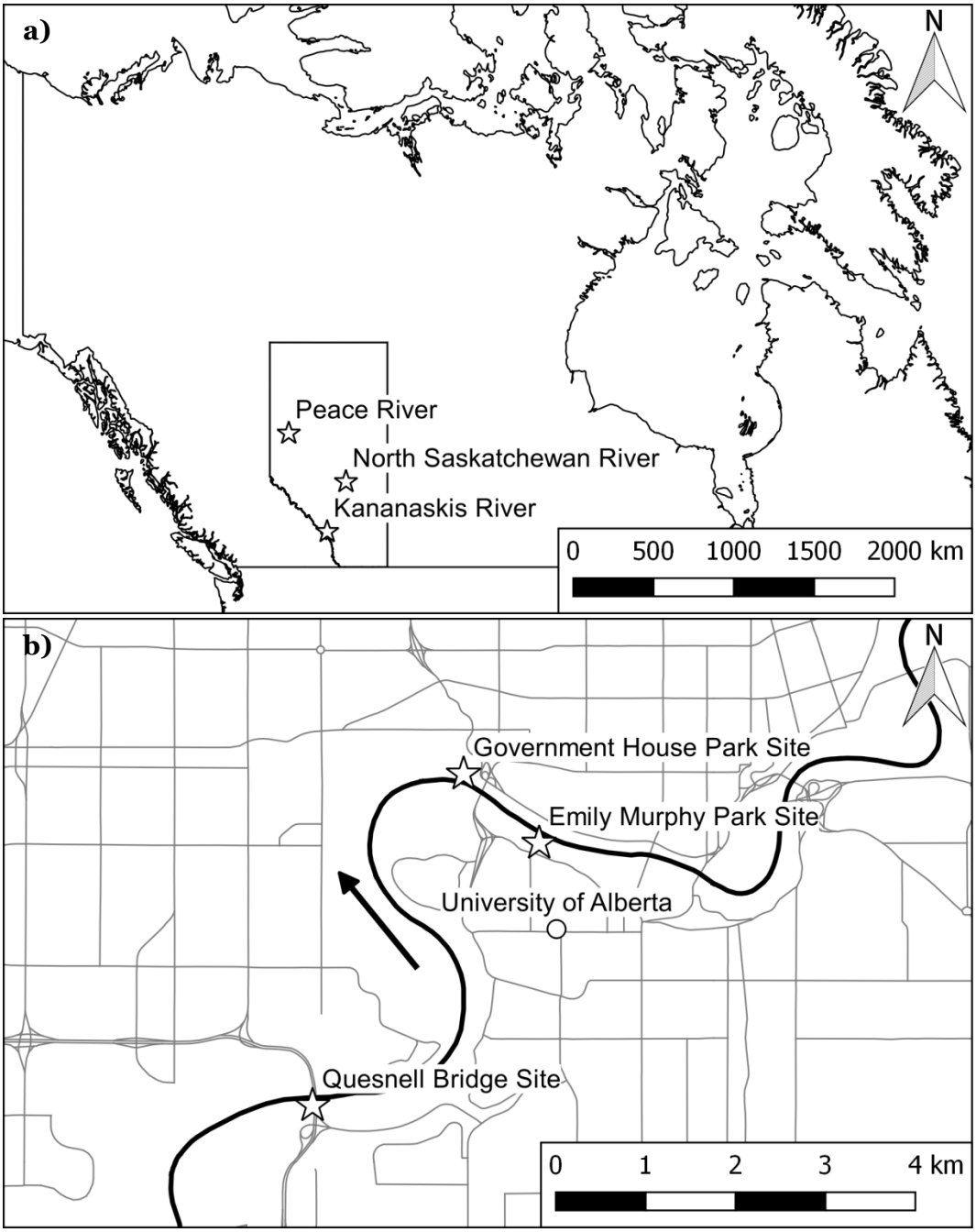
a)
N
Peace River
North Saskatchewan River
Kananaskis River
0 500 1000 1500 2000 km
b)
N
Government House Park Site
Emily Murphy Park Site
University of Alberta
Quesnell Bridge Site
0 1 2 3 4 km

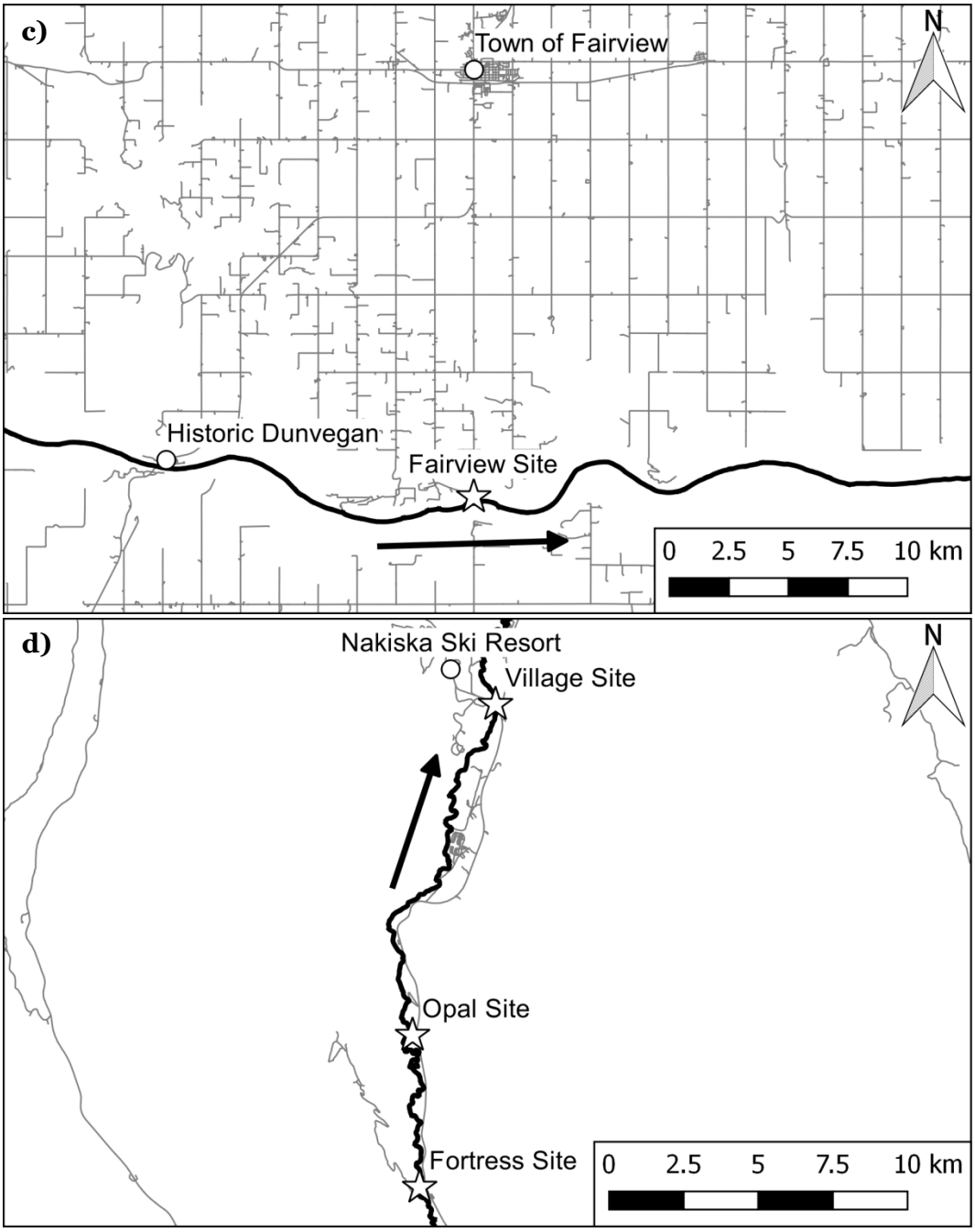

Figure 3-1: The geographic location (☆) of each of the study sites a) within Canada, b) on the North Saskatchewan River, c) the Peace River, and d) the Kananaskis River. The black line indicates the river, the black arrow indicates flow direction, and the dark grey lines indicate roadways.

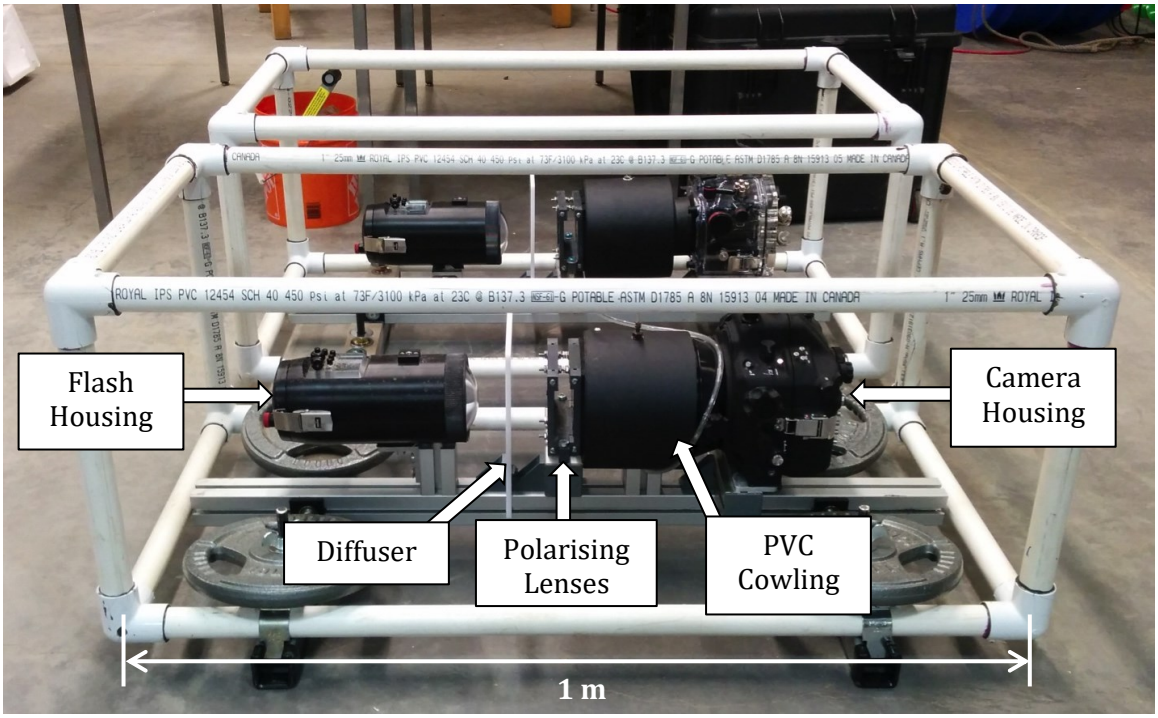

Figure 3-2: Digital image showing the final configuration of the two FrazilCam systems.

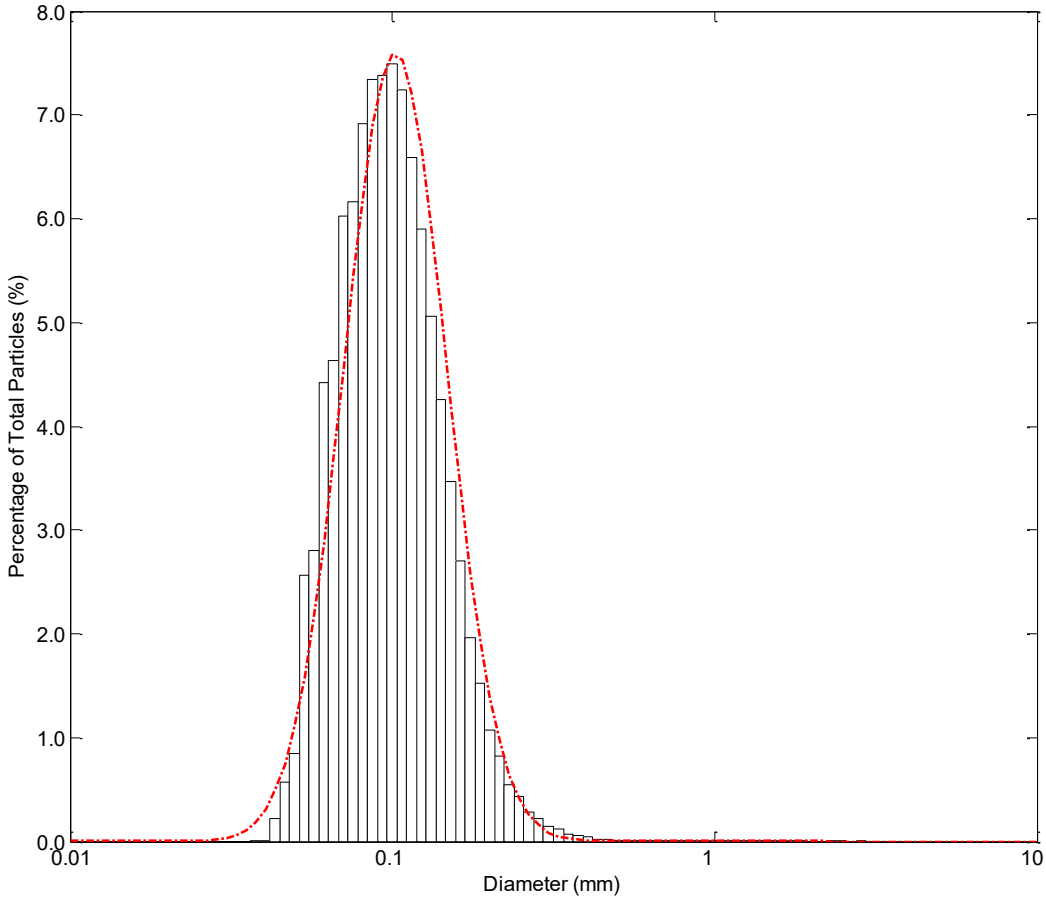

Figure 3-3: The size distribution of sediment particles observed at the Village Bridge on the Kananaskis River March 2, 2015. The dashed line represents the corresponding lognormal distribution calculated using the same mean and standard deviation as the measured size distribution.

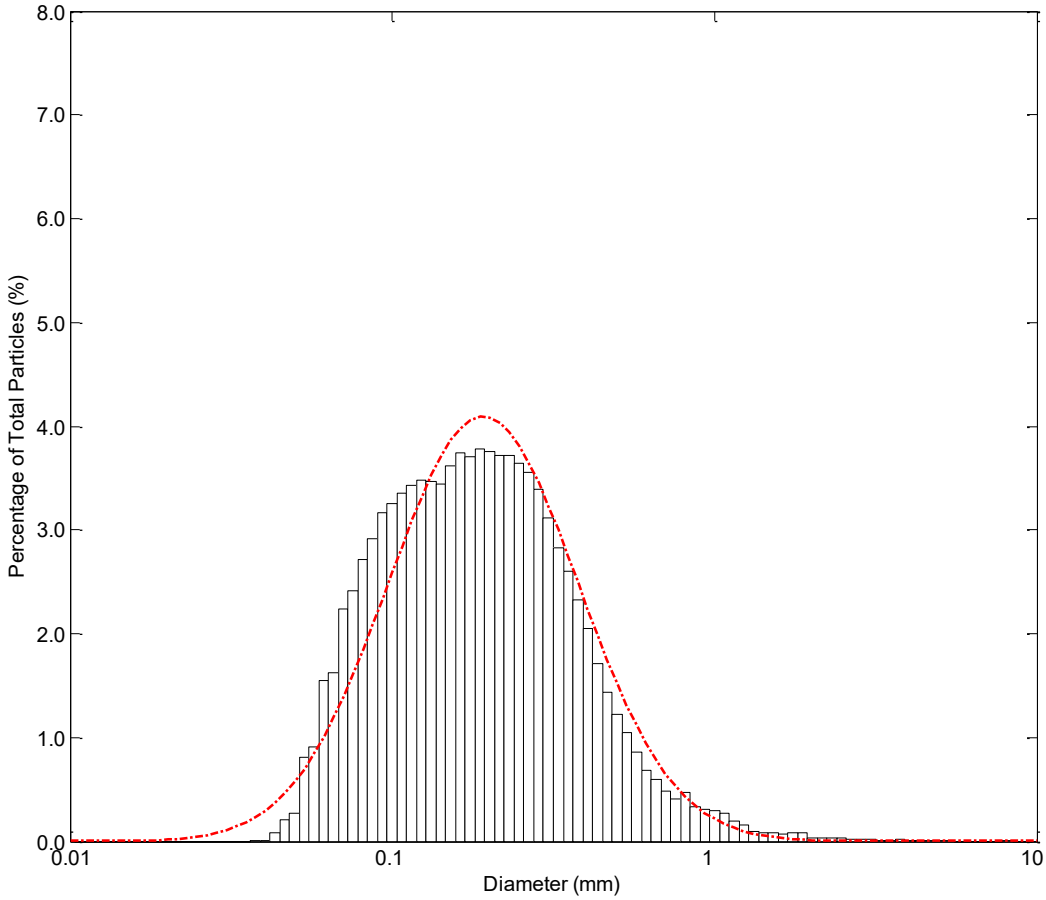

Figure 3-4: The raw size distribution of all particles (i.e. ice and sediment) observed at the Village Bridge on the Kananaskis River March 1, 2015. The dashed line represents the corresponding lognormal distribution calculated using the same mean and standard deviation as the measured size distribution.

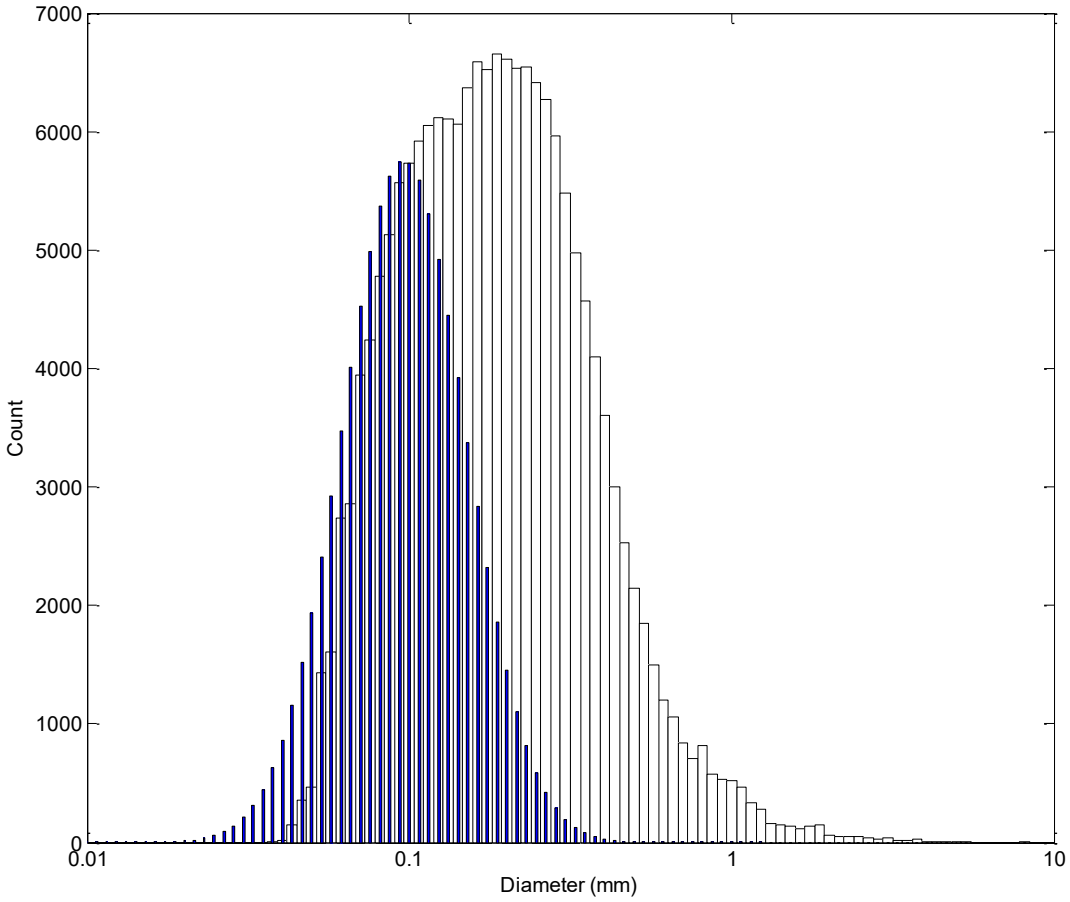

Figure 3-5: The raw size distribution of ice and sediment particles (white bars) at the Village Bridge site on the Kananaskis River March 1, 2015. The ensemble averaged randomly generated lognormal sediment size distribution (blue bars) computed using the mean and standard deviation of the sediment particles observed at the same site on March 2, 2015 is also shown.

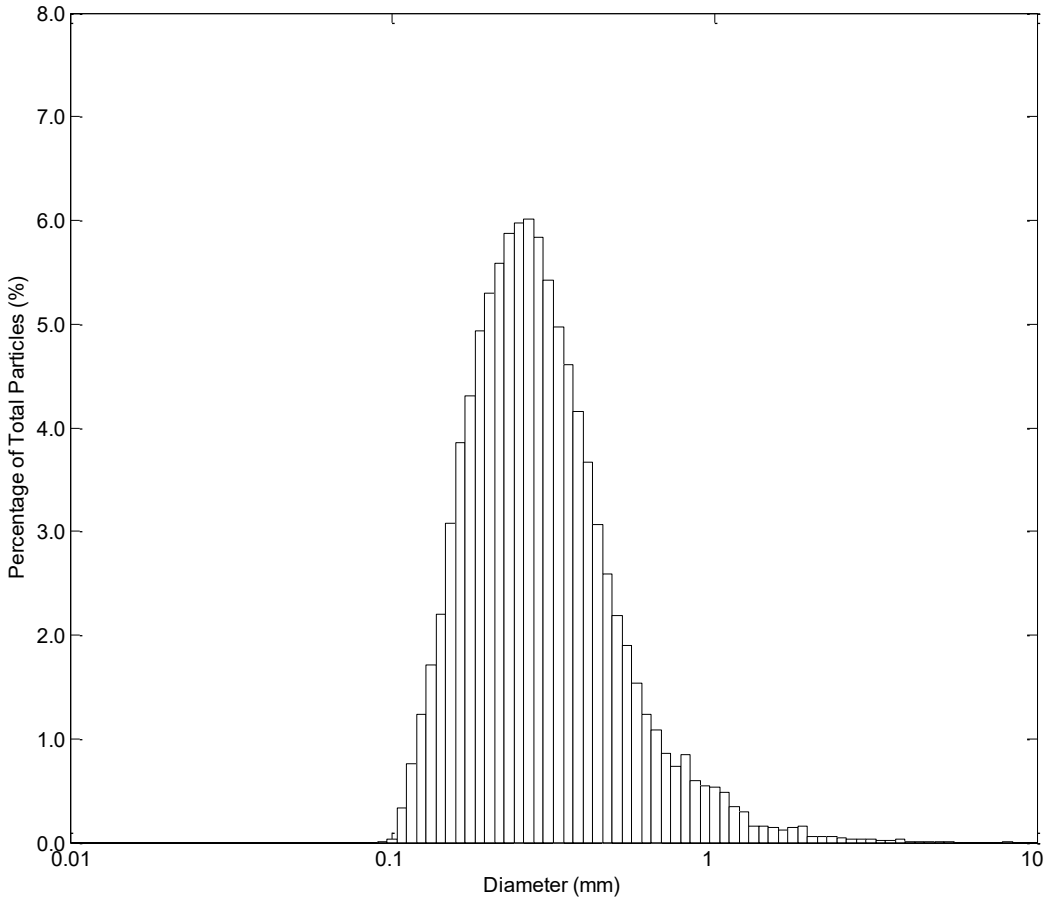

Figure 3-6: The size distribution of frazil ice particles at the Village Bridge site on the Kananaskis River March 1, 2015.

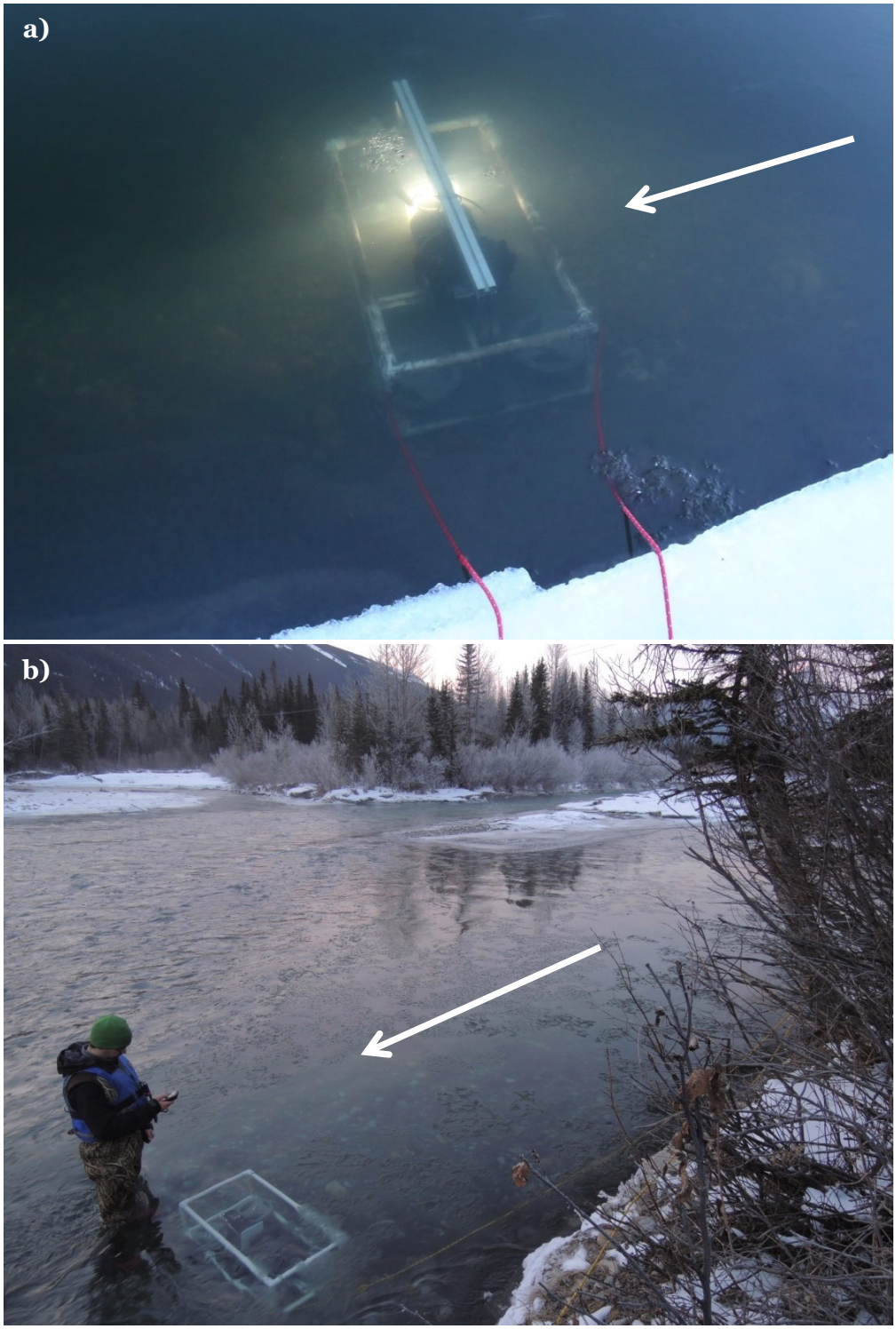

Figure 3-7: Digital image of the FrazilCam deployed a) at the Fairview site on the Peace River December 19, 2014 (photo credit: Martin Jasek), and b) at the Village Bridge site on the Kananaskis River March 1, 2015. Arrow indicates flow direction.

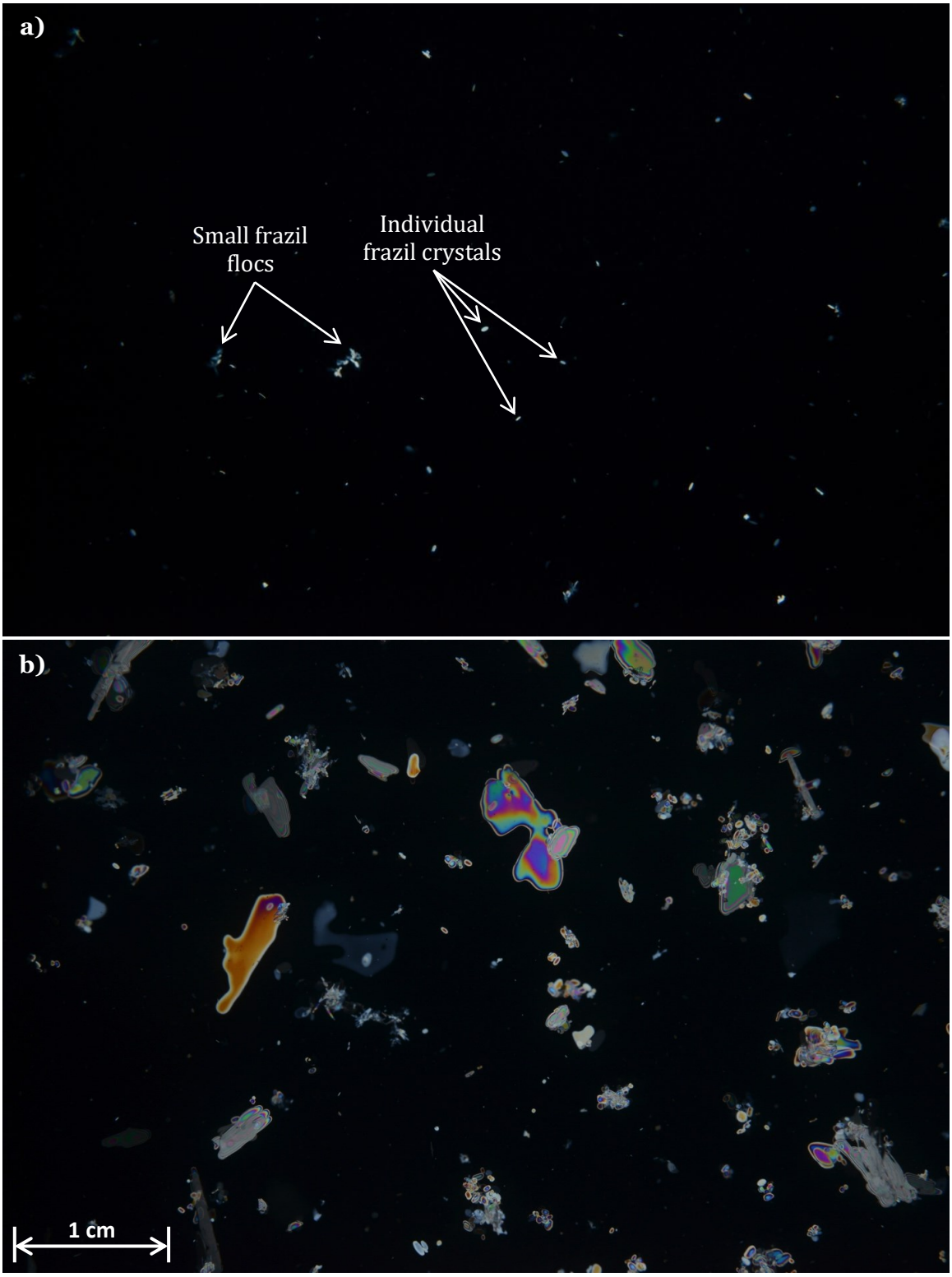

Figure 3-8: Two FrazilCam images captured in the North Saskatchewan River, November 27, 2014. a) Disc-shaped frazil particles and a few small flocs, and b) irregularly shaped ice particles observed in the flow.

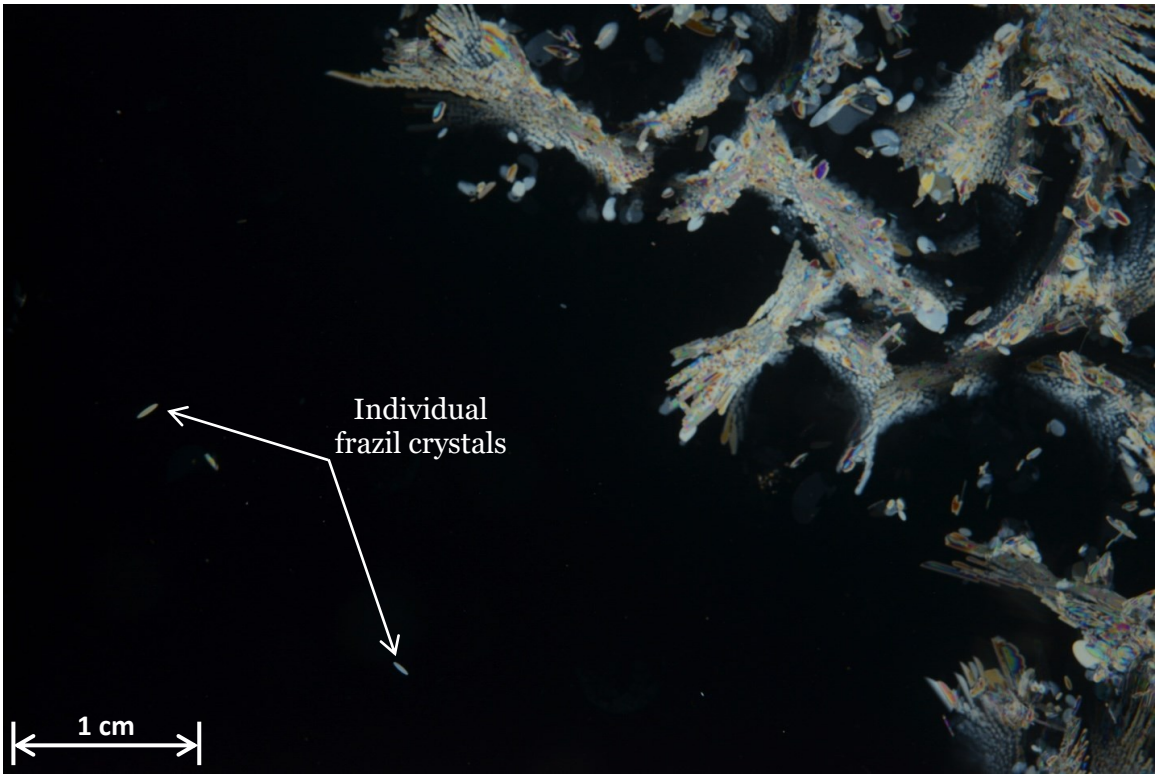

Figure 3-9: Raw digital FrazilCam image captured at the Fairview site on the Peace River on December 19, 2014. The irregularly shaped ice crystals concentrated on the right side of the image formed on the surface of the polariser nearest the camera lens as the camera was submerged.

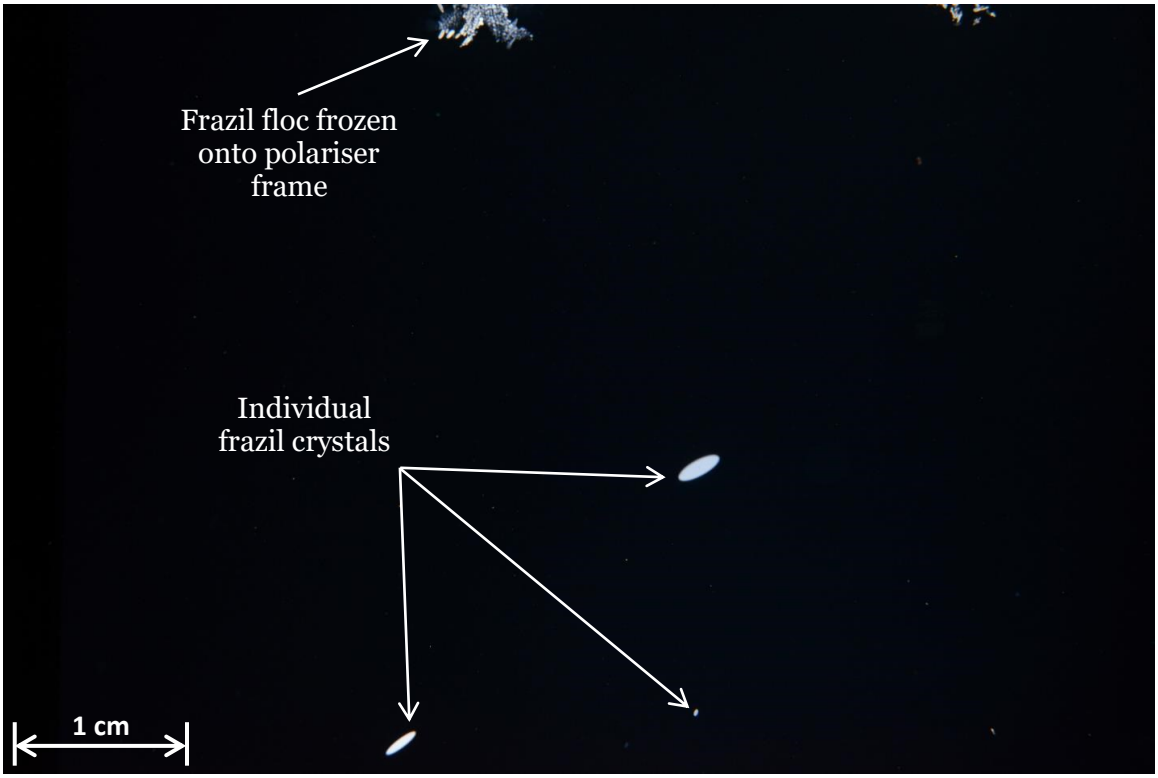

Figure 3-10: A FrazilCam image captured in the Kananaskis River at the Opal site, March 1, 2015.

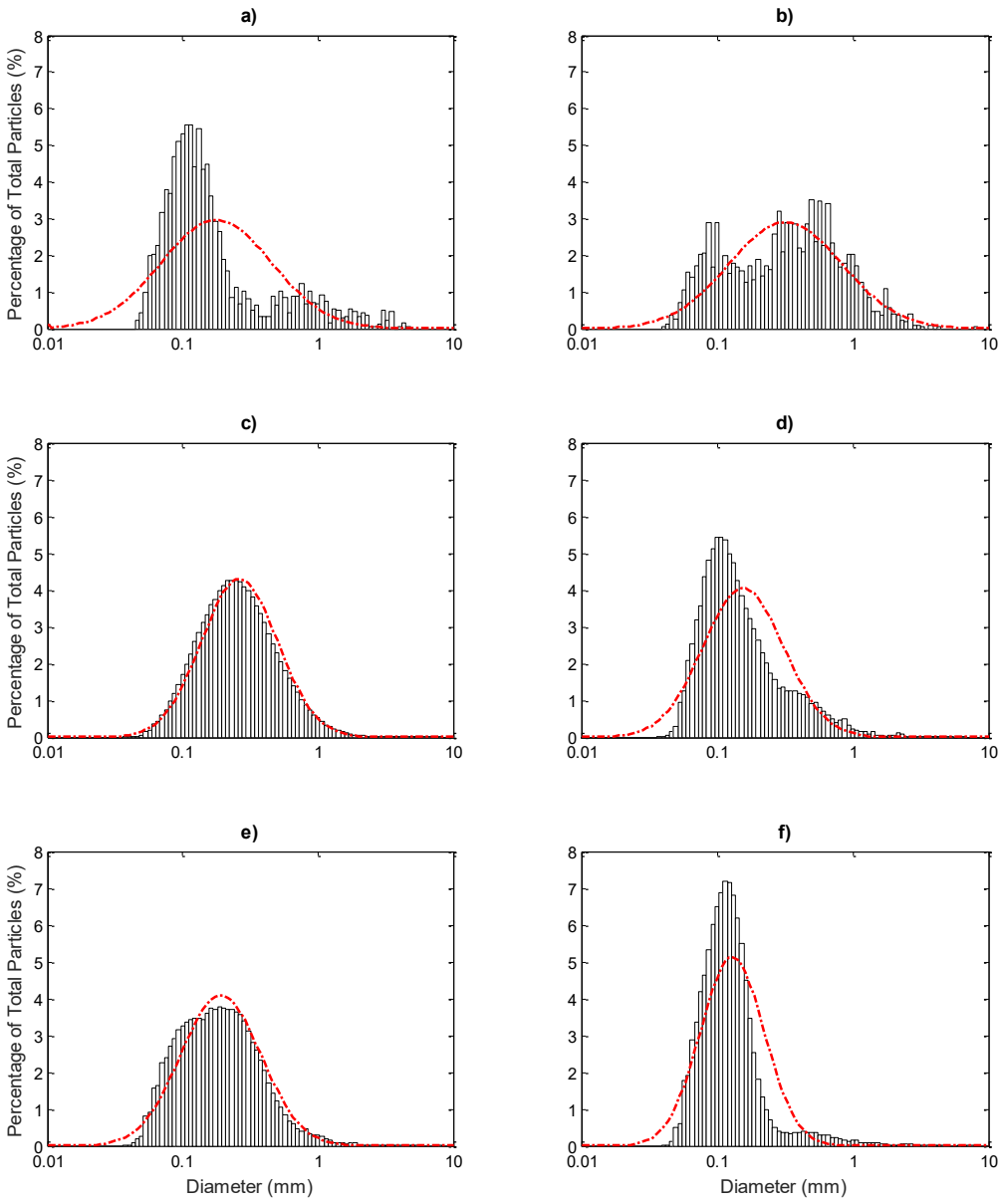

Figure 3-11: The raw size distributions containing ice and sediment particles calculated for the a) Government House Park, b) Quesnell Bridge, c) Emily Murphy Park, d) Fairview Water Intake, e) Village Bridge, and f) Opal sites. The red dashed lines indicate the theoretical lognormal distribution with the same mean and standard deviation as the observed particles.

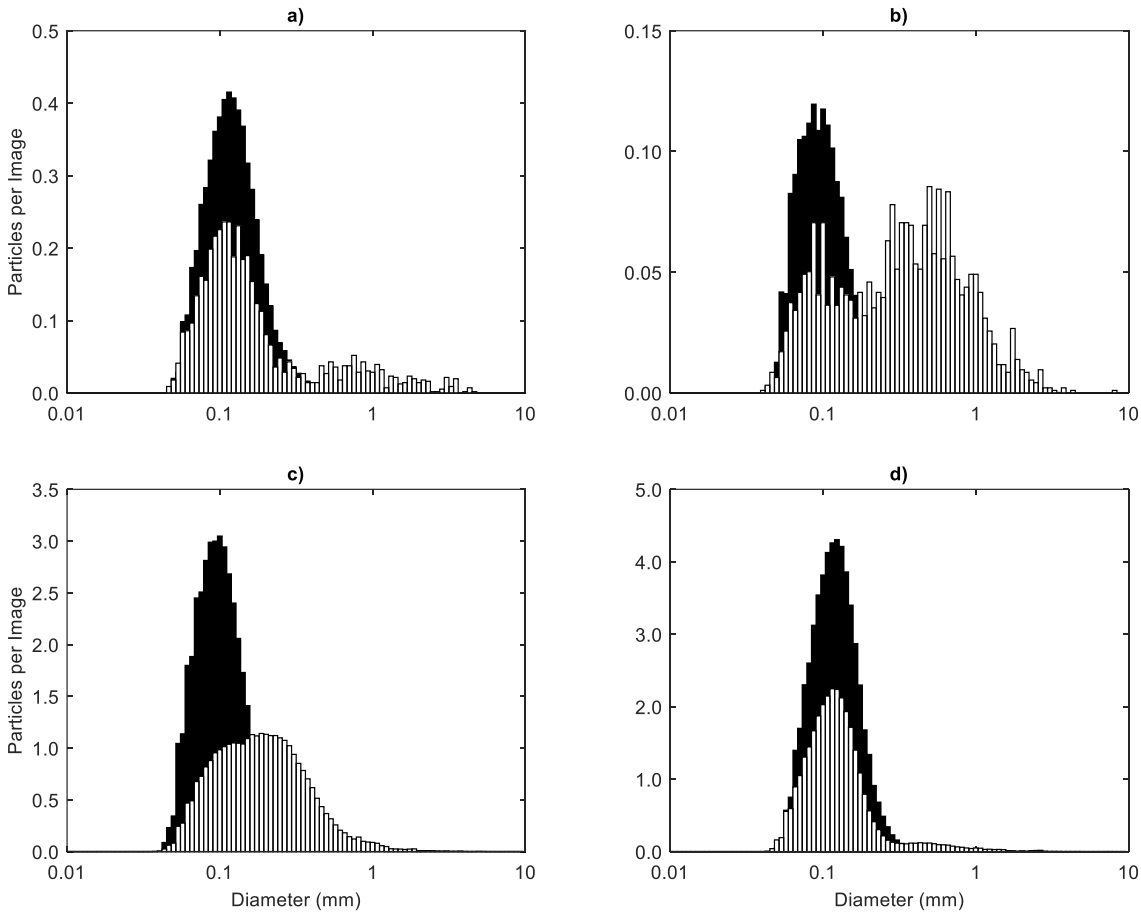

Figure 3-12: A comparison of the suspended sediment (black bars) and raw (white bars) size distributions at the a) Government House Park, b) Quesnell Bridge, c) Village Bridge, and d) Opal sites.

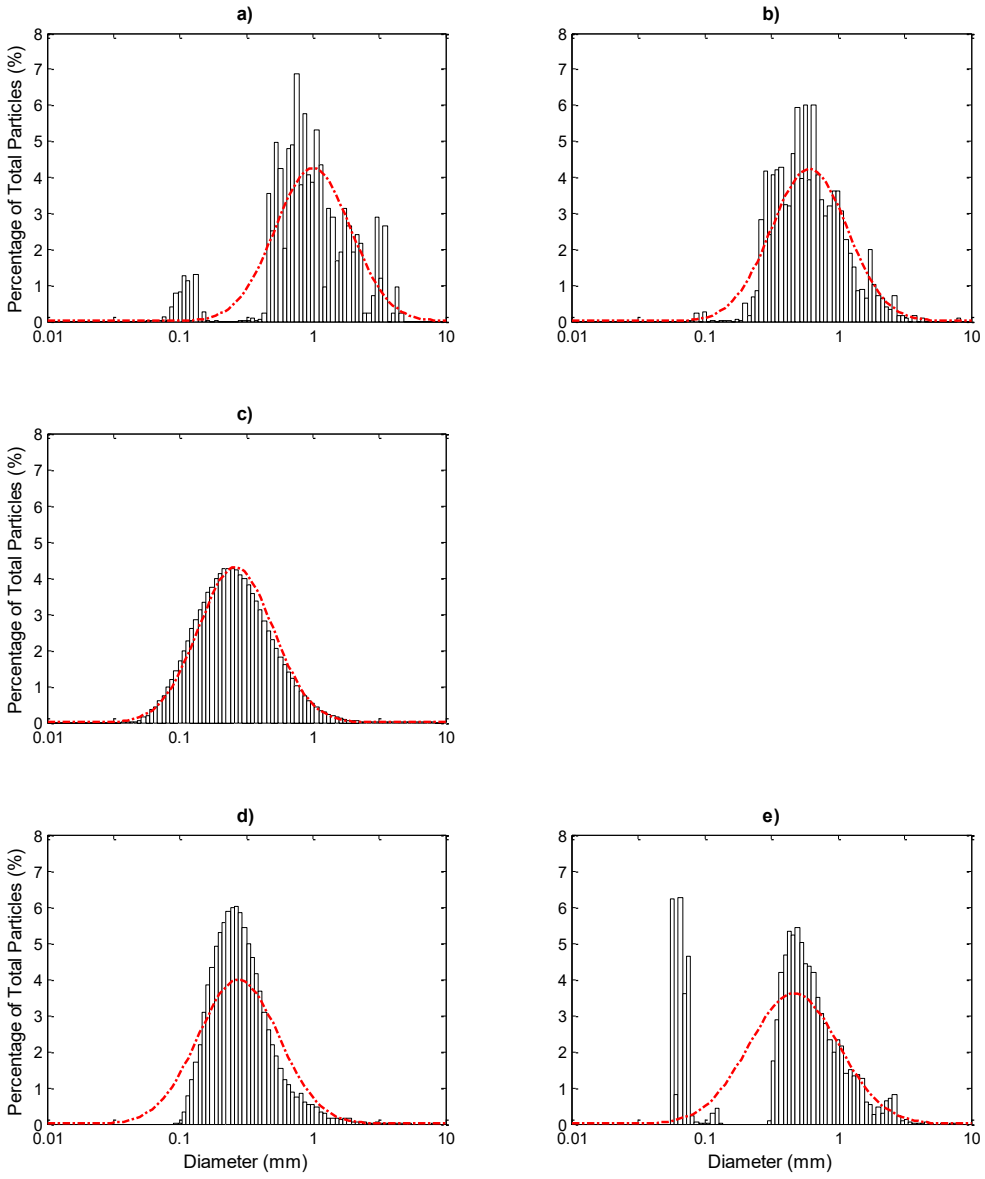

Figure 3-13: The frazil ice size distributions calculated for the a) Government House Park, b) Quesnell Bridge, c) Emily Murphy Park, d) Village Bridge, and e) Opal sites. The red dashed lines indicate the theoretical lognormal distribution with the same mean and standard deviation as the observed particles.

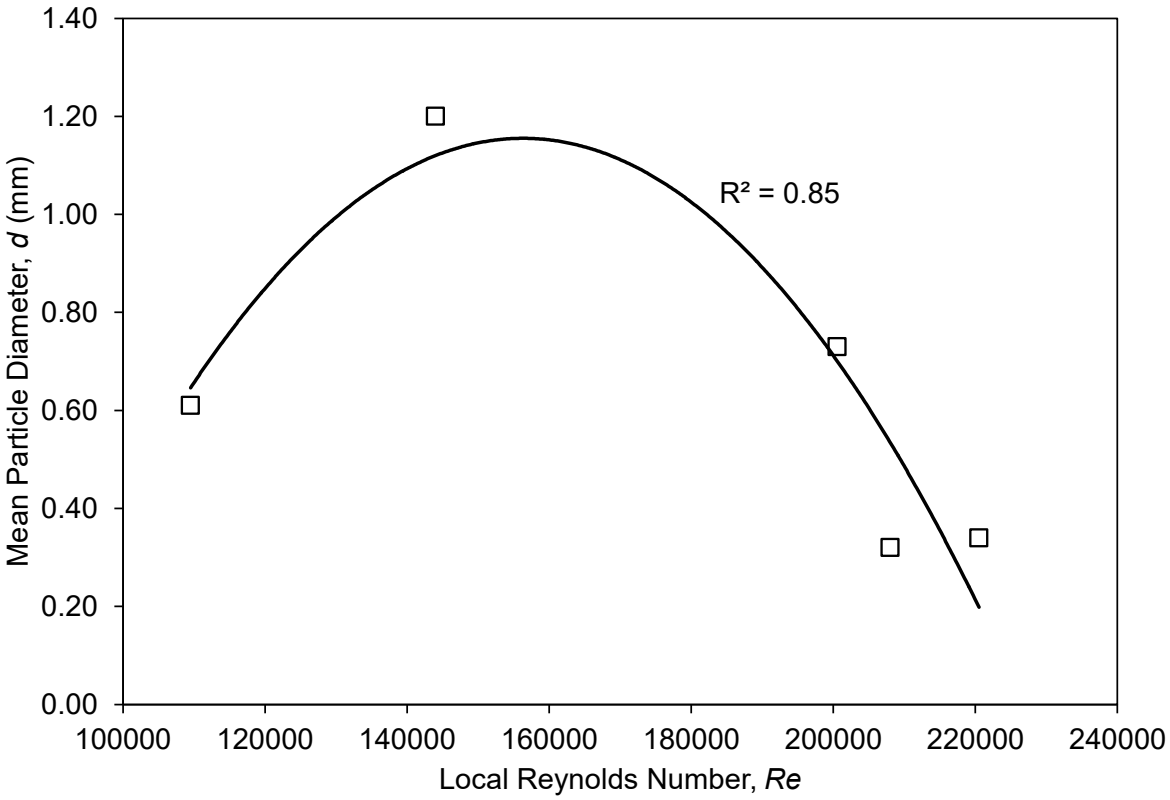

Figure 3-14: The mean frazil ice particle diameter plotted as a function of the local Reynolds number. The solid line is a second-order polynomial trendline.

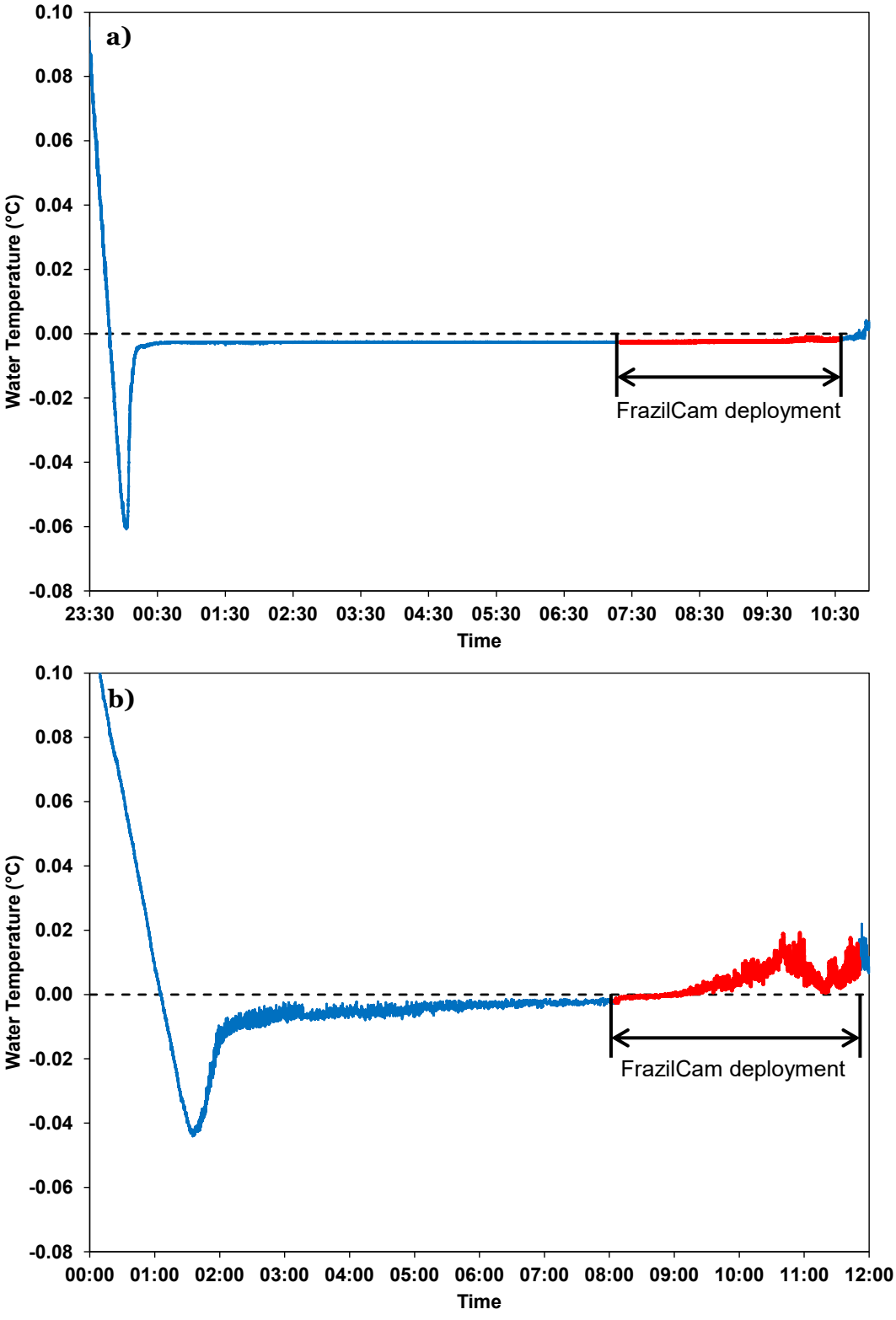

Figure 3-15: Time series of water temperatures during the supercooling events observed on the Kananaskis River a) at the Village Bridge overnight from February 28 to March 1, 2015, and b) at the Opal site on March 1, 2015.

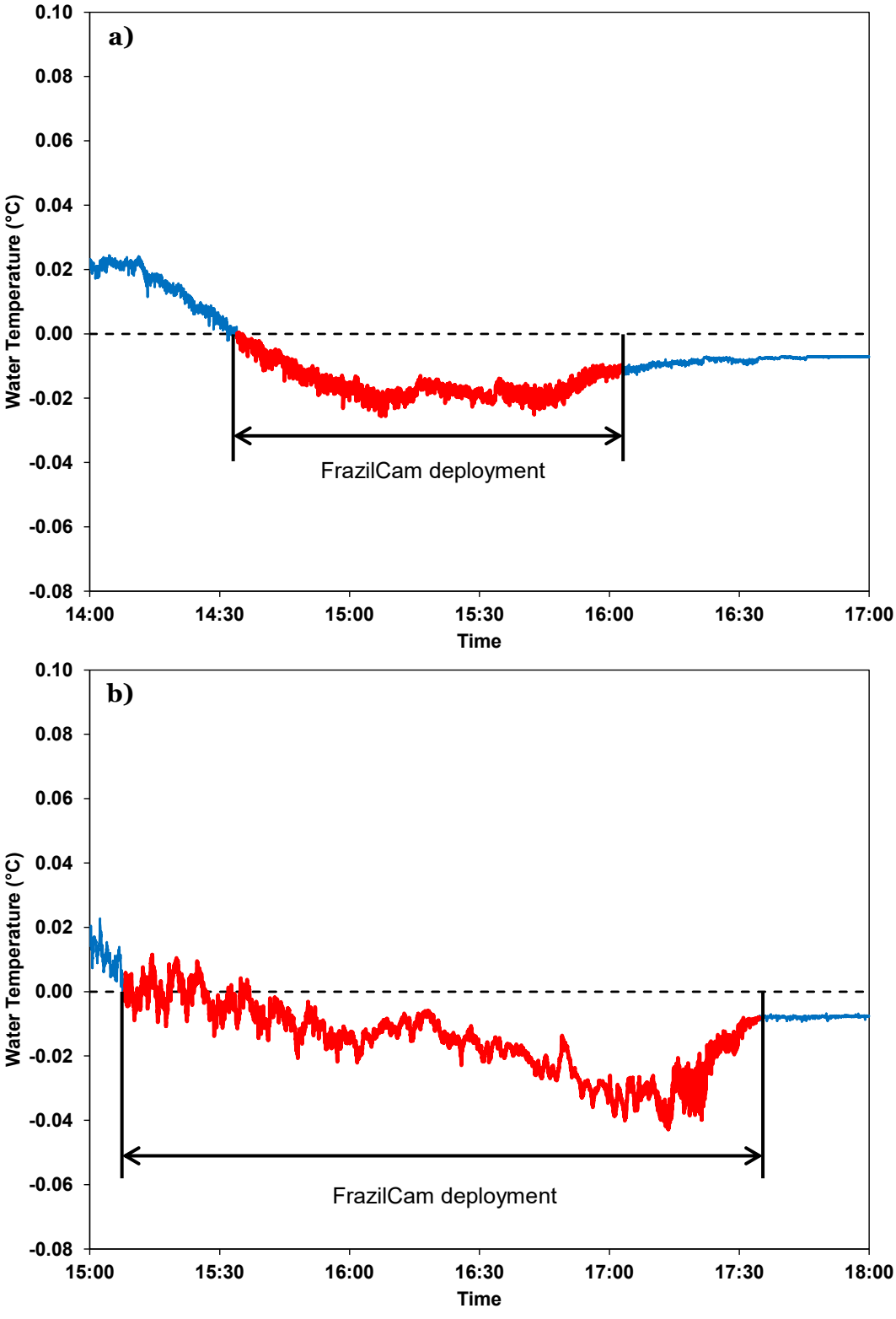

Figure 3-16: Time series of the water temperatures during the supercooling events observed at a) the Government House Park site, and b) the Quesnell Bridge site on the North Saskatchewan River, November 10, 2014.

TABLES

Table 3-1: Study site locations, sampling dates, and average river characteristics.

River	Site	Date	Coordinates	Slope[1]	Average Flow Rate[2] (m^3/s)	Average Water Depth[2] (m)	Average Channel Width[2] (m)	Range of D_{50} of Suspended Sediment[3] (mm)
North Saskatchewan River	Quesnell Bridge	November 10, 2014	53°30'20.5"N 113°34'00.7"W	0.00035	220	1.40	136	0.0091 to 0.030
	Government House Park	November 10, 2014	53°32'19.4"N 113°32'30.9"W					
	Emily Murphy Park	November 27, 2014	53°31'54.8"N 113°31'46.0"W					
Peace River	Fairview Water Intake	December 19, 2014	55°54'34.3"N 118°23'30.7"W	0.00025	1,586	2.56	227	0.0055 to 0.029
Kananaskis River	Opal Day Use Area	March 1, 2015	50°49'58.74"N 115°10'9.5"W	0.005	15	0.61	32	––
	Village Bridge	March 1, 2015	50°55'53.2"N 115° 7'48.3"W	0.005				––

[1] Bed slope data for the North Saskatchewan and Peace Rivers were obtained from Kellerhals et al. (1972). The North Saskatchewan River slope was given at Edmonton and the Peace River slope was given at Dunvegan, ~13 km upstream of where the FrazilCam was deployed. The Kananaskis River slope was measured using real-time kinematic (RTK) survey data obtained between the Fortress and Village Bridge sites.

[2] Average flow rate, water depth, and channel width data for all three rivers were obtained from Kellerhals et al. (1972). The North Saskatchewan River data were given at Edmonton, ~3.5 km downstream of the Emily Murphy Park site; the Peace River data were given at Dunvegan, ~13 km upstream of the Fairview site; and the Kananaskis River data were given at Seebe, ~28 km downstream of the Village Bridge site.

[3] Suspended sediment values interpolated from size distribution data obtained from the Water Survey of Canada website in May 2017. http://wateroffice.ec.gc.ca/. Sediment data for the Peace River were measured at Dunvegan, ~13 km upstream of the Fairview site. Sediment data for the North Saskatchewan River were measured ~3.5 km downstream of the Emily Murphy Park site. No sediment data were available for the Kananaskis River.

Table 3-2: Site conditions during FrazilCam deployments.

River	Site	Date	Mean Air Temperature[4] (°C)	Minimum Water Temperature (°C)	Local Water Depth (m)	Depth-Averaged Water Velocity (m/s)
North Saskatchewan River	Quesnell Bridge	November 10, 2014	−15	−0.043	1.08	0.24
	Government House Park	November 10, 2014	−15	−0.026	0.95	0.38
	Emily Murphy Park	November 27, 2014	−11	−0.011	0.72	0.52
Peace River	Fairview Water Intake	December 19, 2014	−9	−0.014	~0.75	~0.5
Kananaskis River	Opal Day Use Area	March 1, 2015	−12	−0.002	0.73	0.27
	Village Bridge	March 1, 2015	−12	−0.007	0.63	0.63

[4] Air temperature data obtained from the Environment Canada website in March 2016. http://weather.gc.ca/.

Table 3-3: Location, date, time and image sampling data for each FrazilCam deployment.

River	Site	Date	Start Time	End Time	Image Capture Frequency	Number of Images Captured
North Saskatchewan River	Quesnell Bridge	November 10, 2014	09:45	19:03	9 images at 1 Hz every 90 s	3,355
	Government House Park	November 10, 2014	10:30	18:13		3,020
	Emily Murphy Park	November 27, 2014	08:00	10:29	1 Hz	8,991
Peace River	Fairview Water Intake	December 19, 2014	16:38	17:44		3,996
Kananaskis River	Opal Day Use Area	March 1, 2015	08:05	11:50	9 images at 1 Hz every 18 s	7,176
	Village Bridge	March 1, 2015	07:20	10:34		5,845

Table 3-4: Summary of the raw particle size distributions calculated at each site.

River	Site	Number of Images	Number of Total (Ice & Sediment) Particles	Percentage of Particles that were Disc Shaped (%)	Mean, μ (mm)	Standard Deviation, σ (mm)	Particles per Image
North Saskatchewan	Government House Park	559	2,369	64	0.32	0.55	4.2
	Quesnell Bridge	936	2,279	61	0.48	0.50	2.4
	Emily Murphy Park	8,445	862,057	87	0.32	0.26	102.1
Peace	Fairview Water Intake	3,645	87,852	--[5]	0.20	0.24	24.1
Kananaskis	Opal Day Use Area	6,777	211,444	64	0.16	0.19	31.2
	Village Bridge	5,835	176,097	83	0.24	0.23	30.2

[5] Not calculated due to the unknown sediment size distribution for this site.

Table 3-5: Summary of the suspended sediment size distribution data computed from FrazilCam images at various field sites.

River	Site	Number of Images	Number of Sediment Particles	Mean, μ (mm)	Standard Deviation, σ(mm)	Particles per Image
North Saskatchewan	Government House Park	8,991	53,552	0.13	0.083	6.0
	Quesnell Bridge	4,950	8,316	0.12	0.10	1.7
Kananaskis	Opal Day Use Area	3,215	178,422	0.13	0.052	55.5
	Village Bridge	3,315	134,852	0.11	0.050	40.7

Table 3-6: Properties of the frazil ice size distributions estimated for five deployments.

River	Site	Number of Images	Average Number of Frazil Ice Particles	Mean, μ (mm)	Standard Deviation, σ(mm)
North Saskatchewan	Government House Park	559	413	1.20	0.88
	Quesnell Bridge	936	1,262	0.73	0.54
	Emily Murphy Park	8,445	862,057	0.32	0.26
Kananaskis	Opal Day Use Area	6,777	14,419	0.61	0.55
	Village Bridge	5,835	97,341	0.34	0.34

Table 3-7: Summary of frazil particle sizes reported in previous laboratory and field studies. (Continued on next page).

Study	Particle sizes reported	Setting	Apparatus and Measurement Type
Schaefer (1950)	1 to 5 mm	Field	Visual estimate of particles photographed after removal from the Mohawk River, NY
Arakawa (1954)	0.1 to 3 mm	Laboratory	Photographs of particles produced in various apparatuses using different seeding mechanisms
Carstens (1966)	Up to 2-3 mm	Laboratory	Visual observations of particles produced in a recirculating flume
Muller (1978)	Calculated mean of 0.15 to 0.98 mm	Laboratory	Mean diameter estimated based on concentrations measured of particles suspended in a turbulence jar
Gosink and Osterkamp (1983)	1 to 6 mm	Field & Laboratory	Visual observations of crystals scooped from supercooled water into a graduated cylinder
Osterkamp and Gosink (1983)	Mostly 0.1 to 1 mm, up to 3-5 mm	Field	In-situ photographs of particles in the Chatanika River, AK
Ettema et al. (1984)	Up to 2-3 mm	Laboratory	Visual observations of particles removed from the turbulence jar in which they were produced
Wuebben (1984)	0.5 to 4 mm	Laboratory	Visual observations of particles produced in a large clear plastic cylinder
Daly and Colbeck (1986)	35 μm to 0.5 mm, mean generally above 0.1 mm	Laboratory	Microscopic images of particles produced in a refrigerated flume
Kempema et al. (1986)	1 to 5 mm	Laboratory	Visual observations of particles produced in a race-track flume
Doering and Morris (2003)	1.25 mm to 4.75 cm	Laboratory	Cross-polarised images of particles produced in a counter-rotating flume
Clark and Doering (2004)	Mean ranging from 0.49 to 1.40 mm throughout experiment, plateauing at 1.2 to 1.4 mm	Laboratory	Cross-polarised images of particles produced in a counter-rotating flume
Ye et al. (2004)	1 mm to 1.5 cm, larger particles attributed to flocs	Laboratory	Cross-polarised images of particles produced in a counter-rotating flume
Clark and Doering (2006)	0.165 to 5 mm, mean from 1.25 to 2.1 mm	Laboratory	Cross-polarised images of particles produced in a counter-rotating flume
Clark and Doering (2008)	Mean from 0.79 to 1.58 mm, standard deviation from 0.44 to 1.00 mm	Laboratory	Cross-polarised images of particles produced in a counter-rotating flume
Morse and Richard (2009)	Mean of 3.15 mm, median of 3.0 mm, standard deviation 2.5 mm	Field	Rouse analysis of particles detected using a 420 kHz Ice Profiling Sonar (IPS)
Marko and Jasek (2010b)	0.4 to 1.09 mm	Field	Acoustic backscattering models applied to data from 235 and 546 kHz Shallow Water IPS (SWIPS) instruments

Richard et al. (2011)	Particles as small as 0.12 to 0.36 mm, mean from 0.4 to 0.86 mm	Field	Various acoustic backscattering models applied to data from 420 kHz IPS and 1228.8 kHz acoustic Doppler current profiler (ADCP) instruments
McFarlane et al. (2012)	0.04 to 5 mm, mean of 0.8 mm	Laboratory	Cross-polarised images of particles produced in a 1.44 m^3 mixed tank
Ghobrial et al. (2012)	0.25 to 4.25 mm, mean of 1.97 mm, standard deviation of 0.89 mm	Laboratory	Microscopic photographs of particles sieved out of a 1.44 m^3 mixed tank
Ghobrial et al. (2013b)	0.26 to 0.42 mm	Field	Various acoustic backscattering models applied to data obtained from 235 and 546 kHz SWIPS instruments
Dubé et al. (2014)	Maximum size of ~1 mm	Field	Estimation from underwater photograph
Yoshikawa et al. (2014)	0.2 to 2 mm	Field	Photographs of particles scooped out of the flow of the Teshio River, Japan
Marko et al. (2015)	Median from 0.6 to 1.6 mm	Field	Multifrequency acoustic backscattering sonar relationship calibrated with laboratory data applied to a four-frequency SWIPS instrument
McFarlane et al. (2015)	Particles ranging from 22 µm to 5.5 mm; means of 0.59, 0.66, and 0.94 mm with standard deviations of 0.45, 0.51, and 0.73, respectively	Laboratory	Cross-polarised images of particles produced in a 1.44 m^3 tank mixed at three different intensities

ACKNOWLEDGEMENTS

This research was supported by the Natural Sciences and Engineering Research Council of Canada (NSERC). We would like to thank Perry Fedun for technical assistance with the project, Jeff Kemp for his assistance in the field, Martin Jasek for providing field assistance and additional data for the Peace River, and Dr. Ying Tsui and Zach Tchir for their help testing the flash pulse duration.

Maps contained in this publication were produced using QGIS software (QGIS Development Team, 2017) and using data © OpenStreetMap contributors (http://www.osm.org/copyright) and data obtained from AltaLIS (2017) which contains information licensed under the Open Government License – Alberta.

REFERENCES

AltaLIS [WWW Document], 2017. URL http://www.altalis.com/altalis/ (accessed 6.7.17).

Arakawa, K., 1954. Studies on the Freezing of Water (II) Formation of Disc Crystals. J. Fac. Sci. Hokkaido Univ. Japan 4, 311–349.

Carstens, T., 1966. Experiments with supercooling and ice formation in flowing water. Geofys. Publ. 26, 1–18.

Clark, S., Doering, J., 2006. Laboratory Experiments on Frazil-Size Characteristics in a Counterrotating Flume. J. Hydraul. Eng. 132, 94–101. doi:10.1061/(ASCE)0733-9429(2006)132:1(94)

Clark, S., Doering, J., 2008. Experimental investigation of the effects of turbulence intensity on frazil ice characteristics. Can. J. Civ. Eng. 35, 67–79. doi:10.1139/L07-086

Clark, S., Doering, J.C., 2004. A laboratory study of frazil ice size distributions, in: Proceedings of the 17th International Symposium on Ice. International Association of Hydraulic Engineering and Research, Saint Petersburg, Russia, pp. 291–297.

Clark, S.P., Doering, J.C., 2009. Frazil flocculation and secondary nucleation in a counter-rotating flume. Cold Reg. Sci. Technol. 55, 221–229. doi:10.1016/j.coldregions.2008.04.002

Daly, S.F., 1984. Frazil ice dynamics. U.S. Army Cold Regions Research and Engineering Laboratory, Hanover, N. H.

Daly, S.F., 2013. Frazil Ice, in: Beltaos, S. (Ed.), River Ice Formation. Committee on River Ice Processes and the Environment, CGU-HS, Edmonton, Alberta, pp. 107–134.

Daly, S.F., Colbeck, S.C., 1986. Frazil ice measurements in CRREL's flume facility, in: Proceedings of the IAHR Ice Symposium 1986. International Association for Hydraulic Research, Iowa City, Iowa, USA, pp. 427–438.

Doering, J.C., Morris, M.P., 2003. A digital image processing system to characterize frazil ice. Can. J. Civ. Eng. 30, 1–10.

Dubé, M., Turcotte, B., Morse, B., 2014. Inner structure of anchor ice and ice dams in steep channels. Cold Reg. Sci. Technol. 106–107, 194–206. doi:10.1016/j.coldregions.2014.06.013

Ettema, R., Karim, M.F., Kennedy, J.F., 1984. Frazil ice formation. U.S. Army Cold Regions Research and Engineering Laboratory, Hanover, N. H.

Ettema, R., Karim, M.F., Kennedy, J.F., 1984. Laboratory experiments on frazil ice growth in supercooled water. Cold Reg. Sci. Technol. 10, 43–58. doi:10.1016/0165-232X(84)90032-6

Ghobrial, T.R., Loewen, M.R., Hicks, F., 2012. Laboratory calibration of upward looking sonars for measuring suspended frazil ice concentration. Cold Reg. Sci. Technol. 70, 19–31. doi:10.1016/j.coldregions.2011.08.010

Ghobrial, T.R., Loewen, M.R., Hicks, F.E., 2013b. Characterizing suspended frazil ice in rivers using upward looking sonars. Cold Reg. Sci. Technol. 86, 113–126. doi:10.1016/j.coldregions.2012.10.002

Gosink, J.P., Osterkamp, T.E., 1983. Measurements and Analyses of Velocity Profiles and Frazil Ice-Crystal Rise Velocities during periods of Frazil-Ice Formation in Rivers. Ann. Glaciol. 79–84.

Government of Alberta, 2017. Alberta Environment and Parks - Alberta River Basins flood alerting, advisories, reporting and water management [WWW Document]. URL https://rivers.alberta.ca/ (accessed 6.16.17).

Kellerhals, R., Neill, C.R., Bray, D.I., 1972. Hydraulic and Geomorphic Characteristics of Rivers in Alberta. Alberta Cooperative Research Program in Highway and River Engineering, Edmonton, Alberta.

Kempema, E.W., Ettema, R., 2016. Fish, Ice, and Wedge-Wire Screen Water Intakes. J. Cold Reg. Eng. 30, 19. doi:10.1061/(ASCE)CR.1943-5495.0000097

Kempema, E.W., Reimnitz, E., Hunter, R.E., 1986. Flume studies and field observations of the interaction of frazil ice and anchor ice with sediment. U.S. Geological Survey, Menlo Park, California.

Kondolf, G.M., Adhikari, A., 2000. Weibull vs. Lognormal Distributions for Fluvial Gravels. J. Sediment. Res. 70, 456–460. doi:10.1306/2DC4091E-0E47-11D7-8643000102C1865D

Marko, J.R., Jasek, M., 2010b. Sonar detection and measurement of ice in a freezing river II: Observations and results on frazil ice. Cold Reg. Sci. Technol. 63, 135–153.

Marko, J.R., Jasek, M., Topham, D.R., 2015. Multifrequency analyses of 2011–2012 Peace

River SWIPS frazil backscattering data. Cold Reg. Sci. Technol. 110, 102–119. doi:10.1016/j.coldregions.2014.11.006

Mazumder, B.S., Ray, R.N., Dalal, D.C., 2005. Size distributions of suspended particles in open channel flow over bed materials. Environmetrics 16, 149–165. doi:10.1002/env.690

McFarlane, V., Loewen, M., Hicks, F., 2012. Laboratory Experiments to Determine Frazil Ice Properties, in: Proceedings of the Annual Conference and General Meeting of the CSCE - 2012. Edmonton, Alberta, p. 10.

McFarlane, V., Loewen, M., Hicks, F., 2014. Laboratory measurements of the rise velocity of frazil ice particles. Cold Reg. Sci. Technol. 106–107, 120–130. doi:10.1016/j.coldregions.2014.06.009

McFarlane, V., Loewen, M., Hicks, F., 2015. Measurements of the evolution of frazil ice particle size distributions. Cold Reg. Sci. Technol. 120, 45–55. doi:10.1016/j.coldregions.2015.09.001

Morse, B., Richard, M., 2009. A field study of suspended frazil ice particles. Cold Reg. Sci. Technol. 55, 86–102. doi:10.1016/j.coldregions.2008.03.004

Muller, A., 1978. Frazil ice formation in turbulent flow. Iowa City, Iowa, USA.

Osterkamp, T.E., Gosink, J.P., 1983. Frazil ice formation and ice cover development in interior Alaska streams. Cold Reg. Sci. Technol. 8, 43–56. doi:10.1016/0165-232X(83)90016-2

QGIS Development Team, 2017. QGIS Geographic Information System. Open Source Geospatial Foundation Project. URL http://qgis.osgeo.org.

Reimnitz, E., Clayton, J.R., Kempema, E.W., Payne, J.R., Weber, W.S., 1993. Interaction of rising frazil with suspended particles: tank experiments with applications to nature. Cold Reg. Sci. Technol. 21, 117–135.

Richard, M., Morse, B., Daly, S.F., Emond, J., 2011. Quantifying suspended frazil ice using multi-frequency underwater acoustic devices. River Res. Appl. 27, 1106–1117. doi:10.1002/rra.1446

Schaefer, V.J., 1950. The formation of frazil and anchor ice in cold water. Trans. Am. Geophys. Union 31, 885–893.

Verma, P.K., 2010. Optical Mineralogy. CRC Press, Boca Raton, FL.

Wuebben, J.L., 1984. The Rise Pattern and Velocity of Frazil Ice, in: Proceedings of the 3rd Workshop on the Hydraulics of Ice Covered Rivers. Committee on River Ice Processes and the Environment, Fredericton, New Brunswick, Canada, pp. 297–316.

Ye, S.Q., Doering, J., 2004. Simulation of the Supercooling Process and Frazil Evolution in Turbulent Flows. Can. J. Civ. Eng. 31, 915–926. doi:10.1139/L04-055

Ye, S.Q., Doering, J., Shen, H.T., 2004. A laboratory study of frazil evolution in a counter-rotating flume. Can. J. Civ. Eng. 31, 899–914. doi:10.1139/l04-056

Yoshikawa, Y., Watanabe, Y., Abe, T., Ito, A., 2014. Study of Frazil Particle Distribution and Frazil Transport Capacity, in: Proceedings of the 22nd IAHR International Symposium on Ice. International Association of Hydro-Environment Engineering and Research, Singapore, SG, pp. 679–686. doi:10.3850/978-981-09-0750-1

4 Field measurements of suspended frazil ice. Part I: A support vector machine learning algorithm to identify frazil ice particles

4.1 Introduction

Frazil ice particles form in turbulent, supercooled river flows as predominantly disc-shaped crystals. These particles have been observed to range from 22 μm to 6 mm in diameter in a variety of laboratory and field experiments (e.g. Clark and Doering, 2008; Daly and Colbeck, 1986; Gosink and Osterkamp, 1983; McFarlane et al., 2017, 2015; Osterkamp and Gosink, 1983). Osterkamp and Gosink (1983) were the first to provide underwater photographs of frazil ice crystals in the Chatanika River, Alaska. They estimated that the suspended frazil concentration ranged from 10^4 to 10^7 particles per m^3 and that most discs had diameters between 0.1 and 1 mm. McFarlane et al. (2017) obtained the first estimates of frazil ice particle size distributions using in-situ photographic techniques. The FrazilCam camera system developed at the University of Alberta was used to capture images of frazil ice crystals in the Kananaskis, North Saskatchewan, and Peace Rivers in Alberta. These measurements produced mean frazil ice particle diameters ranging from 0.73 to 1.20 mm and from 0.32 to 0.61 mm during the principal (i.e. the period between when the water temperature first drops below 0°C and when a relatively stable, residual supercooling temperature is reached) and residual supercooling phases, respectively. It was also noted that the frazil ice size distributions were "reasonably well described by a lognormal distribution" (McFarlane et al., 2017).

McFarlane et al. (2017) also uncovered a major issue that must be overcome when photographing suspended frazil ice particles in rivers: the ice particles are indistinguishable from small suspended sediment particles to the naked eye. This presents

a significant challenge when trying to calculate the size distribution and concentration of frazil ice particles, especially at the low concentrations observed during the principal supercooling process. Accurate identification of suspended sediment particles in images captured using the FrazilCam, or other similar photographic systems, is essential if accurate frazil ice measurements are to be obtained. McFarlane et al. (2017) attempted to minimise the impact of suspended sediment particles on their data by subtracting an appropriately scaled, randomly generated lognormal sediment size distribution. The mean and standard deviation of the sediment size distribution were computed from FrazilCam images collected when no ice was present at each site. This method produced reasonable size distributions of the frazil ice particles but at diameters of less than approximately 0.3 mm the accuracy varied greatly. In many cases the method completely eliminated all particles within a range of diameters from approximately 0.1 to 0.3 mm, resulting in frazil ice size distributions that were bimodal or abruptly cut-off.

A method that could accurately distinguish between the ice and sediment particles during the initial image processing, rather than trying to correct the distributions afterwards, should provide more accurate results. The new method that was developed is a type of machine learning algorithm called a classification support vector machine (SVM). SVM algorithms were trained specifically for each river to classify the particles detected in the images as either ice or sediment particles during the image processing stage. This methodology is shown to produce more accurate estimates of frazil ice size distributions as long as the suspended sediment concentration is not too high.

This paper has been split into two parts to allow for both the methodology and results to be covered with sufficient detail: Part I describes the development and validation of the

SVM and Part II (McFarlane et al., 2018a) presents and discusses the frazil ice particle size distributions calculated using the machine learning algorithm.

4.1.1 Brief Introduction to Machine-Learning

Machine-learning algorithms fall into two basic categories: supervised and unsupervised (Liang et al., 2011). A supervised machine-learning algorithm learns to differentiate between data classes by analysing examples of each and determining the differences between them. This requires that the algorithm be presented with examples of both the input variables and the desired output class for each data point in the training dataset (Liang et al., 2011). For example, the algorithm could be trained by analysing a large number of sediment particles and a large number of ice particles. Then, when applied to an image containing both ice and sediment, the algorithm would classify each particle based on its similarity to the ice and sediment particles that the algorithm had been trained on. An unsupervised algorithm, on the other hand, learns by observing input variables for multiple data classes at the same time without knowing which class any of the data points belong to (Cristianini and Shawe-Taylor, 2000). The algorithm breaks the data down into separate classes by finding patterns in the input variables. In this case, that would mean training the algorithm using images that contain both ice and sediment particles and asking the algorithm to break the data down into two distinct groups. The problem with using an unsupervised algorithm for this type of data lies in the validation process; since the ice and sediment particles are indistinguishable to the naked eye, it would be impossible to verify that the algorithm is accurately classifying the ice and sediment particles. For this reason, a supervised algorithm was considered the best option in this study.

The type of supervised algorithm that was used was a classification support vector machine (SVM). An SVM takes a set of n-dimensional input data that is difficult to classify and transforms it into an N-dimensional "feature space" (where $N > n$) wherein the data can be separated into two data classes using a linear separator called a hyperplane (Cortes and Vapnik, 1995). The function used to map the data in the feature space is called a kernel function. In the simplest case the dot-product of the input vectors is used for this transformation; this is a linear kernel function. However, other kernel functions can be used including higher-order polynomial functions. The kernel function is applied to each of the input vectors to produce a symmetric matrix called the kernel matrix, which represents the convolution of the dot-product between two input vectors and gives a measure of the similarity of the data in the higher-dimensional feature space (Liang et al., 2011).

Kalke and Loewen (2017) demonstrated the suitability of SVM algorithms for solving river ice problems by training an SVM to analyse aerial photographs captured at freeze-up. Once properly calibrated, the SVM was able to calculate accurate surface ice concentrations by determining which pixels corresponded to frazil pans and which were open water. Training images, with various lighting and ice conditions, were used and as a result the SVM could correctly classify the pixel regardless of the lighting and ice conditions of the input image.

4.2 METHODOLOGY

4.2.1 FIELD MEASUREMENTS

Images of suspended frazil ice crystals were captured using the FrazilCam system described by McFarlane et al. (2017). This system consists of a Nikon D800 digital single-lens reflex (DSLR) camera contained in a waterproof housing, which photographs frazil

ice crystals as they pass between two Cavision 7 cm × 7 cm glass polarising filters. The polarising filters are backlit with a 1/38,500 s pulse of light from a Nikon SB-910 Speedlight within a Subal SN-910 submersible housing. Water temperature data were also recorded during each deployment of the FrazilCam using an RBR SoloT temperature recorder (accuracy ± 0.002°C) at a frequency of 1 Hz.

Data were collected using the FrazilCam during three consecutive winter seasons: 2014-15, 2015-16, and 2016-17. However, only a handful of these deployments will be discussed in Part I in order to demonstrate both the accuracy and limitations of the SVMs. These deployments are briefly summarised in Table 4-1 and a naming convention is defined that will be used to refer to each deployment from this point onward. The deployments from the 2014-15 winter season have been described in detail by McFarlane et al. (2017) and are included again here as they will be re-analysed using the SVM. Four of the seven deployments that will be discussed in Part I were captured during the residual supercooling phase, with one principal supercooling event recorded at two different sites on the North Saskatchewan River (deployments NSR-1 and NSR-2) and one on the Peace River (PR-2).

At each of the sites listed in Table 4-1 (aside from the Fairview Water Intake on the Peace River) images were also captured when no ice was present, resulting in a set of ice-free images that could be used to determine the size distribution of the sediment particles visible to the FrazilCam at that site. It is important to note that the sediment distributions observed by the FrazilCam are not believed to represent the total suspended sediment size distribution in the river; instead, only particles that were thin enough to allow the polarised light to pass through them were visible in the images. These sediment data were used to train the SVM to identify the optical properties of sediment particles in the

photographs. The deployments during which sediment data were captured are outlined in Table 4-2. In some cases, sediment data were captured immediately prior to the supercooling events that would subsequently be processed using the SVMs. However, in other cases the sediment data were captured days, weeks, or even years before or after the frazil ice images were captured. Since the SVM was trained to identify sediment particles based on their optical properties, the size distribution and concentration of the sediment particles were not important. Therefore, if the optical properties of the visible sediment particles did not vary significantly with time, then the amount of time between when the sediment and frazil images were captured was irrelevant. It was assumed that the optical properties of the observed sediment particles were invariant as long as the sediment and ice images were captured under comparable flow conditions (e.g. sediment images captured at a high flow rate during a large runoff event would not be representative of the sediment present during the lower flows at freeze-up).

4.2.2 Machine Learning Methodology

Figure 4-1a shows a small region of an image captured in the Kananaskis River. The image contains several ice and sediment particles, but it is impossible to tell which particles are which simply by observing the image. To illustrate this, the final processed image showing the particles as classified by the SVM is shown in Figure 4-1b. Since the differences between the ice and sediment particles were indistinguishable to the naked eye, it was necessary to determine some sort of threshold that could be applied based on the characteristic properties of each particle. First, individual image characteristics such as the pixel intensities in different colour spaces were examined to see if there was a simple way to separate the two particle classes; for example, if sediment particles had a decidedly higher green intensity than ice particles in the red, green, blue (RGB) colour space then this could be used as a threshold to separate the two. However, after examining a number

of different characteristics manually, it was clear that a simple threshold did not exist. For this reason, the next logical step was to attempt to use multiple optical characteristics at once in a higher-dimensional space by training an SVM. Since all three rivers had different flow characteristics it was assumed that the optical properties of the sediment particles would vary from one river to the next; therefore, a different SVM would be trained for each river.

4.2.2.1 Pre-Processing

Pre-processing of each image series was required before it could be used for training the SVM. First, each image was processed to identify and label the individual particles present in the image, and to determine exactly which pixels in the image corresponded to each particle. This was done using the particle sizing algorithm described in detail by McFarlane et al. (2014). Next, the image was converted into three different colour spaces, each with three layers, which highlight different characteristics of the image. These colour spaces were the RGB colour space of the original image; the hue, saturation, value (HSV) colour space; and the L*a*b* colour space, in which L* represent the lightness, a* represents the red-green colour intensity, and b* gives the blue-yellow colour intensity. The L*a*b* colour space was formulated to represent the full range of colours both visible and invisible to the human eye. Six different properties were then calculated for each particle based on the intensity of each pixel in all three layers of each colour space. These were the minimum, maximum, mean, standard deviation, variance, and root mean square (RMS). This resulted in 54 properties that could be used to train the SVM. Additional properties were also tested but were not found to increase the accuracy of the SVM, so they were discarded to avoid overfitting the algorithm.

This process was performed on a number of different image sets that were used to train the SVM. For each river, the properties were calculated for at least one set of sediment images that had been captured when no ice was present in the river. These sets of sediment images were used to train the algorithm to identify the characteristics of the sediment particles in the corresponding river. In examining the sediment size distributions it was observed that the distribution from the Quesnell Bridge site had a slightly different shape than any of the other distributions. Figure 4-2 illustrates this by comparing the suspended sediment distributions observed during deployments NSR-S3 at Emily Murphy Park and NSR-S4 at the Quesnell Bridge. The different shape and the presence of larger particles in the NSR-S4 distribution indicated that slightly different sediment particles were present at this site than elsewhere in the North Saskatchewan River. For this reason a site-specific SVM was trained for the Quesnell Bridge site.

The other set of images that was required to train the algorithm was one that contained exclusively ice particles with no sediment particles present. However, since there were always sediment particles present in the three rivers when ice was photographed, such a dataset did not exist. Instead, a single set of images in which the ice particles vastly outnumbered the sediment particles was used. It was assumed that the optical properties of the frazil ice particles would not vary between rivers and therefore a single image set would be sufficient. These data were collected in the North Saskatchewan River on November 27, 2014 while it was snowing quite heavily (deployment NSR-3), which resulted in a very large number of seed particles and therefore produced an extremely high concentration of suspended frazil ice particles. This dataset was discussed in detail in McFarlane et al. (2017), where it was shown that the ice concentration was so much greater than the sediment concentration that the effects of suspended sediment on the frazil ice size distribution were negligible. This is supported by the fact that a concentration of 102

particles per image was observed during deployment NSR-3, while the largest concentration of sediment particles observed in the North Saskatchewan River using the FrazilCam when no ice was present that winter was only 6 particles per image.

4.2.2.2 Support Vector Machine Training

Training matrices were assembled using the pre-processed sediment data from each river and ice data from the North Saskatchewan River. Each of the training matrices was an $n \times 55$ array, where n was the combined number of ice and sediment particles. Columns 1 to 54 contained the properties calculated for each particle in each colour space, and column 55 was used to inform the training algorithm if a particular row corresponded to a sediment or ice particle, with one representing sediment and two representing ice. Details regarding when each of the training image sets was captured are presented in Table 4-3. Since there were a small number of sediment particles present in the 'ice' data used for training the SVM, greater emphasis was placed on training the algorithm to correctly identify sediment particles rather than ice particles. It was more desirable to accurately classify sediment particles because this would remove sediment from the raw distributions with greater certainty, even if a small number of ice particles were inadvertently removed as well. This was achieved by adjusting the ratio of sediment to ice particles used in training the SVMs, and it was found that a 3:1 sediment to ice ratio resulted in a greater accuracy when classifying the sediment particles. For the Kananaskis and Peace Rivers, and for the Emily Murphy Park site on the North Saskatchewan River, 15,000 sediment particles and 5,000 ice particles were used in training. However, since only 6,637 sediment particles were captured at the Quesnell Bridge site, only 2,212 ice particles were used to train the algorithm in order to maintain the 3:1 ratio at that site.

The training matrices for each river were loaded into the Classification Learner application that is included in Statistics and Machine Learning Toolbox in MATLAB. Using the Classification Learner application a number of different classification SVMs can be trained simultaneously, and the performance of each can then be compared by assessing their accuracy when applied to subsets of the training data. Comparing the validation results for linear, quadratic, cubic, and Gaussian SVMs, the quadratic SVM was found to be the most accurate model for each river. The quadratic SVM uses the quadratic kernel function shown in Equation 1 below (Cortes and Vapnik, 1995):

$$K(\boldsymbol{x_j}, \boldsymbol{x_k}) = \left(1 + \boldsymbol{x_j} \bullet \boldsymbol{x_k}\right)^2 \qquad [1]$$

where $K(\boldsymbol{x_j},\boldsymbol{x_k})$ is an entry in the kernel matrix, $\boldsymbol{x_j}$ and $\boldsymbol{x_k}$ are $n \times 1$ input vectors for a particular data point with n input variables, and • denotes the dot-product of two vectors. Detailed validation results for each SVM are presented in Table 4-4, as calculated using five-fold cross-validation by the Classification Learner app. Five-fold cross-validation works by splitting the training dataset into five different segments, or "folds", and using four of the five folds to train the model while the fifth fold is withheld and used to test the model. This procedure is repeated five times, with a different fold being withheld for validation each time. The final validation result is the result of averaging the five validation scores obtained from each individual fold. The SVMs for each river were able to identify sediment particles with ~98% accuracy, and determined that ~86% of the 'ice' particles used in training were, in fact, ice. A lower validation accuracy for the ice particles was expected since there was a small amount of sediment present in the ice training data. This decreases the validation accuracy for the ice particle training set because the sediment particles in the 'ice' training data will be identified as sediment, leading the algorithm to label them as having been misclassified.

4.2.2.3 Image Analysis Using the SVM

The four trained SVM algorithms were then added into the image-processing algorithm used for the bulk analysis of the FrazilCam images. The SVM was used to classify each individual particle as ice or sediment on an image-by-image basis. Each ice particle was also checked using the same fitted ellipse criteria described by McFarlane et al. (2014) to determine whether it was disc-shaped or not, with only the disc-shaped particles being classified as frazil while the non-disc particles included frazil particles that had begun to grow in a dendritic manner, pieces of skim ice, released anchor ice, and frazil flocs. In the case of three deployments (PR-1, KR-1, and KR-2) where a large floc or ice growth on the polarisers obstructed a relatively constant portion of the images throughout the deployment, the processing efficiency and accuracy was further improved by applying a mask to that portion of the images during processing (i.e. blacking out that section of the images completely).

4.3 Results

Each of the deployments from the winter of 2014-15 that were previously analysed by McFarlane et al. (2017) were reanalysed using the SVM algorithms, with one exception: the deployment from November 27, 2014 at Emily Murphy Park was used in training all four of the SVMs and thus could not be reanalysed. The size distribution properties for each of these deployments are presented in Table 4-5 and compared to the estimates obtained by McFarlane et al. (2017) (shown in brackets). Each of these size distributions were also plotted for comparison to the distributions obtained by McFarlane et al. (2017). These are shown in Figure 4-3 with a non-dimensionalised y-axis to allow for a direct comparison of the size distribution shapes. It is clear when comparing the distributions calculated using the two different methods that the SVM retained a much larger number of particles in the 0.1 to 0.3 mm diameter range. As a result, the mean particle diameter

decreased by 7% to 23% in all four cases. While the number of retained frazil particles increased for deployments NSR-1 and NSR-2, it actually decreased for the two KR deployments. For KR-1, this was primarily due to the removal of the spike in particles less than 0.1 mm in diameter that appear in Figure 4-3a but not in Figure 4-3b. The cause of the decrease in particle numbers for KR-2 is instead due to the elimination of more particles in the 0.12 to 2.1 mm diameter range, as a large amount of sediment in this size range was evidently present but not accounted for using the sediment subtraction technique.

Use of the SVM also made it possible to determine the size distribution of frazil ice particles observed on the Peace River on December 19, 2014 (deployment PR-1) for the first time; this deployment could not be adjusted for the effects of sediment by McFarlane et al. (2017) since ice-free images had not yet been captured on the Peace River. The raw size distribution and the frazil ice particle size distribution computed with the application of the SVM for deployment PR-1 are compared in Figure 4-4. The frazil ice distribution very closely resembles the lognormal distribution calculated with the same mean and standard deviation as the observed frazil ice particles and the effect of sediment on the frazil ice distribution is minimal, despite the large peak in the raw distribution caused by the sediment particles at a diameter of ~0.08 mm.

4.4 Discussion

Comparison of the frazil ice size distributions obtained using the SVM to those estimated by subtracting the sediment distribution (presented in Figure 4-3) demonstrates the advantages of using the SVM algorithms. Numerous laboratory studies (e.g. Clark and Doering, 2008, 2006; Daly and Colbeck, 1986; McFarlane et al., 2015) have concluded that the size distribution of frazil ice particles tends to be lognormal in shape, and the most

accurate size distribution from field measurements reported by McFarlane et al. (2017), for deployment NSR-3, was almost perfectly lognormal. The SVM frazil ice distributions have a greater similarity to the expected lognormal distribution in all cases, and do not have a sudden drop-off or gap in the data for particles with diameters in the range of 0.1 to 0.2 mm. This is particularly evident for deployments NSR-2 and KR-2. However, the distributions from deployments NSR-1 and KR-1, though improved, are not as lognormal as those for NSR-2 and KR-2. It seems as though these three deployments were right on the limit of the sediment to ice ratio that the SVM can handle.

Table 4-6 presents the sediment to frazil ice particle ratio calculated using the SVM for each deployment, and size distributions plotted in terms of raw particle counts obtained from deployments NSR-1, NSR-2, KR-1, and KR-2 with and without the application of the SVM are compared in Figure 4-4 and Figure 4-5. It is clear in the cases of NSR-1 (Figure 4-5a), and KR-1 (Figure 4-5c) that the number of sediment particles outnumbers the ice particles, as evidenced by the large peak in the raw size distributions at a diameter of ~0.1 mm. These two deployments had sediment to frazil ice ratios of 3.7 and 14, respectively. If there had been much more sediment present in any of the three cases, the impact of sediment on the resulting frazil ice distribution after application of the SVM would have been too significant to draw any conclusions about the size distribution properties. For deployments NSR-2 and KR-2 (Figure 4-5b and Figure 4-5d, respectively) the influence of sediment is much less pronounced in the raw distribution and the sediment to frazil ice ratios are 1.1 and 1.5, respectively. The resulting frazil ice distributions obtained using the SVM have a much stronger resemblance to the expected lognormal distribution for both of those deployments.

Despite the prevalence of sediment in NSR-1 and KR-1, the resulting SVM frazil ice distributions are still useable, and an improvement over the methodology used by McFarlane et al. (2017) as demonstrated in Figure 4-3. However, since the SVM is not able to identify sediment particles with 100% accuracy, the computed frazil ice size distribution becomes inaccurate if the ratio of sediment particles to frazil ice particles is too high. This is demonstrated in Figure 4-6 where the raw particle size distribution and the frazil ice size distribution computed using the SVM algorithm for deployment PR-2 are compared. This deployment had an extremely high sediment concentration and, as it took place during a principal supercooling event when frazil production was just beginning, relatively few ice particles were present. Even though the SVM was still functioning as expected, correctly identifying and eliminating ~98% of the sediment particles (e.g. 98.1% of particles in the 0.1 mm bin and 97.3% in the 0.12 mm bin were eliminated), there was such a large number of sediment particles that the ~2% that were misclassified as ice greatly outnumbered the actual ice particles. As a result, the sediment to frazil ice ratio was 25 and the SVM frazil ice size distribution in Figure 4-6 still had a dominant peak centred at ~0.15 mm that corresponded to the sediment particles.

This is a limitation that must be considered when applying the SVM to future datasets. If the amount of sediment present outnumbers the ice to the extent that the ice particles are hardly visible in the raw size distribution, the SVM will not be effective enough to salvage the frazil ice distribution from the raw data. Considering the sediment to frazil ice ratios presented inTable 4-6, the largest ratio that resulted in acceptable data was 14 for deployment KR-1, and even this appeared to be right on the limit of the sediment to frazil ratio that the SVM could handle. This suggests that for sediment to frazil ratios greater than 14 the algorithm cannot be relied on to produce accurate frazil ice size distributions. In cases where this ratio is very near 14, a judgment call must be made based on the

resulting frazil ice size distribution produced by the SVM. If it appears that there is still a large peak in the 0.1 to 0.15 mm diameter range, the frazil ice distribution is likely compromised by suspended sediment particles. On the other hand, if the most prominent peak in the frazil ice size distribution corresponds to the ice particles and not the sediment, then the distribution may be representative of the suspended frazil crystals. This must be evaluated on a case-by-case basis.

In order to avoid situations where the frazil ice distribution cannot be resolved, efforts must be made to minimise the amount of sediment in the raw images. Based on the deployments that are analysed in this paper, a few recommendations can be made that will be taken into account during any future FrazilCam deployments. The most important consideration is to choose a deployment location with coarse bed material. The deployment locations for KR-1 and PR-2 had very fine, sandy material on the bed that, with the slightest disturbance, would become entrained in the flow. Other deployments that had more favourable sediment to frazil ice ratios (e.g. KR-2 and PR-1) had much coarser bed material. Alternatively, great care must be taken to avoid disturbing the bed material near the FrazilCam while the deployment is underway. Additionally, deployment locations with moderate flow velocities (i.e. greater than ~0.5 m/s) should be selected. Comparing deployments KR-1 and KR-2, for example, the local depth-averaged water velocities were 0.27 and 0.63 m/s, respectively, and KR-2 resulted in a far more favourable sediment to frazil ice ratio. However, there is a practical limit to the water velocity in which the FrazilCam can be deployed. As the velocity approaches one metre per second at a suitable depth for the FrazilCam (i.e. greater than 0.5 m) certain tasks that are required while operating the FrazilCam become impossible, and if the velocity and depth are too great it is no longer safe to wade in the water. Velocities that are too high could also result in increased suspended sediment concentrations in the flow.

In addition to these recommendations, future studies should focus on improving the accuracy of the machine learning algorithm. If a dataset were collected that contained exclusively ice particles with no suspended sediment present, this would almost certainly help with the development of a more accurate SVM. Alternatively, the use of another type of machine learning algorithm could potentially improve upon the accuracy of the SVM algorithms. However, until improvements to the accuracy of the algorithm are made, the SVM algorithms still offer many advantages over the previous size distribution subtraction method used by McFarlane et al. (2017). The subtraction method required the assumption that the shape and size of the sediment size distribution was the same before and after ice formed in the river, meaning the sediment images should ideally be captured at the deployment site immediately prior to the beginning of a supercooling event. This assumption is not required when applying the SVM algorithms. Instead, the SVM algorithms simply require the assumption that the optical properties of the visible sediment particles in a particular river do not vary with time. Therefore, training images of sediment particles must only be captured at a comparable flow rate in order to determine their optical properties, and these images can easily be acquired in the weeks leading up to freeze-up. This is more realistic and less restrictive than assuming the shape of the sediment size distribution is invariant with time and allows for much more flexibility in the timing of field work.

4.5 CONCLUSIONS

Classification SVM algorithms have been successfully trained to distinguish between suspended frazil ice and fine sediment particles captured using the FrazilCam in the Kananaskis, North Saskatchewan, and Peace Rivers in Alberta. By processing sets of training images corresponding to the ice and sediment particle classes and presenting the SVM with 54 input variables to aid in classifying each particle, the algorithm can

successfully identify and remove sediment particles with 98% accuracy. This has made it possible to analyse data presented by McFarlane et al. (2017) with greater accuracy and confirm the overall trends that they reported. The SVM method also allows for more flexibility in the timing of when the sediment data are captured, as the exact shape of the sediment size distribution present during the supercooling event does not need to be known, but only the optical properties of the sediment particles present at that site. This method can also be easily adapted for use in different rivers provided that the necessary training data is available.

However, there are limitations to the SVM algorithms. If the suspended sediment concentration is too high during the deployment, the sediment particles will still have an impact on the resulting size distribution. This impact is too large to ignore at sediment to frazil ice ratios greater than 14. In order to avoid this scenario it is recommended that efforts are made during future FrazilCam deployments to choose locations with coarse bed material and moderate flow velocities. It is also important to focus on improving the classification accuracy of the machine learning algorithms. Although the SVMs presented in this paper were 98% accurate in classifying sediment particles, a higher accuracy would result in greater confidence in the resulting frazil ice size distributions, and make it possible to study frazil particles produced at lower concentrations in slower flows with finer bed material.

FIGURES

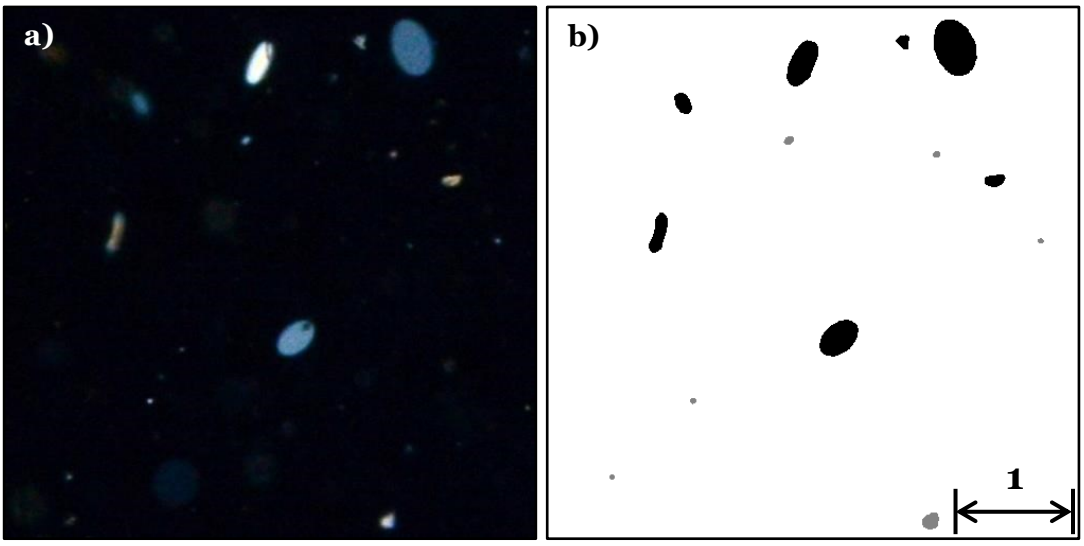

Figure 4-1: a) A small portion of a raw image captured in the Kananaskis River, and b) the SVM processed image where gray particles are sediment and black particles are ice. Note the small scale of the particles, with the largest particle being 0.5 mm in diameter.

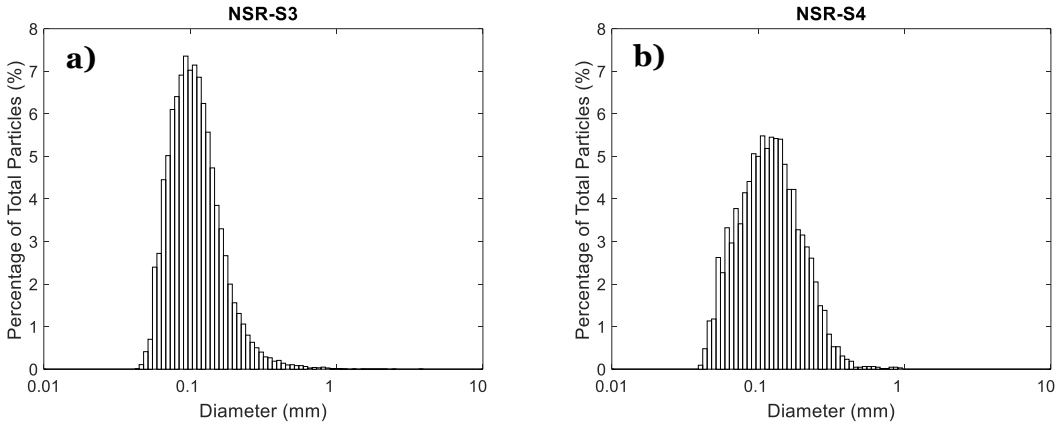

Figure 4-2: Comparison of the sediment size distributions observed during deployments a) NSR-S3 at Emily Murphy Park and b) NSR-S4 at the Quesnell Bridge. The different sediment distribution at the Quesnell Bridge site led to the creation of a site-specific SVM.

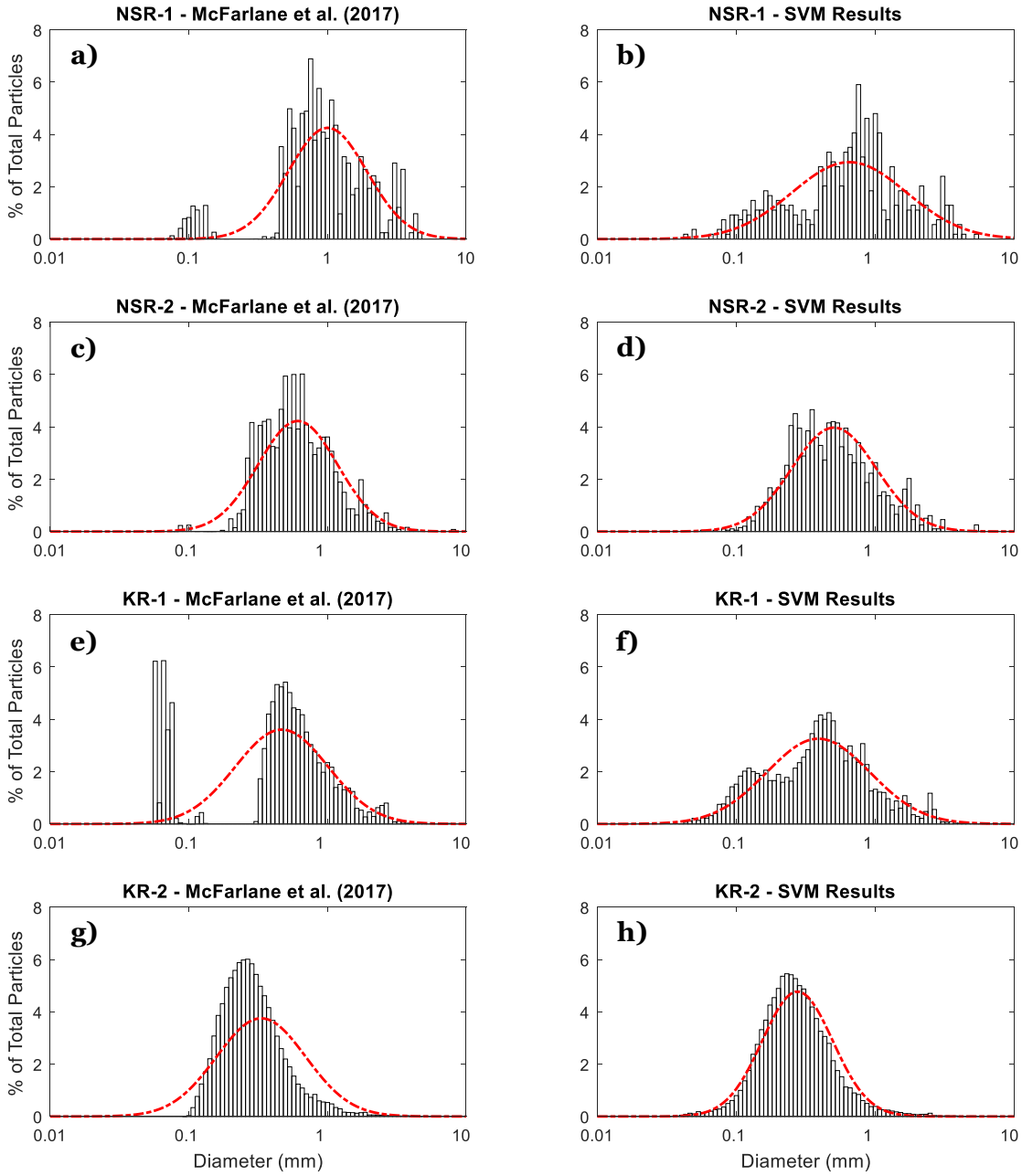

Figure 4-3: Comparison of the frazil ice size distributions estimated by McFarlane et al. (2017) (left column) to those calculated using the SVM (right column). The red dashed line indicates a lognormal distribution with the same mean and standard deviation as the observed particles.

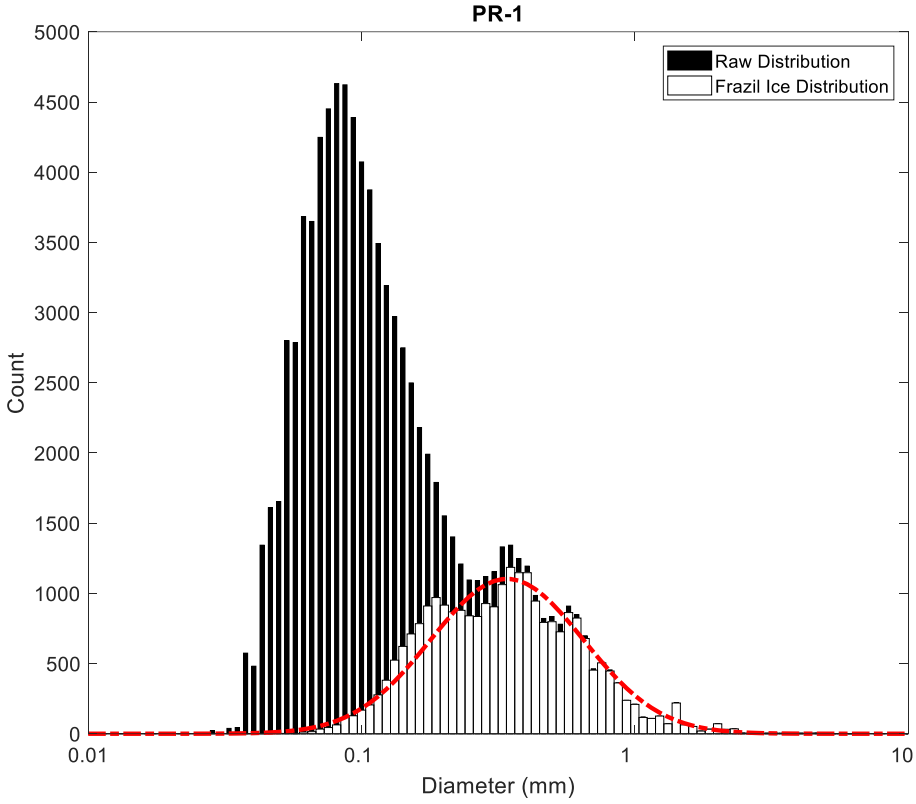

Figure 4-4: Comparison of the size distribution from deployment PR-1 before (black bars) and after (white bars) the SVM had been applied. The red dashed line indicates a lognormal distribution with the same mean and standard deviation as the observed particles.

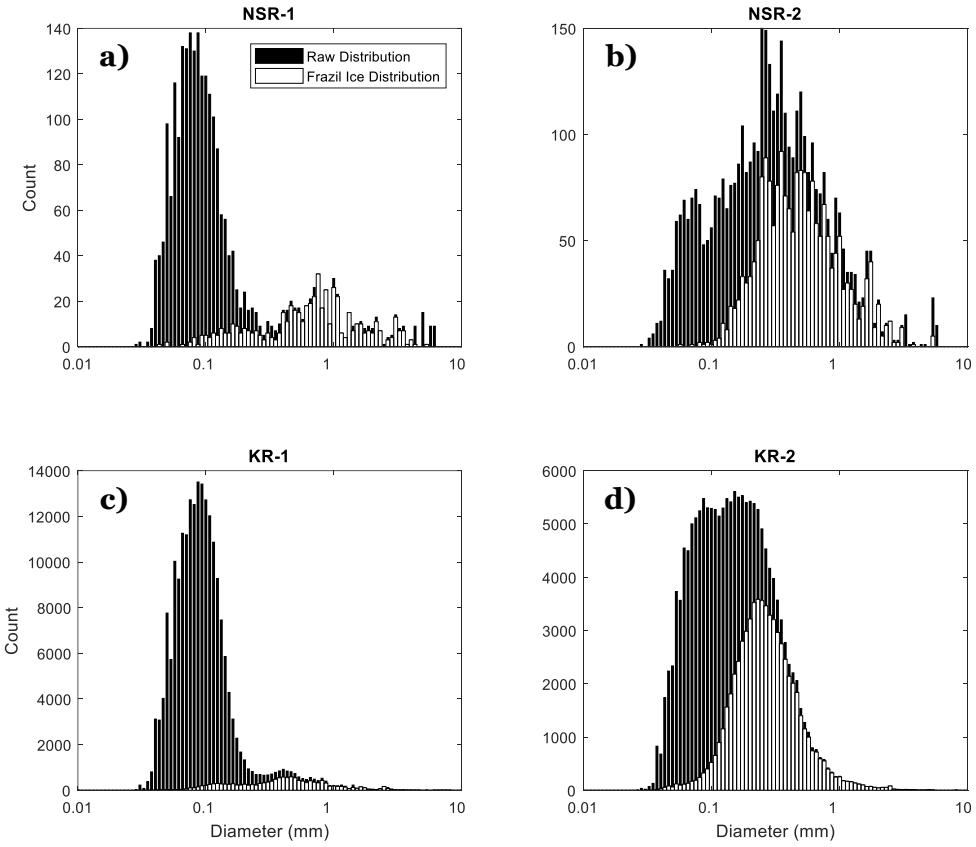

Figure 4-5: Comparison of the raw distributions to the frazil ice distributions obtained using the SVM for deployments a) NSR-1, b) NSR-2, c) KR-1, and d) KR-2.

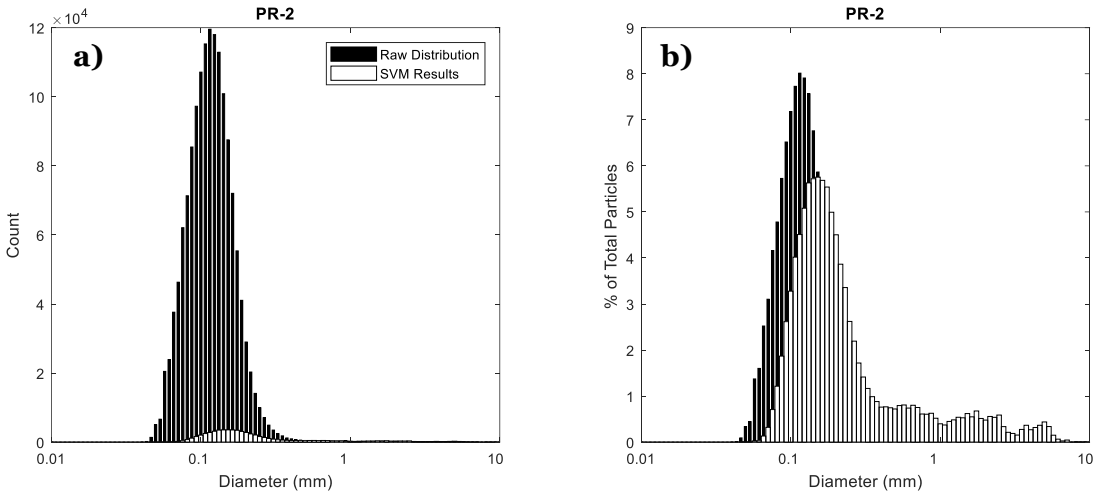

Figure 4-6: Comparison of the size distribution observed for deployment PR-2 before and after the SVM had been applied, plotted a) in terms of raw particle count to demonstrate the difference in magnitude between the sediment and ice crystals, and b) non-dimensionalised to illustrate the resulting shape of the distribution after the SVM had been applied. The effects of suspended sediment are still clearly visible after application of the SVM since such a large concentration of sediment was observed.

TABLES

Table 4-1: Summary of the FrazilCam deployments

River	Deployment name	Site	Date	Image capture frequency	Stage of supercooling
North Saskatchewan	NSR-1	Government House Park	November 10, 2014	9 images at 1 Hz every 90 s	Principal
	NSR-2	Quesnell Bridge	November 10, 2014	9 images at 1 Hz every 90 s	Principal
	NSR-3	Emily Murphy Park	November 27, 2014	1 Hz	Residual
Peace	PR-1	Fairview Water Intake	December 19, 2014	1 Hz	Residual
	PR-2	Shaftesbury Ferry	January 22, 2017	1 Hz	Principal
Kananaskis	KR-1	Opal Day Use Area	March 1, 2015	9 images at 1 Hz every 18 s	Residual
	KR-2	Village Bridge	March 1, 2015	9 images at 1 Hz every 18 s	Residual

Table 4-2: The sites on each river where sediment size distribution data were recorded.

River	Deployment name	Site	Date(s)
North Saskatchewan	NSR-S1	Government House Park	November 10, 2014
	NSR-S2 NSR-S4	Quesnell Bridge	November 10, 2014 November 19, 2016
	NSR-S3	Emily Murphy Park	November 5, 2015
Peace	PR-S1	Shaftesbury Ferry Crossing	January 21, 2017
Kananaskis	KR-S1	Opal Day Use Area	March 2, 2015
	KR-S2	Village Bridge	March 2, 2015

Table 4-3: Details of the image sets used to train the SVM.

River	Site	Date	Data type	Number of particles used for training
North Saskatchewan	Emily Murphy Park	November 27, 2014	Ice	5,000 (2,212)[6]
North Saskatchewan	Emily Murphy Park	November 5, 2015	Sediment	15,000
North Saskatchewan	Quesnell Bridge	November 19, 2016	Sediment	6,637
Kananaskis	Opal Day Use Area	March 2, 2015	Sediment	15,000
Peace	Shaftesbury Ferry	January 21, 2017	Sediment	15,000

Table 4-4: The percentage of sediment and ice particles correctly identified by each SVM.

SVM	Sediment Particles	Ice Particles
Kananaskis	98 %	85 %
North Saskatchewan-1	97 %	89 %
North Saskatchewan-2	97 %	84 %
Peace	98 %	86 %

[6] In order to maintain the 3:1 sediment to ice particle ratio, 2,212 ice particles were used when training the SVM for the Quesnell Bridge site since only 6,637 sediment particles were observed at that site.

Table 4-5: Frazil ice size distribution properties determined using the SVM algorithms, compared to the results of McFarlane et al. (2017) (in brackets).

Deployment name	Mean, μ (mm)	Standard deviation, σ(mm)	Number of particles
NSR-1	0.93 (1.20)	0.85 (0.88)	542 (413)
NSR-2	0.63 (0.73)	0.55 (0.54)	1,975 (1,262)
PR-1	0.41	0.33	25,511
KR-1	0.54 (0.61)	0.53 (0.55)	13,871 (14,419)
KR-2	0.32 (0.34)	0.27 (0.34)	65,736 (97,341)

Table 4-6: Sediment to frazil ice particle ratio calculated based on the SVM results.

Deployment name	Sediment to frazil ice particle ratio
NSR-1	3.7
NSR-2	1.1
PR-1	2.6
PR-2	25
KR-1	14
KR-2	1.5

ACKNOWLEDGMENTS

We would like to thank the Natural Sciences and Engineering Research Council of Canada (NSERC) for supporting this project (RGPIN-2015-04670 and RGPAS 477890-2015), Perry Fedun for his valuable technical assistance, and Hayden Kalke and Chris Schneck for their help with field work.

REFERENCES

Clark, S., Doering, J., 2006. Laboratory Experiments on Frazil-Size Characteristics in a Counterrotating Flume. J. Hydraul. Eng. 132, 94–101. doi:10.1061/(ASCE)0733-9429(2006)132:1(94)

Clark, S., Doering, J., 2008. Experimental investigation of the effects of turbulence intensity on frazil ice characteristics. Can. J. Civ. Eng. 35, 67–79. doi:10.1139/L07-086

Cortes, C., Vapnik, V., 1995. Support-vector networks. Mach. Learn. 20, 273–297. doi:10.1007/BF00994018

Cristianini, N., Shawe-Taylor, J., 2000. An Introduction to Support Vector Machines and Other Kernel-based Learning Methods. Cambridge University Press, Cambridge. doi:10.1017/CBO9780511801389

Daly, S.F., Colbeck, S.C., 1986. Frazil ice measurements in CRREL's flume facility, in: Proceedings of the IAHR Ice Symposium 1986. International Association for Hydraulic Research, Iowa City, Iowa, USA, pp. 427–438.

Gosink, J.P., Osterkamp, T.E., 1983. Measurements and Analyses of Velocity Profiles and Frazil Ice-Crystal Rise Velocities During Periods of Frazil-Ice Formation in Rivers. Ann. Glaciol. 4, 79–84. doi:10.3189/S0260305500005279

Kalke, H., Loewen, M., 2017. Predicting Surface Ice Concentration using Machine Learning, in: Proceedings of the 19. CGU HS Committee on River Ice Processes and the Environment, Whitehorse, YK, Canada, p. 17.

Liang, Y., Xu, Q.-S., Li, H.-D., Cao, D.-S., 2011. Support vector machines and their application in chemistry and biotechnology. CRC Press, Boca Raton, FL.

McFarlane, V., Loewen, M., Hicks, F., 2014. Laboratory measurements of the rise velocity of frazil ice particles. Cold Reg. Sci. Technol. 106–107, 120–130. doi:10.1016/j.coldregions.2014.06.009

McFarlane, V., Loewen, M., Hicks, F., 2015. Measurements of the evolution of frazil ice particle size distributions. Cold Reg. Sci. Technol. 120, 45–55. doi:10.1016/j.coldregions.2015.09.001

McFarlane, V., Loewen, M., Hicks, F., 2017. Measurements of the size distribution of frazil ice particles in three Alberta rivers. Cold Reg. Sci. Technol. 142, 100–117.

doi:10.1016/j.coldregions.2017.08.001

McFarlane, V., Loewen, M., Hicks, F., 2018a. Field measurements of suspended frazil ice. Part II: Observations and analyses of frazil ice properties during the principal and residual supercooling phases. Submitted to Cold Reg. Sci. Technol.

Osterkamp, T.E., Gosink, J.P., 1983. Frazil ice formation and ice cover development in interior Alaska streams. Cold Reg. Sci. Technol. 8, 43–56. doi:10.1016/0165-232X(83)90016-2

5 FIELD MEASUREMENTS OF SUSPENDED FRAZIL ICE. PART II: OBSERVATIONS AND ANALYSES OF FRAZIL ICE PROPERTIES DURING THE PRINCIPAL AND RESIDUAL SUPERCOOLING PHASES

5.1 INTRODUCTION

Frazil ice particles form during the earliest stages of the river freeze-up process when the water temperature supercools to a fraction of a degree below zero. These typically disc-shaped particles have been extensively studied in laboratory environments and it has been determined by many researchers that the size distribution of the particles is well described by a lognormal distribution (e.g. Clark and Doering, 2008, 2004; Daly and Colbeck, 1986; McFarlane et al., 2015; Ye et al., 2004). Frazil particles have been observed to range in diameter from 22 μm to 6 mm (Gosink and Osterkamp, 1983; McFarlane et al., 2015), and the parameters describing the size distribution evolve throughout the supercooling process (Clark and Doering, 2008; McFarlane et al., 2015; Ye et al., 2004). These properties include the mean and standard deviation of the particle diameter and the number of suspended frazil crystals. Ye et al. (2004), Clark and Doering (2009, 2008, 2006), and McFarlane et al. (2015) all observed that the number of frazil particles increased quite slowly at the beginning of a supercooling event and then much more rapidly as the maximum degree of supercooling was reached, with the peak number of particles being achieved shortly thereafter. The number of particles subsequently decreased as particles began to flocculate and, eventually, rose to the surface. McFarlane et al. (2015) also noted that the mean particle diameter reached a maximum at approximately the same time as the maximum supercooling occurred, then decreased and leveled off at a stable value. The standard deviation of the particle sizes followed a similar

trend to the mean particle diameter, although the peak standard deviation was reached slightly before the maximum supercooling (McFarlane et al., 2015).

One of the most difficult properties to quantify for frazil ice crystals is the volume concentration, and there have been some discrepancies between the values obtained using various methods. Few laboratory studies have attempted to measure frazil volume concentration, with Ettema et al. (2003) reporting volume concentrations of 6.6 to 61 × 10^{-4} m^3/m^3 and Ghobrial et al. (2012) finding concentrations of 1.3 to 14.7 × 10^{-4} m^3/m^3. Both of these values were obtained by collecting the frazil from a known volume of water using a fine mesh or sieve, and weighing the collected ice. Tsang (1986, 1984) developed comparative resistance probes to measure volume concentrations and reported mean values of ~6 × 10^{-3} m^3/m^3 in the laboratory and ~2.5 × 10^{-3} m^3/m^3 in the field. Many other measurements have been attempted in field settings using acoustic instruments (e.g. Ghobrial et al., 2013b; Jasek et al., 2011; Marko et al., 2015; Marko and Jasek, 2010a, 2010b; Richard et al., 2011) and have yielded volume concentrations ranging from 0.2 to 45 × 10^{-5} m^3/m^3 and number concentrations of 10^5 to 4 × 10^7 particles/m^3. Jasek et al. (2011) found that volume concentrations in the Peace River predicted using a numerical model were approximately an order of magnitude larger than those measured using acoustic instruments, reporting typical values of 1.5 × 10^{-3} and 1.5 × 10^{-4}, respectively. Other studies using photographic methods have only reported the number concentration, with Osterkamp and Gosink (1983) giving an estimate on the order of 10^4 to 10^7 particles/m^3 in the Chatanika River, Alaska; Daly and Colbeck (1986) observing 0.17 to 0.982 × 10^6 particles/m^3 in a refrigerated flume facility; and McFarlane et al. (2015) reporting 0.29 to 1.8 × 10^6 particles/m^3 in the cold room facility at the University of Alberta.

Attempts at measuring frazil ice particle sizes in field environments have been relatively few and met with various levels of success. Most measurements of particle size have been made via indirect means such as acoustic devices (e.g. Ghobrial et al., 2013b; Marko et al., 2015; Marko and Jasek, 2010b; Richard et al., 2011). Direct, in-situ measurements have been far less common with only Osterkamp and Gosink (1983) and McFarlane et al. (2017) reporting particle sizes based on underwater photographs of suspended frazil ice crystals. Osterkamp and Gosink (1983) deployed a camera in the Chatanika River, Alaska, and observed discs with diameters that were predominantly in the range of 0.1 to 1.0 mm but some were as large as 5 mm. McFarlane et al. (2017) measured the size distribution of particles in the Kananaskis and North Saskatchewan Rivers in Alberta and estimated mean particle sizes ranging from 0.32 to 1.2 mm. However, their results were affected by the presence of very small suspended sediment particles in the images that were optically very similar to small frazil crystals. To minimise the impact of these suspended sediment particles on the frazil ice size distributions a portion of each size distribution centering on a particle size of 0.10-0.12 mm had to be subtracted from the overall distribution. However, this method completely eliminated certain portions of the frazil ice size distribution corresponding to frazil particles with very small diameters, potentially causing an overestimation of the mean frazil particle diameter. A summary of the size distribution properties observed in these and other laboratory and field studies of frazil crystals is provided by McFarlane et al. (2017).

In order to improve on the results presented by McFarlane et al. (2017), a type of machine learning algorithm known as a classification support vector machine (SVM) was trained for use in each of the three rivers. This improved upon the analysis method used by McFarlane et al. (2017) as the SVM decides on a particle-by-particle basis whether it should be classified as ice or sediment, rather than attempting to correct the size

distribution in an approximate manner once the image processing is complete. The SVM algorithm is presented and discussed in detail by McFarlane et al. (2018b) and its efficacy demonstrated by reanalysing the data presented by McFarlane et al. (2017). After reanalysis, the mean particle diameters were found to range from 0.32 to 0.93 mm.

In the current study, additional frazil ice particle size distribution data were captured in the Kananaskis, North Saskatchewan, and Peace Rivers in Alberta using the same FrazilCam system described by McFarlane et al. (2017). These images were captured during both the principal (i.e. between when supercooling is first achieved and when the residual supercooling temperature is reached) and residual (i.e. when the water temperature levels off at a relatively stable temperature slightly below 0°C) supercooling phases in all three rivers, and data were also collected when no ice was present to determine the suspended sediment characteristics at each site. The SVMs described by McFarlane et al. (2018b) were applied to data collected during the 2014-15, 2015-16, and 2016-17 winter seasons to calculate the frazil ice particle size distributions and suspended frazil ice volume concentration.

5.2 METHODOLOGY

The locations of the Kananaskis, North Saskatchewan, and Peace Rivers within the province of Alberta are shown in Figure 5-1a. These three rivers were selected based on several factors, including: accessibility, prior-knowledge, and scale. The North Saskatchewan was the most accessible since it runs through Edmonton and there are multiple access points near the University of Alberta, making it convenient to work in on short notice. The other two rivers are both within a five-hour drive of Edmonton and offered a selection of access points along the study reach. This was important since it is difficult to predict exactly where and when supercooling will occur on the river, and having

multiple access points allows some flexibility; if principal supercooling had already occurred at a downstream site, it may not yet have occurred at a site further upstream.

The North Saskatchewan River was also the easiest to monitor since it was nearby, but prior-knowledge and experience were very valuable in deciding when to plan fieldwork trips for the other two rivers. A previous University of Alberta study had focussed on the Kananaskis River as part of a different project, and as such an extensive history of water temperatures at several sites and over multiple winter seasons was available to assist in decision making. As for the Peace River, it is continuously monitored and modelled by BC Hydro, who kindly provided updates regarding the ice conditions on the river and predictions of when supercooling would occur. The mean flow rate, water depth, and channel width for each of the three rivers are presented in Table 5-1. As these three rivers were all of different scales they also offered the opportunity to examine frazil particles in rivers with varying flow characteristics.

5.2.1 INSTRUMENTATION

All of the frazil ice images were captured using the FrazilCam system described by McFarlane et al. (2017) and shown in Figure 5-2. Each FrazilCam consisted of a Nikon D800 digital single-lens reflex (DSLR) camera using a Micro-Nikkor 60 mm f/2.8D lens, focused to capture images of frazil crystals as they passed through a 2.2 cm gap between two glass 7 cm × 7 cm Cavision polarising filters. The polarisers were rotated 90° with respect to each other to filter out any light passing through them that was not refracted by an ice crystal or sediment particle. The images were backlit by a Nikon SB-910 Speedlight with a pulse duration of 1/38,500 s, diffused by a 5 mm thick sheet of white acrylic and directed through the polarising filters and towards the camera lens. Each of the electronic components were enclosed in waterproof housings; one Aquatica AD800 housing and one

Ikelite D800 housing were used for the two cameras, and Subal SN-910 housings were used for both of the SB-910 Speedlights.

During each deployment an RBR SoloT temperature logger (accuracy ± 0.002°C) was mounted to the frame of each FrazilCam to collect temperature data at a frequency of 1 Hz throughout the deployment. In the winters of 2015-16 and 2016-17, RBR SoloT loggers were also mounted on the bed at many of the sites throughout the entire winter to collect a seasonal temperature profile, and an RBR SoloTu turbidity logger (< 2% deviation 0-750 FTU) was also affixed to each FrazilCam. Onset HOBO weather stations were also deployed on the banks of each river throughout the 2016-17 season to monitor the air temperature, barometric pressure, relative humidity, wind speed and direction, and incoming short-wave (solar) radiation. Flow characteristics were measured during most deployments using a SonTek Flow Tracker handheld acoustic Doppler velocimeter (ADV) and a Nortek Aquadopp acoustic Doppler current profiler (ADCP).

5.2.2 FIELD DEPLOYMENTS

Each of the deployment sites on all three rivers are labelled in Figure 5-1. Frazil ice data were captured during either the principal or residual supercooling phases, and ice-free images were also collected when no ice was present at each of these sites with the exception of Fortress. The deployments from all three seasons are detailed in Table 5-2 and a deployment numbering system is introduced that will be used to refer to specific deployments throughout the rest of this paper. The water velocity was observed to be essentially constant throughout all deployments except for KR-5. This was because a hydropeaking wave reached the deployment site while the deployment was underway, causing a rapid increase the flow rate, depth, and velocity. Deployment KR-5 was aborted early as a result and it was not safe to wade into the river and measure the increased water

velocity with the handheld ADV. The water velocity for deployment NSR-5 was measured at the same location the day before; however, the water level was observed to be the same on both days as was confirmed using water level data downloaded from the Alberta River Basins website (https://rivers.alberta.ca).

In certain cases (denoted with an asterisk next to the deployment number in Table 5-2) the data were affected by flocs adhering to or ice crystals growing on the polarisers. In the case of deployment number NSR-4B ice crystals were not an issue, but there was a long piece of grass that became caught on the polariser frame early in the deployment and it was slightly visible in many of the images. These issues would slightly affect the calculation of the disc-shaped particle percentage during processing because a larger number of non-disc particles would be visible in the images. However, in some cases the region that was obstructed by stationary ice crystals was nearly constant in size and position throughout the deployment, so this region was simply masked out during image processing. This was the case for deployments PR-1, KR-1, and KR-2. In these three cases only the unmasked area of the image was considered when calculating the sampling volume for the purposes of estimating the frazil ice concentration.

5.3 Data Analysis

The frazil ice data were analysed in two stages: first, using an image processing algorithm designed to identify each individual particle and determine its diameter, classify it as ice or sediment using the SVM, and determine which ice particles were frazil ice crystals by checking for a disc-like shape. Second, the data were analysed using a post-processing algorithm written by McFarlane et al. (2015) to calculate how the particle size properties and concentration evolved as a function of time and water temperature. Each of these processing steps is described below.

5.3.1 IMAGE PROCESSING

Image processing was performed using the algorithm described by McFarlane et al. (2014) with a slight improvement: the sensitivity of the threshold used to detect the edges of each disc was reduced by three percent as it was found that the diameters of certain very bright discs were being slightly overestimated. Once each image had been analysed to identify and determine the size of each particle (defined as the major axis length), the optical characteristics of each individual particle were analysed using the SVM to determine whether the particle fell into the ice or sediment class. A total of 54 optical properties over the span of the red, green, blue (RGB), hue, saturation, value (HSV), and L*a*b* colour spaces were examined by the SVM. Each particle was then assigned a value of 1 if it was identified to be sediment, or a 2 if it was confirmed to be ice. A very detailed description of the training and validation processes for the SVMs is provided by McFarlane et al. (2018b).

Any particles identified as ice by the SVM were then compared to a fitted ellipse with the same second-central moments to determine whether they were disc-shaped or not. Using this classification, the ice particles were further classified into disc-shaped frazil crystals and other 'non-disc' ice crystals, and the overall percentage of ice particles found to be disc-shaped was also calculated. The size distribution characteristics, including the mean and standard deviation, were then calculated for both the sediment and disc-shaped frazil ice particle classes. If the ratio of sediment to frazil ice particles was less than 14, the frazil ice data were deemed to be accurate. However, if the sediment to frazil ratio was greater than 14, this meant that the sediment concentration was too high during the deployment to accurately resolve the frazil ice size distribution, even with the 98% accuracy of the SVM. These limitations to the SVM algorithm are demonstrated and discussed in detail by McFarlane et al. (2018b).

5.3.2 POST-PROCESSING

After the processing had been completed using the image analysis and machine learning algorithms, the data were further analysed to examine how the particle properties varied with time. This was accomplished using the algorithm developed by McFarlane et al. (2015) designed to calculate the moving average and standard deviation of the size distribution data, as well as the average number of particles per image and the volume concentration of ice in the measuring volume (m^3/m^3). Calculation of the frazil ice volume required an assumption to be made regarding the thickness of each particle, and it was decided to use an aspect ratio (i.e. diameter to thickness ratio) of 37 to calculate this. This aspect ratio was chosen based on the observations of McFarlane et al. (2014) who measured the diameter and thickness of 38 frazil ice particles and found that the aspect ratio ranged from 11 to 71 with a mean of 37 for particles ranging in thickness from 0.03 to 0.12 mm, and with a mean thickness of 0.07 mm. The other option was to use a constant thickness for all particles; however, this would result in incorrect aspect ratios and artificially high concentrations for particles with small diameters (i.e. diameters less than the assumed thickness) as these particles would appear to be cylinders instead of discs. However, using a constant aspect ratio results in reasonable thicknesses for all particles.

For each of the deployments where images were captured at a high enough frequency, the time series data were calculated by averaging the particle properties over 35 consecutive images for direct comparison to the lab data presented by McFarlane et al. (2015). This corresponded to a 35 second moving average for deployments with an image capture frequency of 1 Hz. Time series data were also calculated for one deployment (KR-1) where the images were captured in 9 image bursts at a frequency of 1 Hz, followed by a 9 second wait until the next burst began, producing a 70 second moving average in this case. The time series data were calculated for both the sediment and frazil ice particles and

synchronised with the water temperature time series that were concurrently measured during each deployment. Time series plots of the volume concentration, number of particles per image, and the mean and standard deviation of the particle diameters were produced for certain deployments. The mean volume concentration and the percentage of ice particles that were disc-shaped were also calculated for each deployment.

5.4 RESULTS

In Table 5-3, the numerical results for each deployment are presented including the mean, standard deviation, and 99th percentile of the frazil diameter; average number and volume concentrations; percentage of ice particles that were disc-shaped; and the sediment to frazil ice ratio. The raw results, which include all ice and sediment particles combined, are presented as well. The frazil ice data for deployment KR-5 were further broken down into pre-peak and post-peak classes to demonstrate how the frazil ice properties changed as the hydropeaking wave passed through the deployment site causing the water level and velocity to increase. It is of note that the percentage of suspended ice crystals that were disc-shaped was greater than 50% in all cases and was greater than 90% for deployments NSR-4A, KR-2, and KR-4A. Deployments NSR-5A and 5B have been excluded from the table since that supercooling event was dominated by the growth of shard-like crystals with very few frazil discs present in the images. Deployment PR-2 was also omitted from Table 5-3 because the sediment to frazil ice ratio was 25, indicating that the data were too heavily influenced by the presence of suspended sediment to give accurate results, which was demonstrated by McFarlane et al. (2018b). All other deployments were found to have sediment to frazil ice ratios less than the limit of 14 that was recommended by McFarlane et al. (2018b). Overall, the smallest frazil ice particles observed were 34 μm in diameter (which was the smallest the FrazilCam was capable of detecting) and the 99th percentile ranged from 1.29 to 5.83 mm.

In Figure 5-3 plots of the raw and frazil ice size distributions calculated for four of the deployments are presented. A lognormal distribution with the same mean and standard deviation as the frazil ice data is included in each plot for comparison. Figure 5-4 includes two distributions from deployment KR-5: the first from before the hydropeaking wave reached the site, and the second from after the wave had arrived. The pre-hydropeaking distribution has only one peak centred at a diameter of ~1 mm, while the post-hydropeaking distribution appears bimodal. It is of note that 15,111 frazil ice particles were observed before and 12,204 were observed after the hydropeaking event, while the numbers of images in those cases were 3,989 and 153, respectively. This resulted in an increase in the average number of particles per image from 3.8 to 80.

Time series plots of frazil ice and sediment properties for deployments NSR-4A, KR-1, PR-1, and KR-5 are presented in Figure 5-5, Figure 5-6, Figure 5-7, and Figure 5-8, respectively. The volume concentrations were not calculated for the sediment particles as this property would not be representative of the actual sediment concentration in the flow, but only the concentration of particles that were thin enough to refract the light and appear visible in the FrazilCam images. Deployments NSR-4A, KR-1, and PR-1 took place during the residual supercooling phase, while KR-5 occurred during the principal supercooling phase. Unfortunately, as mentioned in section 5.2.2, the temperature logger was iced-up during deployment KR-5 and, consequently, the water temperature appears almost constant in Figure 5-8. However, the water temperature had been recorded cooling from 0.25°C at 15:20 down to 0°C at 18:40, just before the deployment began, indicating that this was a principal supercooling event.

There are a number of anomalous spikes in the particles per image and concentration time series plotted in these figures. Although these spikes are quite visible in the time series

they were short in duration and only accounted for a very small fraction of the overall data, and therefore did not impact the overall accuracy of the size distribution characteristics presented in Table 5-3. In Figure 5-5c there are noticeable spikes at approximately 09:04, 10:07, and 10:24. A few images captured at 09:04 had large flocs in them and a higher concentration of individual crystals, indicating that a slush ball or frazil pan had likely collided with the FrazilCam at this point in time and resulted in the increased concentration. At 10:07 and 10:24 there were no abnormalities in the images aside from a higher number of visible particles for a short period of time. The largest anomaly in Figure 5-6 occurred at 08:40 when there was an increase in the number of particles visible for 9 consecutive images. It is not clear what caused this but there was a large floc visible in the first of these images, indicating that released anchor ice or a large, slushy floc colliding with the FrazilCam could have caused this temporary increase in the number concentration of the particles. In Figure 5-7c there was a clear spike at 16:45. Again, examining the images confirms that there were a significantly larger number of particles visible for about 13 images but the reason for this is not clear. It is possible that particles were released from the riverbed by movement when positioning the FrazilCam at the beginning of the deployment or that a natural anchor ice release had occurred upstream of the deployment site. The spike in concentration seen in Figure 5-7d at ~17:22 appears to have been caused by a few crystals that froze onto the polarisers at approximately 17:15. These crystals slowly grew and other crystals froze onto them, causing the increase in concentration while not impacting the number of particles per image in Figure 5-7c. By about 17:25 when the concentration levelled off again, these particles had accumulated enough additional particles to appear as abnormally-shaped flocs and they were rejected by the algorithm.

The plots in Figure 5-8 have the most spikes of those presented. There are a few "jumps" in the time series data that appear where segments of the data were removed. These occurred from 19:19 to 19:21, 19:38 to 19:41, and 19:52 to 19:54 while the polarisers were being cleaned to remove accumulated ice particles. The cleaning apparatus is visible during these times and there are more particles due to the flow disturbance caused by the cleaning procedure, so these images were eliminated from the time series. The spike that occurs at 19:30 was caused by a few very large discs passing through the images at that time. The increase in concentration in Figure 5-8d at 19:45 was caused by a single shard-like crystal that was frozen near the edge of the polarisers for several minutes as it continued to grow. Eventually, it grew to a shape that no longer appeared disc-like to the algorithm and it was rejected, resulting in the drop in concentration. The sharp increase in the number of particles per image in Figure 5-8c at 20:03 indicates when the hydropeaking wave came through the site. It is also interesting to note the change in the moving average particle diameter that occurs in Figure 5-8a at the same time. The mean frazil diameter very quickly drops from ~1 mm to ~0.4 mm, indicating that a large number of smaller particles were produced in the increased flow.

Figure 5-9 shows the water temperature and sediment particles per image time series for deployments NSR-5A and NSR-5B. Although no frazil ice data were obtained from this deployment due to the growth of the shard-like crystals on the polarisers, sediment particles were still visible in the images in the period leading up to the maximum degree of supercooling. After the maximum supercooling was reached and the shard crystals began to grow the sediment data are much noisier due to the obstruction to the images. This figure demonstrates the extreme supercooling temperature of −0.145°C that was reached during deployment NSR-5 and how quickly the water temperature rebounded to the residual supercooling temperature as the shard crystals rapidly grew. However, ice was

observed to grow on the temperature logger as well, which likely impacted the measurements until it was manually removed at ~19:40. It is also of note that the number of sediment particles per image steadily decreased from ~10 before the principal supercooling began down to ~2 when the maximum degree of supercooling occurred.

5.5 Discussion

5.5.1 Frazil Ice Size Distributions

Examining the size distributions presented in Figure 5-3 and Figure 5-4, it is clear that a lognormal distribution provides a very good approximation of the size distribution in almost all cases. This confirms what has been observed in multiple laboratory studies (e.g. Clark and Doering, 2008, 2006; Daly and Colbeck, 1986; McFarlane et al., 2015). McFarlane et al. (2017) also suggested that a lognormal distribution was a good fit for frazil ice particles observed in the field, although there were gaps in the observed size distributions due to the size distribution subtraction method used to minimise the effects of suspended sediment. The use of the SVM algorithms to separate the ice and sediment particles in this study demonstrates with much greater certainty that a lognormal distribution can be used to approximate the size distribution of frazil ice particles in field environments, during both the principal and residual supercooling phases.

The only size distribution that did not fit a lognormal distribution reasonably well was the distribution from deployment KR-5 plotted in Figure 5-4b, which appeared bimodal. However, this size distribution was obtained under unique circumstances as the flow was rapidly increasing due to the arrival of a hydropeaking wave at the site. It seems likely that as the water level increased, a large number of seed particles were collected from snow and frost on parts of the bed and banks that were previously above water, but became submerged with the water level rise. This influx of seed particles likely caused the increase

in small frazil particles, which, along with the large particles already in the flow, caused the bimodal distribution. However, other conditions affected by the change in flow rate including water velocity and turbulence intensity could also have affected the size distribution and caused existing frazil flocs to break apart or frazil particles floating at the surface to become re-suspended. These results indicate that during an unsteady event when conditions are rapidly changing a bimodal rather than lognormal distribution is realistic in field environments.

McFarlane et al. (2017) presented a summary of previously measured frazil ice particle sizes, which had mean diameters ranging from 0.13 mm (Daly and Colbeck, 1986) to 2.1 mm (Clark and Doering, 2006) in laboratory studies and 0.4 mm (Richard et al., 2011) to 3.15 mm (Morse and Richard, 2009) in field environments. The mean frazil ice particle diameters obtained from the FrazilCam deployments in this study ranged from 0.32 to 1.32 mm overall, which falls well within the range of previously reported measurements in both the laboratory and the field. This can be further broken down between the principal and residual supercooling phases: the mean diameter ranged from 0.63 to 1.32 during the principal supercooling events and from 0.32 to 0.93 during the residual phase. This supports the conclusion that the mean frazil diameter tends to be larger during principal supercooling events than once the residual supercooling temperature has been reached, as was observed in the field by McFarlane et al. (2017) and in laboratory studies by Clark and Doering (2008) and McFarlane et al. (2015).

The time series plots from the residual supercooling event in Figure 5-5 indicate that the mean frazil diameter was essentially constant during deployment NSR-4A. This was also the case for deployments NSR-3, NSR-4B, KR-2, KR-3A, KR-3B, and KR-4A, which would seem to indicate that the frazil ice size distribution does not change during the residual

supercooling phase. However, the time series data in Figure 5-6 and Figure 5-7, which were captured during the residual supercooling phase during deployments KR-1 and PR-1, respectively, disagree with this trend. The mean diameter was approximately 0.25 mm at the beginning of deployment PR-1 and nearly 0.5 mm at the end, with spikes up to ~0.75 mm in between. Although this deployment occurred during the 2014-15 season when there were no weather stations set up along the Peace River, the FrazilCam was being continuously monitored during the deployment and no extreme changes to the environmental or flow conditions were observed. However, the deployment began prior to sunset and finished after sunset. It seems likely that the increase in the mean particle diameter throughout the first half of the deployment was caused by a reduction in the heat flux into the water at sunset as there was no more incoming solar radiation. This allowed for greater heat loss from the water and, therefore, more available cooling to facilitate the further growth of the frazil crystals. This is further supported by the fact that the number of frazil ice particles per image remained essentially constant throughout the deployment, indicating that the number of particles in the flow was stable, but they were growing larger. Deployment KR-1 began in the early morning before the sun rose over the mountains and ended when the river was in full sunlight. This caused a gradual increase in water temperature during the deployment, and the local temperature was actually greater than 0°C for the final two thirds of the deployment. The mean frazil diameter was relatively constant until approximately the same time as the water temperature increased above zero degrees (~09:15), then it steadily decreased. Since the local water temperature was above zero, the frazil that remained in the flow must have been produced in upstream reaches of the river that remained supercooled, and the decreasing particle size seems to indicate that these particles were beginning to melt.

The principal supercooling event that was recorded during deployment NSR-5 and is plotted in Figure 5-9 developed in an unusual way despite what seemed like unfavourable environmental conditions. The air temperature was 2.2°C at 16:00 when the water temperature dropped below zero (just before sunset which was at 16:23) and was only −2.3°C when the maximum degree of supercooling was reached at 19:20. The mean wind speed was only 0.2 m/s over this time period; it had been a clear and sunny day and the sky remained clear throughout the event; and there was no snow or frost on the ground to provide readily available seed particles. However, the water steadily cooled to an extremely low temperature of −0.145°C, 3.4 times cooler than the next lowest temperature that was measured during a principal supercooling event, which was −0.043°C during deployment NSR-2. The only environmental condition that had changed significantly from day to night was the loss of incoming solar radiation after sunset. During the daytime the mean incoming solar radiation had been 234 W/m^2 and the mean air temperature had been 4.8°C. Using the radiative heat flux equations provided by Hicks (2016) it was calculated that the water experienced a net radiative heat gain of 161 W/m^2 during the daytime, and a net radiative heat loss of 63 W/m^2 during the supercooling event. This heat loss was sufficient to supercool the water despite the above zero air temperature. At ~19:20 ice began to form very rapidly and the water temperature began to rise quite quickly. However, the majority of the ice did not form as the expected suspended frazil ice crystals, but rather as anchor ice shards that rapidly grew onto any submerged object, including the river bed material, the FrazilCam, and AquaDopp. Despite repeated attempts to keep the polarisers clear of ice using injections of hot, saline water, these shard-like crystals also formed on the faces of the polarising filters and were visible in all of the FrazilCam images. An example image of these crystals is shown in Figure 5-10, captured after the maximum degree of supercooling had been reached and the water temperature was beginning to increase. The crystals grew faster and faster until, eventually, the entire image was

obstructed and the FrazilCam was removed from the river. A photo of the FrazilCam on the bank after this deployment is shown in Figure 5-11. Anchor ice crystals can be seen completely encasing the camera, and most of the flash was covered as well. Similar crystals had also grown on the FrazilCam during a different deployment five days earlier on the morning of November 20, 2016, but the images were too obstructed by these crystals to yield useable results after image processing. A photo of some of these crystals growing on the polarisers is shown in Figure 5-12. These crystals are very similar in appearance to the "interfingered, relatively large ice crystals" observed by Kempema and Ettema (2016) in the Laramie River, Wyoming.

An interesting trend is visible with respect to the sediment particles in the flow during deployment NSR-5: the number of sediment particles per image slowly decreased as the water temperature decreased towards the maximum degree of supercooling (Figure 5-9). Examining the turbidity measurements made during this deployment reveals the same trend, as the turbidity decreased from 12 NTU at 16:00 to 9.1 NTU at 19:20 when the maximum degree of supercooling was reached. This supports the conclusion reached in the lab by Kempema et al. (1986) that the suspended sediment concentration decreases during frazil ice formation, and supports the hypothesis presented by McFarlane et al. (2017) that the "scavenging or mechanical trapping of sediment by frazil flocs" was the reason for apparently decreased sediment concentrations during supercooling events. Conversely, the number of suspended sediment particles steadily increased during deployment KR-1 in Figure 5-6c once the water temperature rose above 0°C, suggesting that as the frazil particles, flocs, and anchor ice melted, additional fine suspended sediment particles were released. However, no turbidity data were collected during deployment KR-1.

The hydropeaking wave that arrived at the measurement site during deployment KR-5 caused a rapid increase in water level and velocity. This is evident in Figure 5-8c where the number of frazil ice crystals increased dramatically at ~20:03. Figure 5-13a shows an image captured before the hydropeaking wave arrived, where there were 3.8 particles per image on average and the mean diameter was 1.32 mm. In Figure 5-13b, captured only one minute and eight seconds later, the average number of particles per image had risen to 80 and the mean diameter had decreased to 0.40 mm. Interestingly, while the average number of particles per image increased by a factor of 21, the volume concentration only increased by a factor of 1.2 from 1.52×10^{-5} to 1.83×10^{-5} since the vast majority of the new particles were small in diameter and therefore small in volume, as well.

5.5.2 Frazil Ice Concentrations

Frazil concentrations reported in previous laboratory and field studies are presented in Table 5-4. Notably, all of the volume concentrations measured in laboratory studies were at least an order of magnitude larger than those measured using acoustic devices in field environments. This suggests that frazil ice events simulated in laboratory settings produce higher concentrations of suspended frazil ice particles, even though the shape of the size distribution has been observed to be lognormal in both settings and the mean particle sizes found have been similar. During the FrazilCam deployments, the frazil ice number concentration ranged from 1.48×10^4 to 1.81×10^6 particles/m^3 (Table 5-3), which is in agreement with the range of 10^4 to 4×10^6 particles/m^3 that has been observed in the previous studies presented in Table 5-4. The volume concentration ranged from 1.0×10^{-6} to 1.8×10^{-5} m^3/m^3 (Table 5-3), and these are the first frazil ice volume concentrations to be measured in field environments using an optical device. However, it should be noted that these volume concentrations are only representative of the individual, disc-shaped crystals suspended in the flow. Conversely, the previous field measurements made using

comparative resistance probes and acoustic devices were representative of the total suspended ice concentration, including frazil flocs, released anchor ice, and abnormally shaped ice crystals. Nonetheless, the volume concentrations observed in this study are very similar to the range of 2 to 6 × 10^{-6} obtained by Richard et al. (2011) from ADCP measurements in the St. Lawrence River. The lower range of some of the concentrations estimated using shallow water ice profiling sonar (SWIPS) instruments in the Peace River (Jasek et al., 2011; Marko et al., 2015; Marko and Jasek, 2010b, 2010c) are also of the same order of magnitude as the upper limit obtained in this study.

5.6 Conclusions

The FrazilCam system was successfully deployed during both the principal and residual supercooling phases in the Kananaskis, North Saskatchewan, and Peace Rivers. By processing the images with an SVM algorithm that had been trained specifically for each river, the size distributions of the suspended frazil ice particles were reliably calculated. All of the frazil ice size distributions captured under steady flow conditions were accurately described by a lognormal distribution with the same mean and standard deviation as the observed data. During the principal and residual supercooling phases the mean frazil ice particle diameter ranged from 0.63 to 1.32 mm and from 0.32 to 0.93 mm, respectively. These particle sizes are within the range of mean diameters that have been observed in numerous laboratory studies, and indicate that the mean tends to be larger during the principal supercooling phase than during the residual phase. The number concentration of frazil ice particles was found to range from 1.48 × 10^{4} to 1.81 × 10^{6} particles/m^3, which is in agreement with previous studies. Estimates of the average frazil ice volume concentration during each deployment were also made using an assumed particle aspect ratio of 37. This resulted in the first direct measurements of frazil ice volume concentrations in field environments, ranging from 1.0 to 18 × 10^{-6} m^3/m^3.

Analysis of the time-series evolution of the frazil ice properties indicated that, in most cases, the mean frazil ice particle size remained approximately constant during the residual supercooling phase. However, changing environmental conditions during the residual phase resulted in changes to the mean particle size. In one deployment that occurred in the evening, the mean particle size was seen to increase after nightfall. In another that occurred in the morning, the mean particle size decreased once the river was exposed to sunlight and the water began to warm. Unfortunately, due to complications during the observed events, no definitive conclusions could be reached about the evolution of the frazil ice characteristics during the principal supercooling phase, although the number of observed sediment particles decreased as supercooling began and increased when the water temperature climbed back above 0°C. Improvements will be made in future studies in order to collect reliable frazil ice time series data during the principal supercooling phase.

Unique shard-like crystals were observed to grow during one supercooling event that reached a minimum temperature of −0.145°C, over three times colder than the next coldest principal supercooling event that was measured. These crystals formed on all submerged objects in the river and were not the result of frazil ice discs or flocs becoming attached. There was no frost or snow and the air temperature was above 0°C at the time the supercooling event began, suggesting a lack of available seed particles. This indicates that the growth of shard-like ice crystals rather than the more common frazil ice crystals can dominate a freeze-up event under the right conditions.

FIGURES

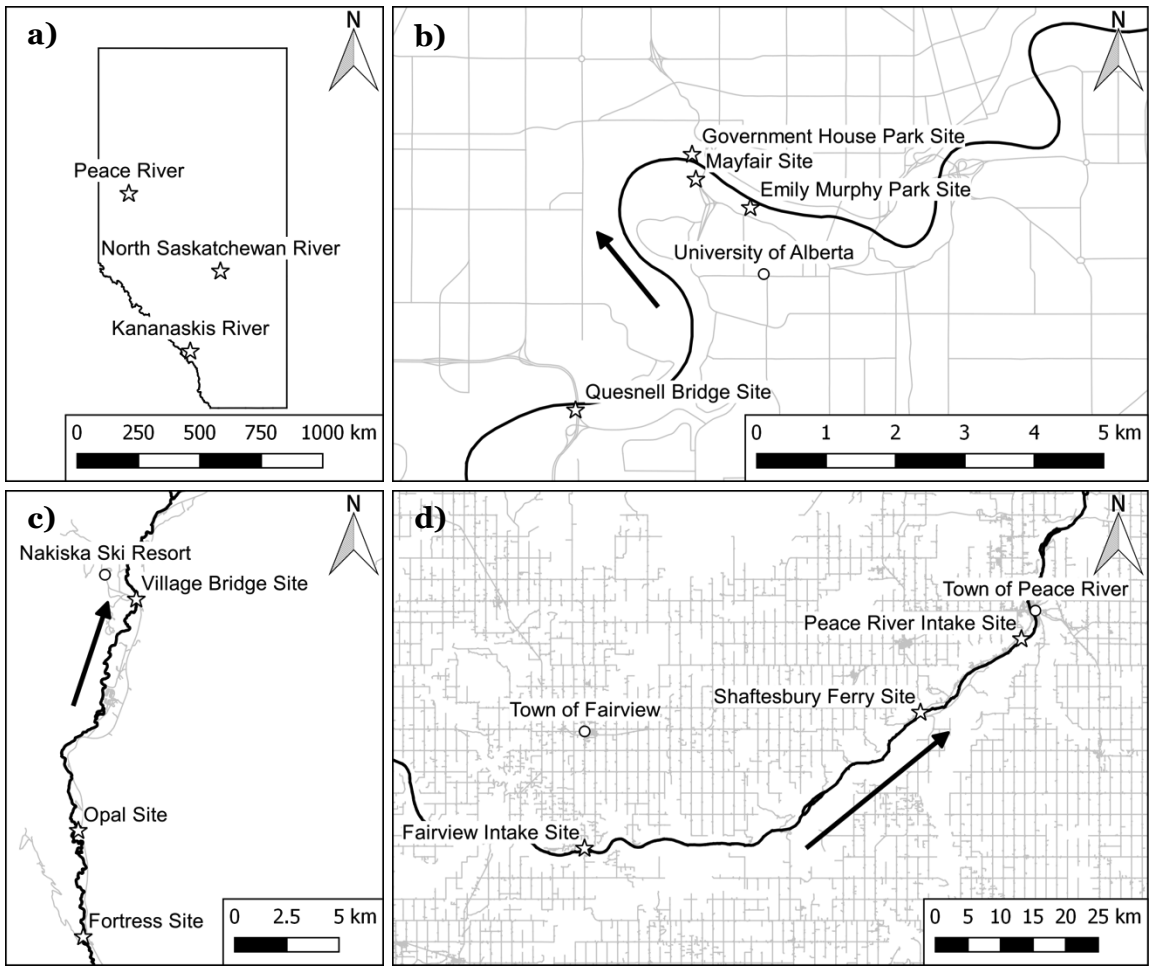

Figure 5-1: Maps showing a) the location of the three rivers in Alberta, b) the location of the study sites on the North Saskatchewan River at Edmonton, c) the study sites on the Kananaskis River, and d) the study sites on the Peace River. Study sites are marked with a ☆, geographical reference points are marked with a ○ , the black arrow indicates flow direction, the black line indicates the river, and the light grey lines indicate roadways.

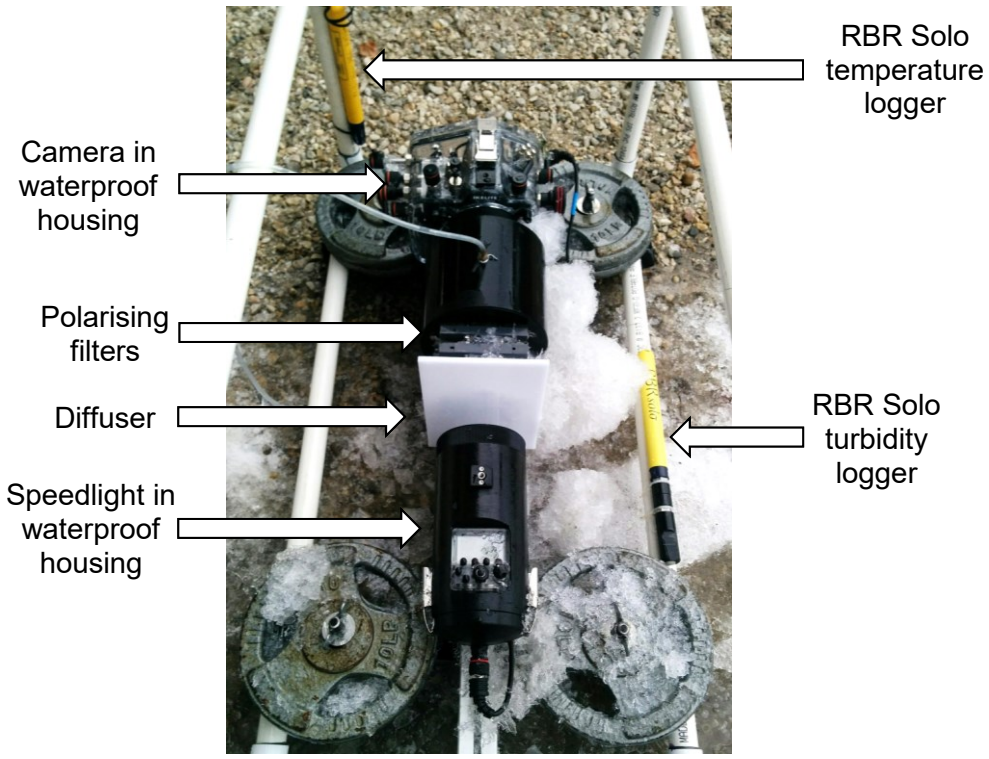

Figure 5-2: Top-down view of the FrazilCam after deployment in the North Saskatchewan River.

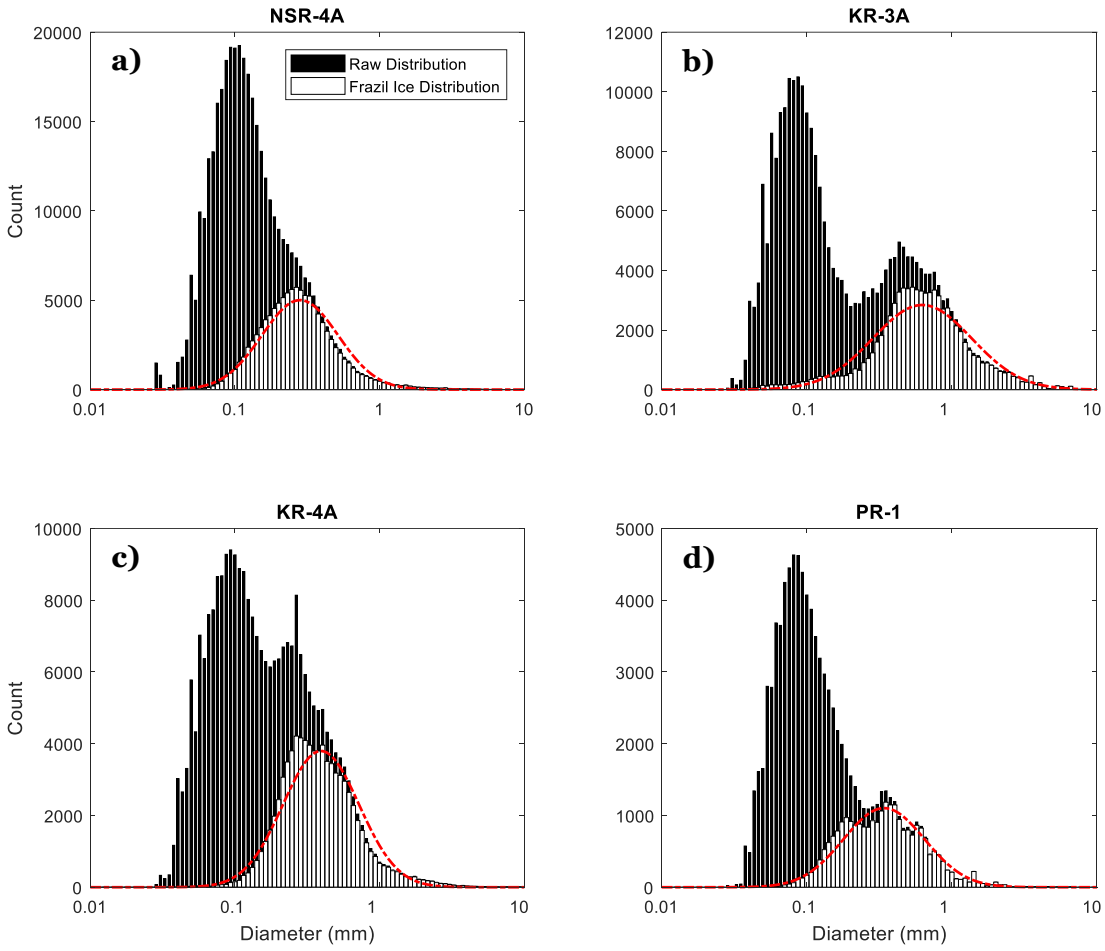

Figure 5-3: A comparison of the raw (black bars) and frazil ice (white bars) size distributions for deployments a) NSR-4A, b) KR-3A, c) KR-4A, and d) PR-1. The red dashed line indicates the lognormal distribution calculated with the same mean and standard deviation as the frazil ice distribution.

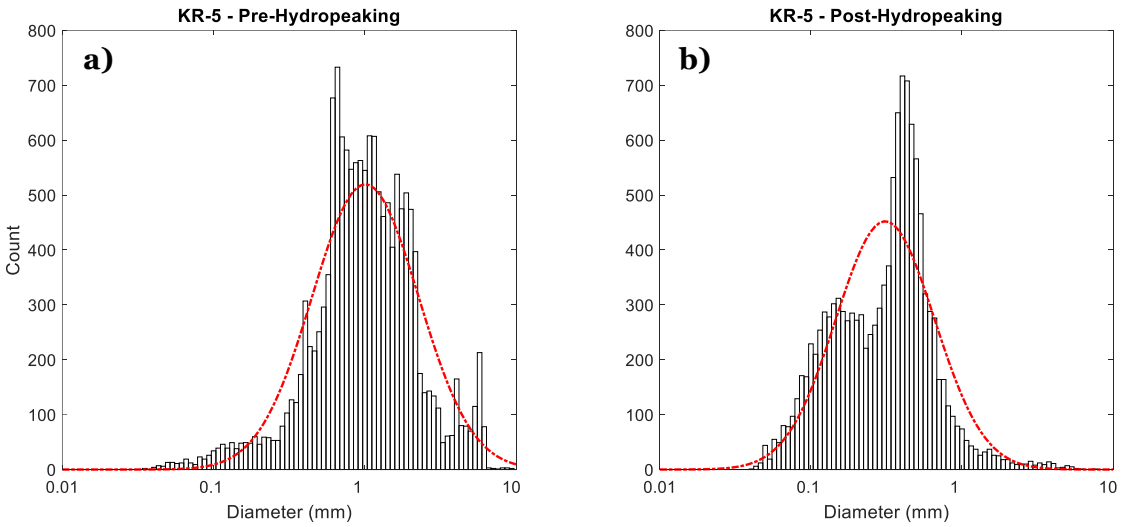

Figure 5-4: The frazil ice size distributions calculated a) before and b) after the hydropeaking event that occurred during deployment KR-5.

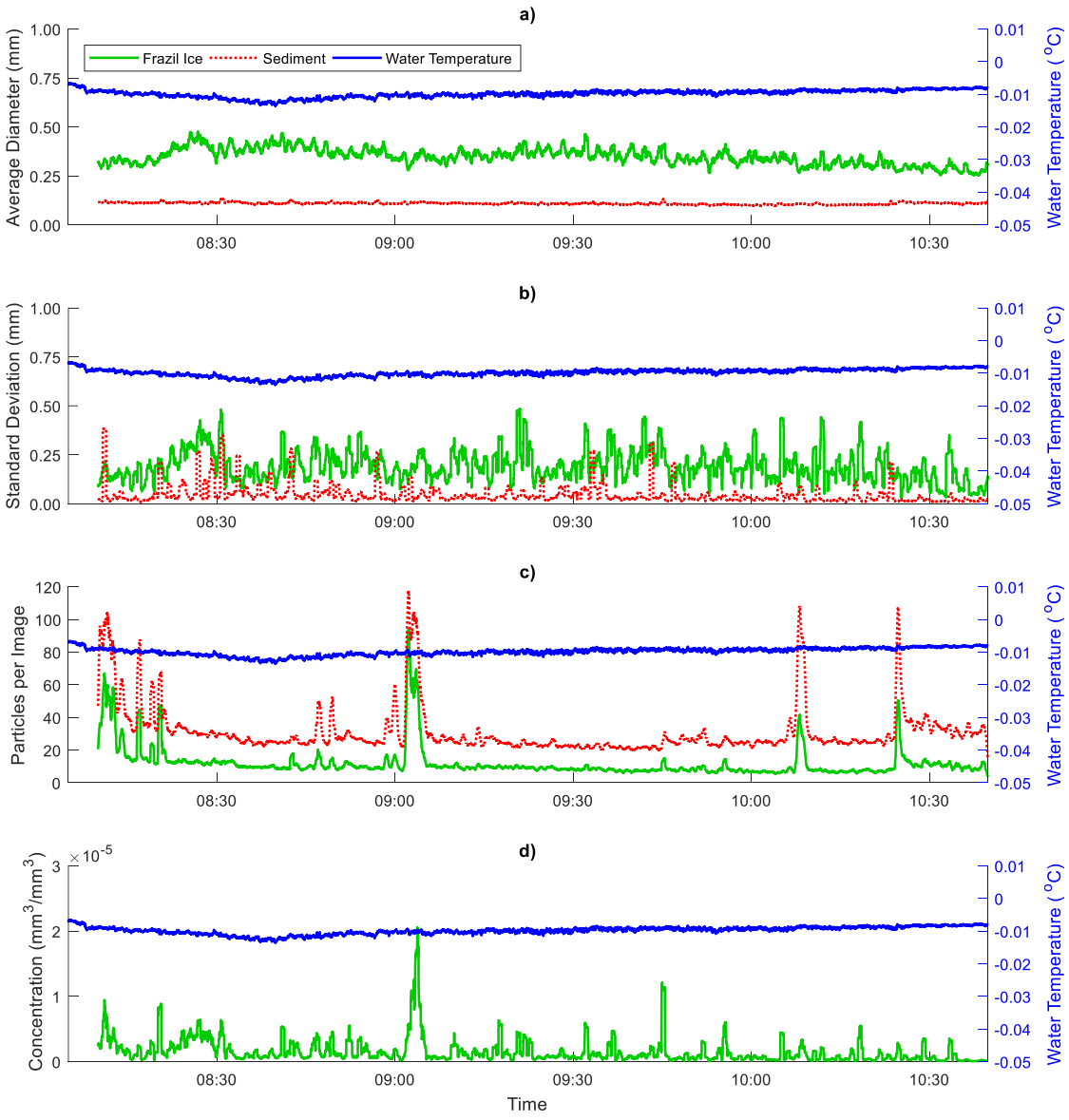

Figure 5-5: Time series data calculated over a period of 35 images for deployment NSR-4A. The variables plotted are a) the average particle diameter, b) the standard deviation of the diameter, c) the number of particles per image, and d) the volume concentration. The solid green line represents frazil ice particles, the red dotted line represents sediment particles, and the solid blue line is the water temperature.

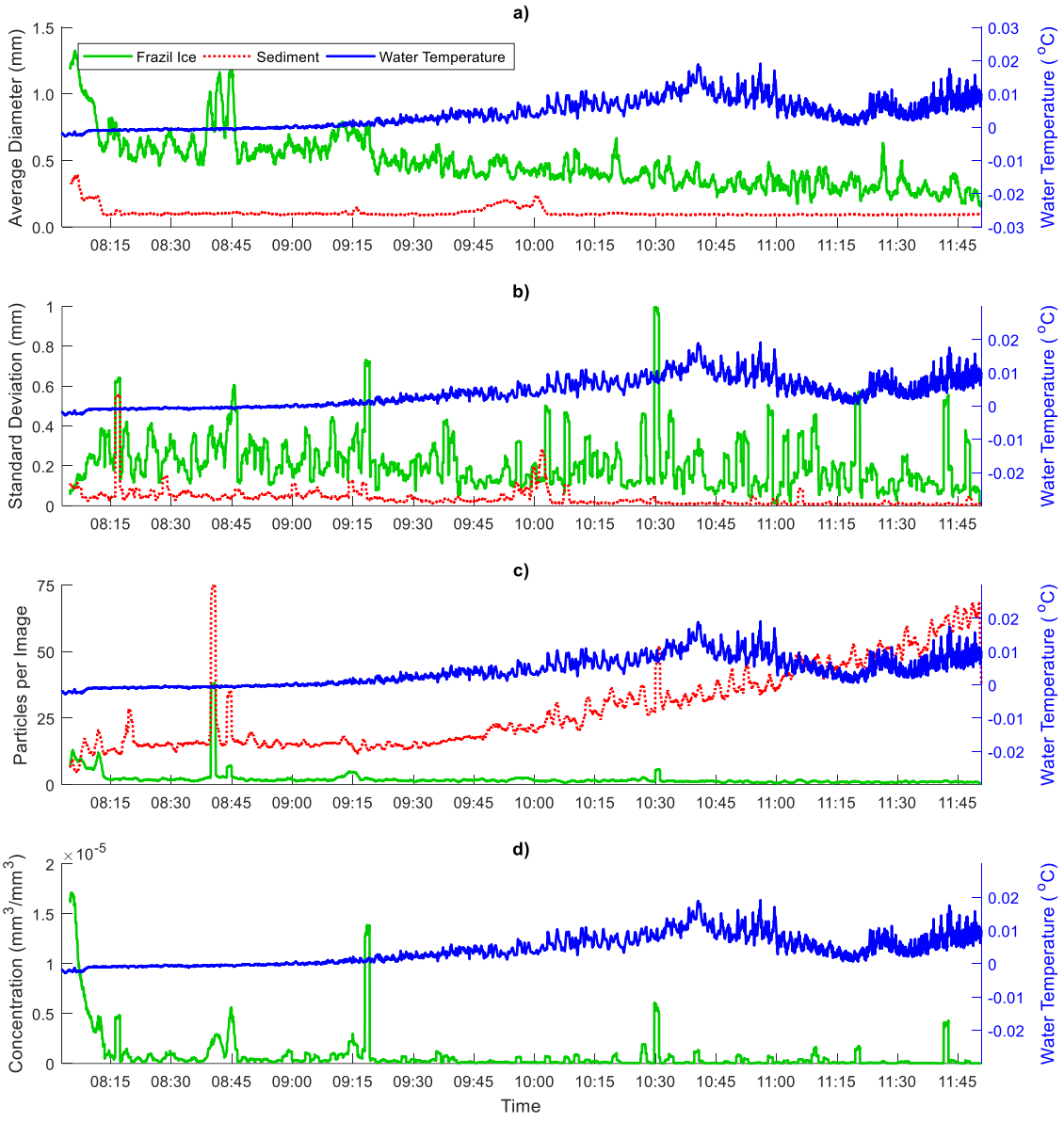

Figure 5-6: Time series data calculated over a period of 35 images for deployment KR-1. The variables plotted are a) the average particle diameter, b) the standard deviation of the diameter, c) the number of particles per image, and d) the volume concentration. The solid green line represents frazil ice particles, the red dotted line represents sediment particles, and the solid blue line is the water temperature.

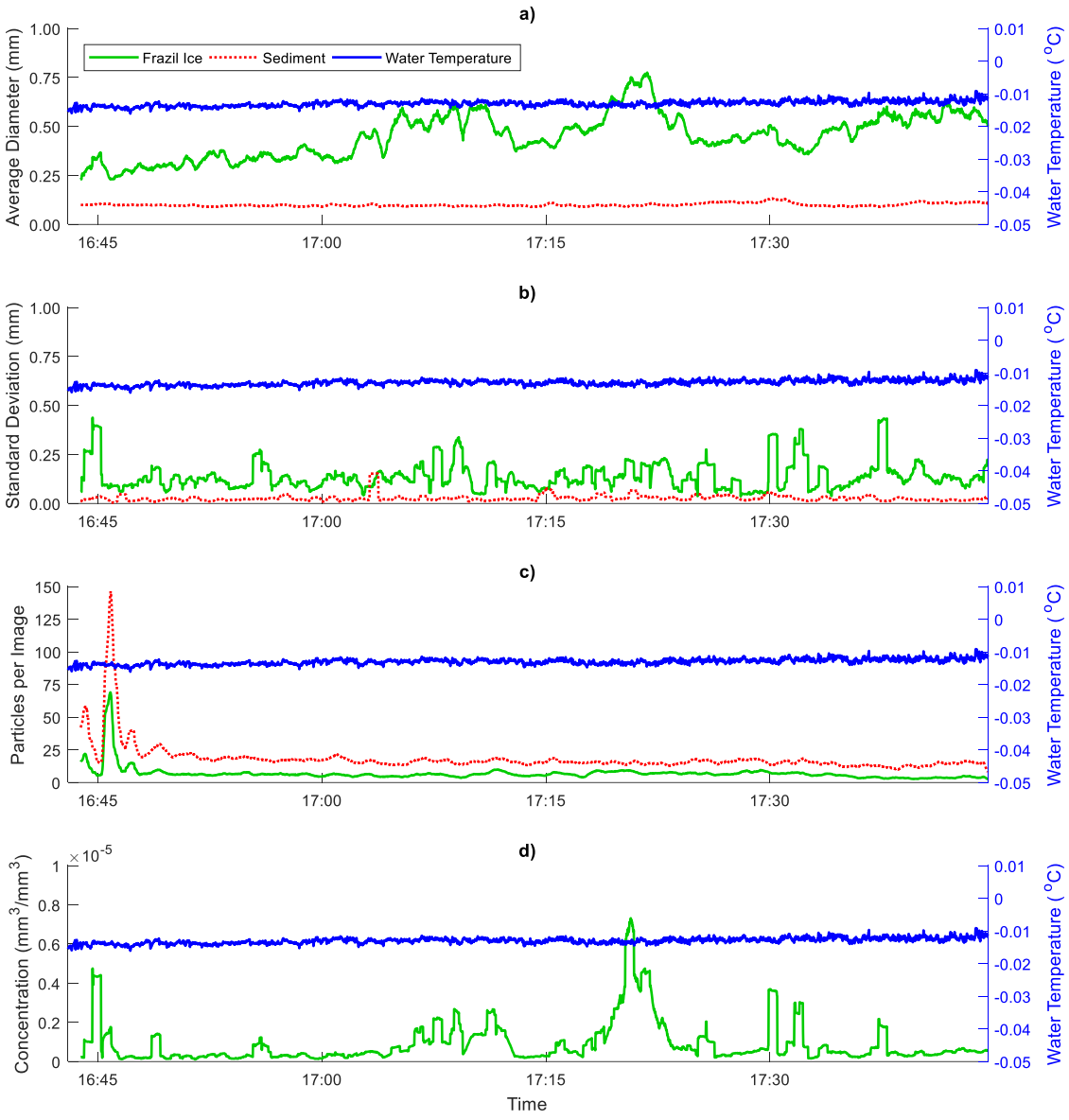

Figure 5-7: Time series data calculated over a period of 35 images for deployment PR-1. The variables plotted are a) the average particle diameter, b) the standard deviation of the diameter, c) the number of particles per image, and d) the volume concentration. The solid green line represents frazil ice particles, the red dotted line represents sediment particles, and the solid blue line is the water temperature.

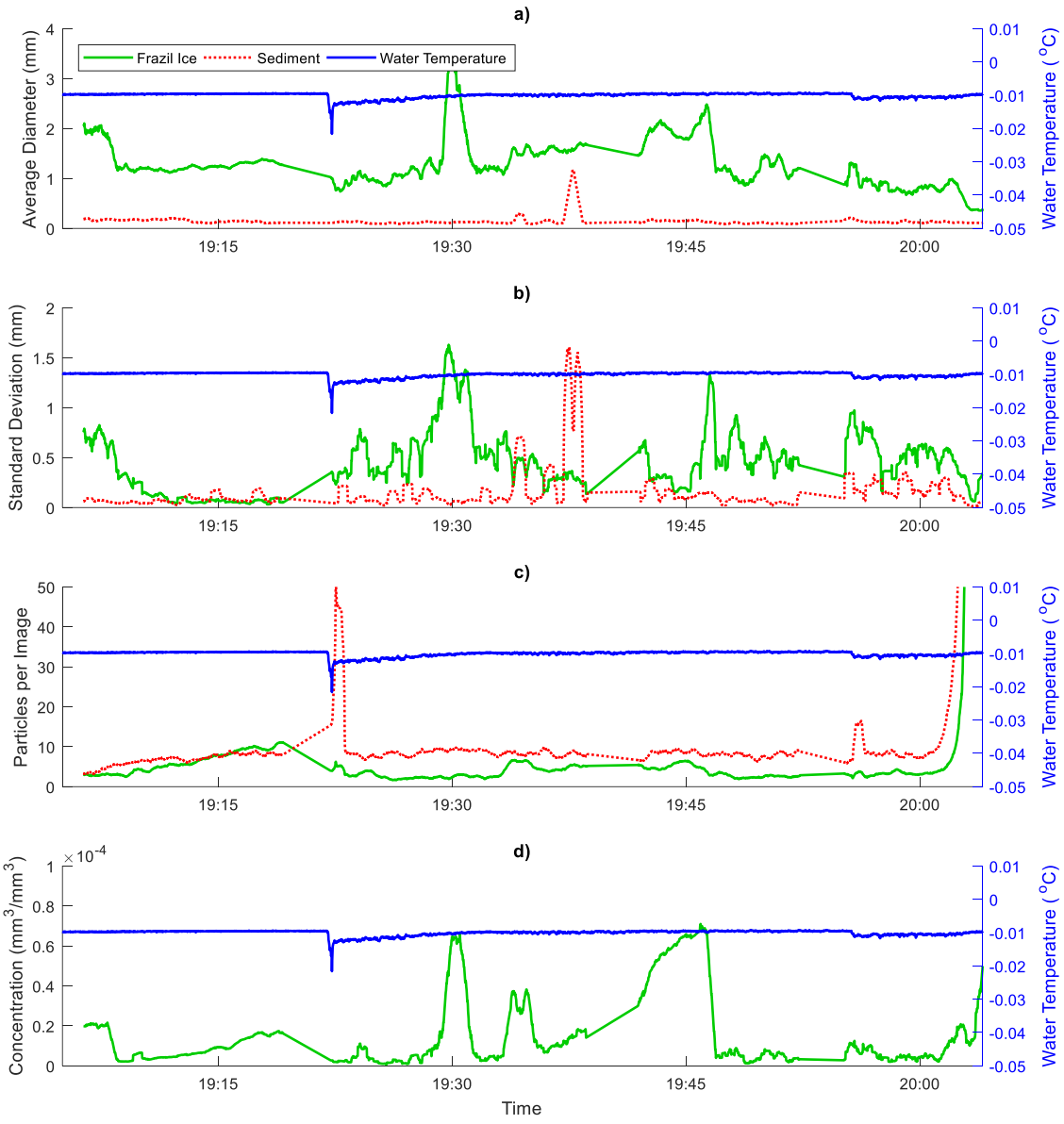

Figure 5-8: Time series data calculated over a period of 35 images for deployment KR-5. The variables plotted are a) the average particle diameter, b) the standard deviation of the diameter, c) the number of particles per image, and d) the volume concentration. The solid green line represents frazil ice particles, the red dotted line represents sediment particles, and the solid blue line is the water temperature.

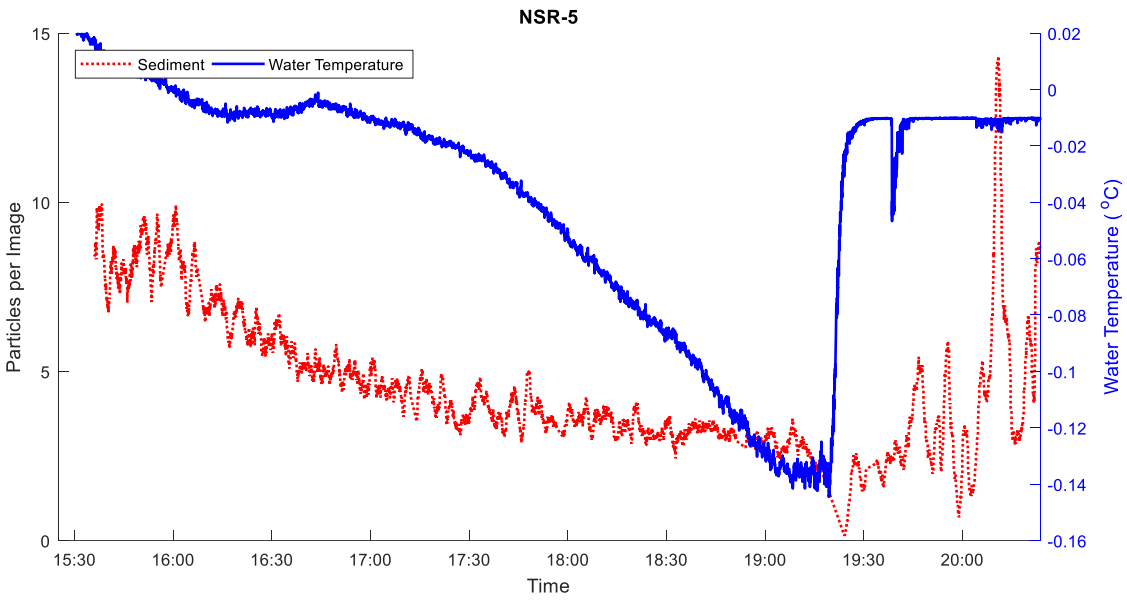

Figure 5-9: Time series data calculated over a period of 35 images for deployments NSR-5A and -5B. The number of sediment particles per image (red dotted line) and the water temperature (blue solid line) are plotted.

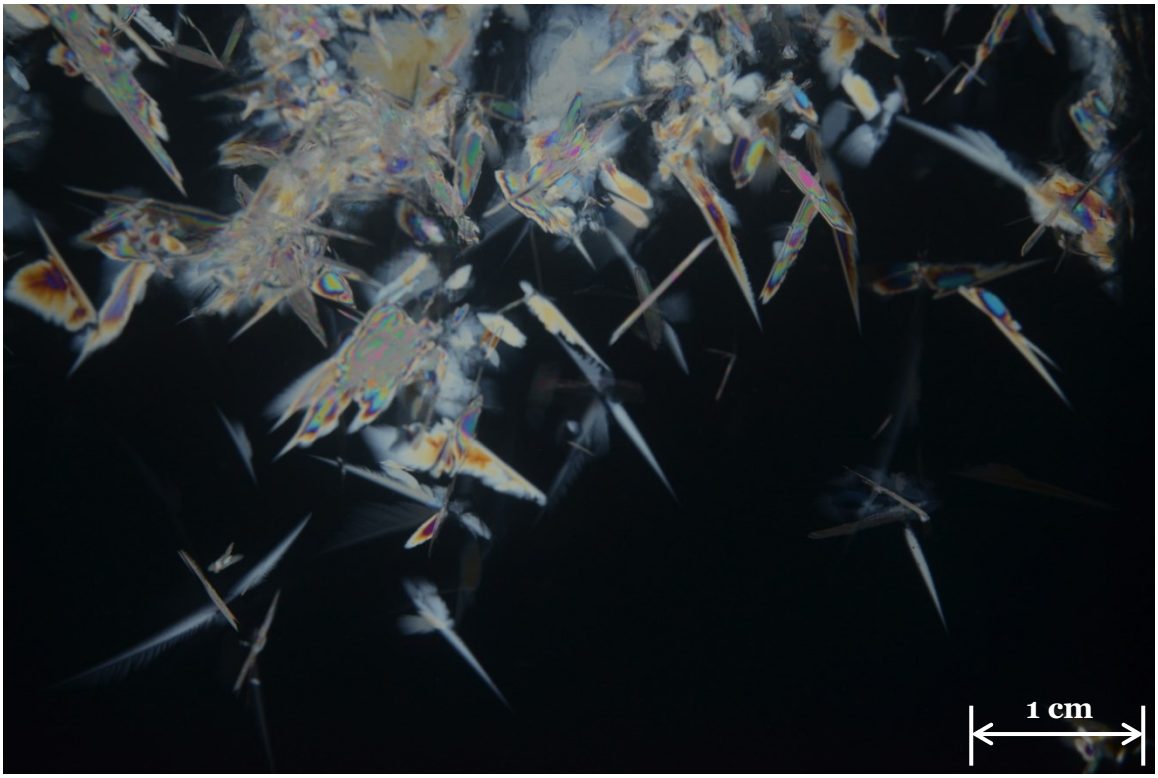

Figure 5-10: Shard-like ice crystals growing on the polarising filters during deployment NSR-5 on November 25, 2016.

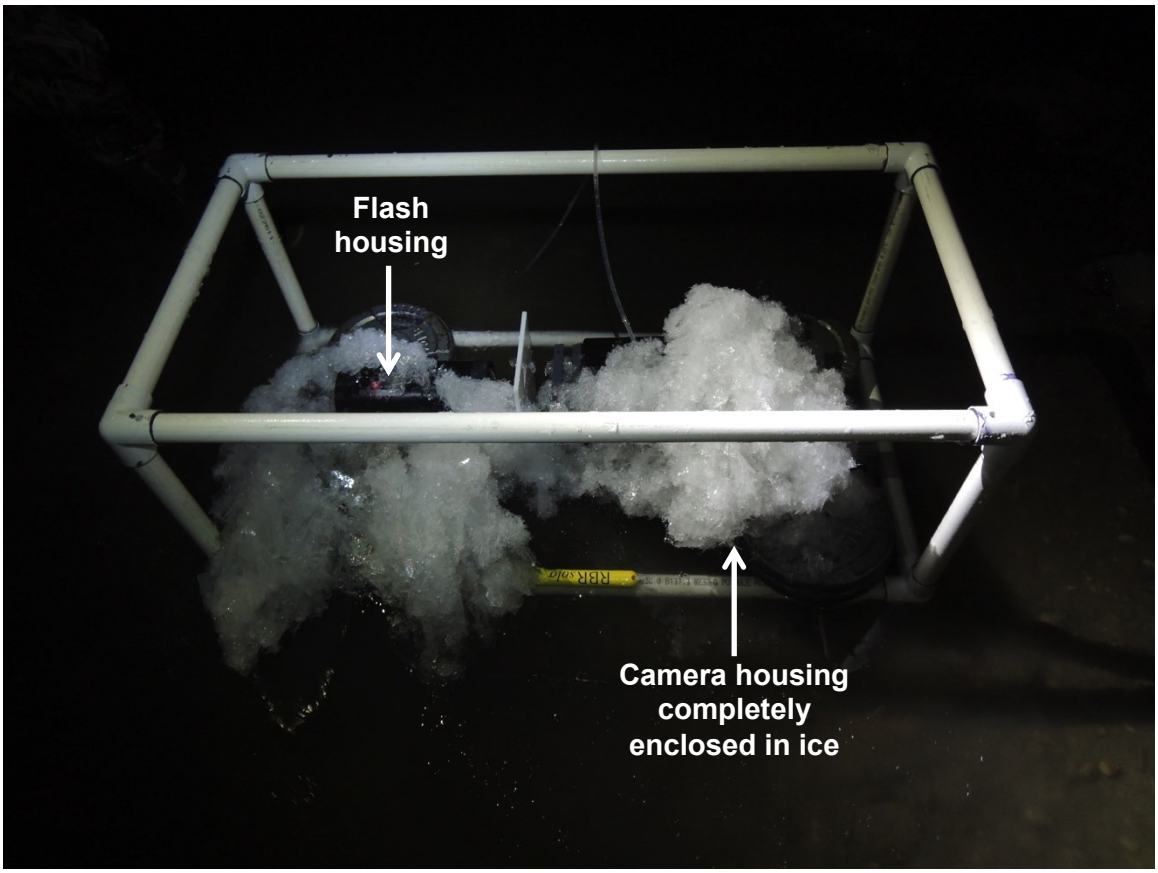

Figure 5-11: A large accumulation of shard-like anchor ice crystals on the FrazilCam following deployment NSR-5 on November 25, 2016. The flash (on the left) and the camera (on the right) are almost entirely covered in anchor ice.

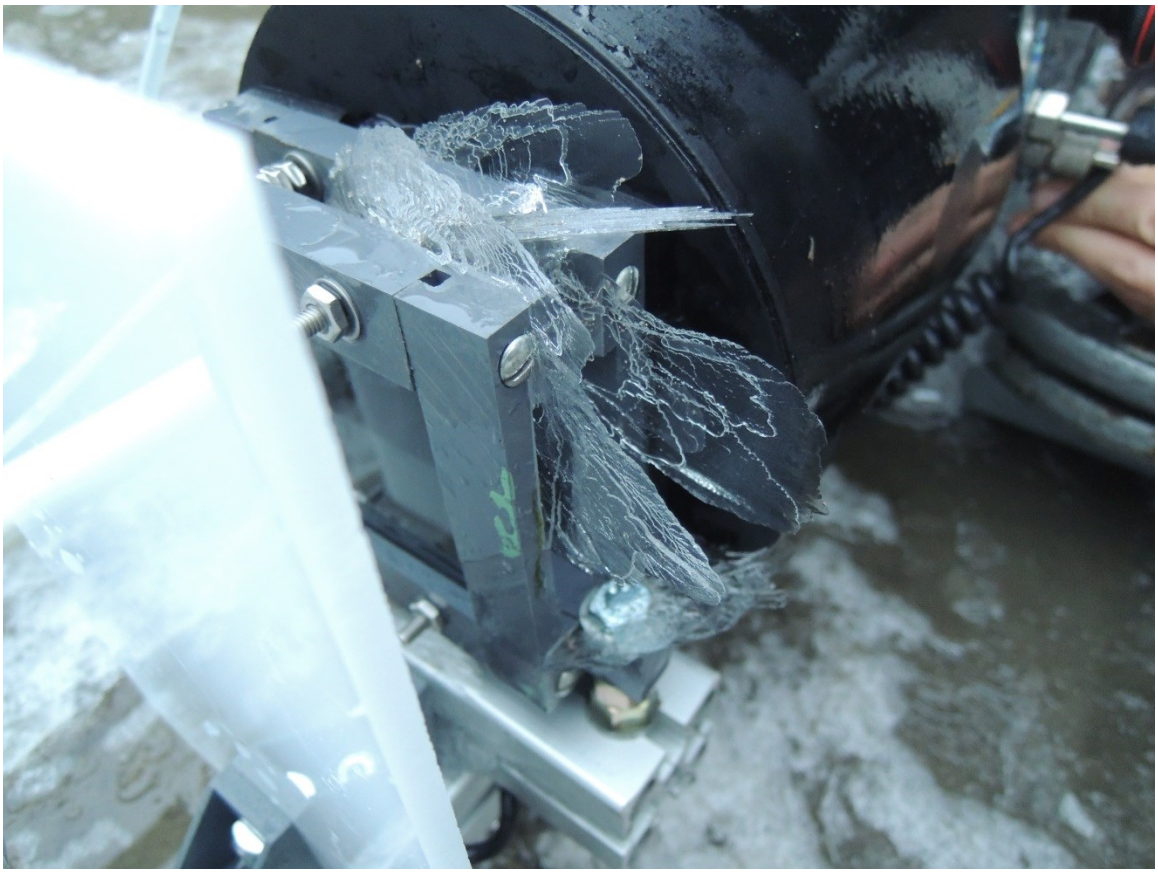

Figure 5-12: Shard-like crystals that grew off of the polariser frame during a FrazilCam deployment on November 20, 2016.

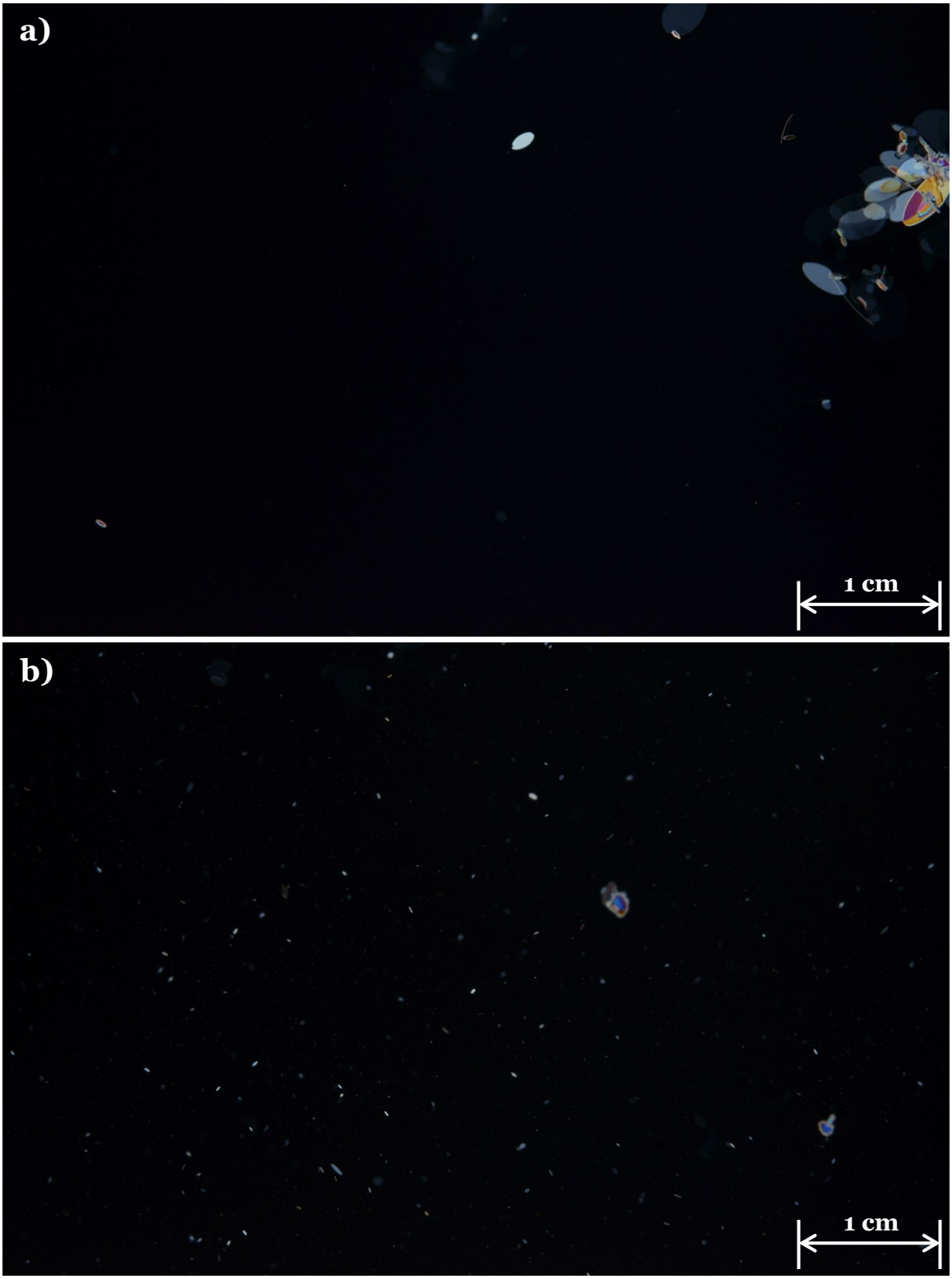

Figure 5-13: Two images captured during deployment KR-5 on February 1, 2017. a) Captured before the hydropeaking wave arrived at the site, and b) captured 68 seconds later as the water level was increasing.

TABLES

Table 5-1: Average channel properties for each of the three rivers (Kellerhals et al., 1972).

River	Average flow rate (m^3/s)	Average water depth (m)	Average channel width (m)
Kananaskis	15	0.61	32
North Saskatchewan	220	1.40	136
Peace	1,586	2.56	227

Table 5-2: Summary of the FrazilCam deployments from all three winters. (Continued on next page).

River	Deployment Number	Date	Site	Image Capture Frequency	Depth-averaged water velocity (m/s)	Minimum recorded water temperature (°C)	Stage of Supercooling
North Saskatchewan	NSR-1	10-Nov-14	Government House Park	9 images at 1 Hz every 90 s	0.38	−0.026	Principal
	NSR-2*		Quesnell Bridge	9 images at 1 Hz every 90 s	0.24	−0.043	Principal
	NSR-3	27-Nov-14	Emily Murphy Park	1 Hz	0.52	−0.011	Residual
	NSR-4A	19-Nov-15	Emily Murphy Park	1 Hz	0.43	−0.014	Residual
	NSR-4B*			1 Hz	0.54	−0.014	Residual
	NSR-5A	25-Nov-16	Quesnell Bridge	1 Hz	0.43	−0.145	Principal
	NSR-5B			1 Hz		−0.145	Principal
Peace	PR-1	19-Dec-14	Fairview Intake	1 Hz	~ 0.5	−0.014	Residual
	PR-2	22-Jan-17	Shaftesbury	1 Hz	~ 0.2 [7]	−0.042	Principal
Kananaskis	KR-1	01-Mar-15	Opal	9 images at 1 Hz every 18 s	0.27	−0.002	Residual
	KR-2		Village Bridge	9 images at 1 Hz every 18 s	0.63	−0.007	Residual

[7] Velocity estimated because the handheld ADV was forgotten at the University of Alberta on this field trip.

	KR-3A*	07-Dec-16	Fortress	1 Hz	0.23	−0.008	Residual
	KR-3B*			9 images at 2 Hz every 9 s		−0.010	Residual
	KR-4A	08-Dec-16	Fortress	1 Hz	0.23	−0.021	Residual
	KR-4B*			1 Hz		−0.011	Residual
	KR-5	01-Feb-17	Fortress	1 Hz	0.30 [8]	−0.014	Principal

[8] This water velocity was measured before the hydropeaking wave reached the deployment site. Once the flow increased the velocity was too high to safely measure using the handheld ADV.

Table 5-3: Particle size and concentration results from each of the FrazilCam deployments. Principal supercooling events are indicated with the superscript ^{P}. An asterisk indicates that there were an artificially large number of non-disc particles identified, resulting in a low disc-shaped ice percentage. (Continued on next page).

Deployment	Particle group	Mean diameter (mm)	Standard deviation (mm)	99th percentile frazil diameter (mm)	Average number concentration (particles/m^3)	Average volume concentration (m^3/m^3)	Disc-shaped ice percentage	Sediment to frazil ice ratio
NSR-1^{P}	Raw	0.32	0.55	3.76	1.48×10^{4}	2.50×10^{-6}	76	3.73
	Sediment	0.22	0.77					
	Frazil	0.93	0.85					
NSR-2^{P*}	Raw	0.48	0.50	2.56	3.73×10^{4}	1.92×10^{-6}	53	1.14
	Sediment	0.35	0.72					
	Frazil	0.63	0.55					
NSR-3	Raw	0.32	0.26	1.29	1.81×10^{6}	5.45×10^{-6}	--	--
NSR-4A	Raw	0.21	0.22	1.72	1.85×10^{5}	1.59×10^{-6}	95	2.53
	Sediment	0.11	0.09					
	Frazil	0.34	0.34					
NSR-4B*	Raw	0.26	0.32	2.26	1.89×10^{5}	2.13×10^{-6}	68	1.51
	Sediment	0.15	0.22					
	Frazil	0.39	0.39					
PR-1	Raw	0.20	0.24	1.64	2.39×10^{5}	1.76×10^{-6}	76	2.63
	Sediment	0.10	0.06					
	Frazil	0.41	0.33					
KR-1	Raw	0.16	0.19	2.59	3.41×10^{4}	1.02×10^{-6}	70	13.9
	Sediment	0.10	0.09					
	Frazil	0.54	0.53					
KR-2	Raw	0.24	0.23	1.44	2.34×10^{5}	1.10×10^{-6}	94	1.49
	Sediment	0.12	0.08					
	Frazil	0.32	0.27					
KR-3A*	Raw	0.34	0.52	3.94	1.35×10^{5}	1.01×10^{-5}	62	2.31
	Sediment	0.15	0.18					
	Frazil	0.82	0.76					
KR-3B*	Raw	0.48	0.80	3.96	1.37×10^{5}	1.31×10^{-5}	58	1.44
	Sediment	0.13	0.21					
	Frazil	0.93	0.85					

KR-4A	Raw	0.27	0.31	2.27	1.40×10^{5}	2.27×10^{-6}	94	2.22
	Sediment	0.13	0.13					
	Frazil	0.47	0.42					
KR-4B*	Raw	0.40	0.56	3.47	1.51×10^{5}	7.78×10^{-6}	63	1.77
	Sediment	0.18	0.24					
	Frazil	0.75	0.70					
KR-5[P]	Raw	0.38	0.67	5.62	1.00×10^{5}	1.53×10^{-5}	63	2.07
	Sediment	0.13	0.28					
	All frazil	0.91	1.00					
	Pre-peak frazil	1.32	1.14	5.83	5.78×10^{4}	1.51×10^{-5}		
	Post-peak frazil	0.40	0.42	2.21	1.22×10^{6}	1.83×10^{-5}		

Table 5-4: Frazil concentrations from previous laboratory and field studies. (Continued on next page).

Study	Number concentration (particles/m^3)	Volume concentration (m^3/m^3)	Method
Osterkamp and Gosink (1983)	10^4 to 10^7		Underwater photographs in Chatanika River, Alaska
Tsang (1984)		$\sim 6 \times 10^{-3}$	Comparative resistance measurements in laboratory flume
		$\sim 2.5 \times 10^{-3}$	Comparative resistance measurements in the Beauharnois Canal
Tsang (1985)		2.1 to 55 $\times 10^{-4}$	Calculated from water temperature in laboratory flume
Tsang (1986)		$\sim 0.5 \times 10^{-3}$ (near bed) $\sim 30 \times 10^{-3}$ (near surface)	Comparative resistance measurements in the Lachine Rapids
Daly and Colbeck (1986)	0.17 to 0.982 $\times 10^6$		Microscopic images captured in a refrigerated flume
Ettema et al. (2003)		6.6 to 61 $\times 10^{-4}$	Ice collected on mesh over intake mouth in laboratory tank
Ye et al. (2004)		1 to 1.7 $\times 10^{-3}$	Calculated from water temperature in laboratory flume
		Up to $\sim 2 \times 10^{-3}$	Estimated from cross-polarised images in laboratory flume

Marko and Jasek (2010b)		2 to 8×10^{-5}	SWIPS measurements in the Peace River
Marko and Jasek (2010c)	10^5 to 4×10^7	~5×10^{-5} to 2.5×10^{-4}	SWIPS measurements in the Peace River
Jasek et al. (2011)		5 to 33×10^{-5} (15×10^{-5} typical)	SWIPS measurements in the Peace River
		0 to 3×10^{-3} (1.5×10^{-3} typical)	CRISSP model for Peace River
Richard et al. (2011)		2.0 to 5.9×10^{-6}	ADCP measurements in the St. Lawrence River
Ghobrial et al. (2012)[9]		1.3 to 14.7×10^{-4}	Ice sieved out of laboratory frazil tank
Ghobrial et al. (2013b)[9]		11 to 20×10^{-5} during freeze-up events 45×10^{-5} during open lead event	SWIPS measurements in the North Saskatchewan River
Marko et al. (2015)		2×10^{-5} to 1×10^{-4}	SWIPS measurements in the Peace River
McFarlane et al. (2015)	0.29 to 1.8×10^6		Digital images captured in laboratory frazil tank

[9] Mass concentrations reported in this publication were converted into volume concentrations assuming the density of frazil ice to be 920 kg/m^3.

ACKNOWLEDGMENTS

We would like to thank the Natural Sciences and Engineering Research Council of Canada (NSERC) for supporting this project (RGPIN-2015-04670 and RGPAS 477890-2015), Perry Fedun for his valuable technical assistance, Hayden Kalke and Chris Schneck for their help with field work, and Martin Jasek for providing estimates of when and where to expect supercooling to occur on the Peace River.

The maps in this publication were generated using QGIS software (QGIS Development Team, 2017) and using data © OpenStreetMap contributors (http://www.osm.org/copyright) and data obtained from AltaLIS (2017) which contains information licensed under the Open Government License – Alberta.

REFERENCES

AltaLIS [WWW Document], 2017. URL http://www.altalis.com/altalis/ (accessed 6.7.17).

Clark, S., Doering, J., 2006. Laboratory Experiments on Frazil-Size Characteristics in a Counterrotating Flume. J. Hydraul. Eng. 132, 94–101. doi:10.1061/(ASCE)0733-9429(2006)132:1(94)

Clark, S., Doering, J., 2008. Experimental investigation of the effects of turbulence intensity on frazil ice characteristics. Can. J. Civ. Eng. 35, 67–79. doi:10.1139/L07-086

Clark, S., Doering, J.C., 2004. A laboratory study of frazil ice size distributions, in: Proceedings of the 17th International Symposium on Ice. International Association of Hydraulic Engineering and Research, Saint Petersburg, Russia, pp. 291–297.

Clark, S.P., Doering, J.C., 2009. Frazil flocculation and secondary nucleation in a counter-rotating flume. Cold Reg. Sci. Technol. 55, 221–229. doi:10.1016/j.coldregions.2008.04.002

Daly, S.F., Colbeck, S.C., 1986. Frazil ice measurements in CRREL's flume facility, in: Proceedings of the IAHR Ice Symposium 1986. International Association for Hydraulic Research, Iowa City, Iowa, USA, pp. 427–438.

Ettema, R., Chen, Z., Doering, J., 2003. Making Frazil Ice in a Large Ice Tank, in: Proceedings of the 12th Workshop on the Hydraulics of Ice Covered Rivers. CGU HS Committee on River Ice Processes and the Environment, Edmonton, Alberta, p. 13.

Ghobrial, T.R., Loewen, M.R., Hicks, F., 2012. Laboratory calibration of upward looking sonars for measuring suspended frazil ice concentration. Cold Reg. Sci. Technol. 70, 19–31. doi:10.1016/j.coldregions.2011.08.010

Ghobrial, T.R., Loewen, M.R., Hicks, F.E., 2013b. Characterizing suspended frazil ice in rivers using upward looking sonars. Cold Reg. Sci. Technol. 86, 113–126. doi:10.1016/j.coldregions.2012.10.002

Gosink, J.P., Osterkamp, T.E., 1983. Measurements and Analyses of Velocity Profiles and Frazil Ice-Crystal Rise Velocities During Periods of Frazil-Ice Formation in Rivers. Ann. Glaciol. 4, 79–84. doi:10.3189/S0260305500005279

Hicks, F., 2016. An introduction to River Ice Engineering for Civil Engineers and Geoscientists. Charleston, SC, USA.

Jasek, M., Ghobrial, T., Loewen, M., Hicks, F., 2011. Comparison of CRISSP modeled and SWIPS measured ice concentrations on the Peace River, in: Proceedings of the 16th Workshop on River Ice. CGU HS Committee on River Ice Processes and the Environment, Winnipeg, Manitoba, p. 25.

Kellerhals, R., Neill, C.R., Bray, D.I., 1972. Hydraulic and Geomorphic Characteristics of Rivers in Alberta. Alberta Cooperative Research Program in Highway and River Engineering, Edmonton, Alberta.

Kempema, E.W., Ettema, R., 2016. Fish, Ice, and Wedge-Wire Screen Water Intakes. J. Cold Reg. Eng. 30, 19. doi:10.1061/(ASCE)CR.1943-5495.0000097

Kempema, E.W., Reimnitz, E., Hunter, R.E., 1986. Flume studies and field observations of the interaction of frazil ice and anchor ice with sediment. U.S. Geological Survey, Menlo Park, California.

Marko, J.R., Jasek, M., 2010a. Sonar detection and measurement of ice in a freezing river II: Observations and results on frazil ice. Cold Reg. Sci. Technol. 63, 135–153. doi:10.1016/j.coldregions.2010.05.003

Marko, J.R., Jasek, M., 2010b. Frazil monitoring by multi-frequency Shallow Water Ice Profiling Sonar (SWIPS): present status, in: Proceedings of the 20th IAHR International Symposium on Ice. International Association of Hydro-Environment

Engineering and Research, Lahti, Finland, p. 13.

Marko, J.R., Jasek, M., Topham, D.R., 2015. Multifrequency analyses of 2011–2012 Peace River SWIPS frazil backscattering data. Cold Reg. Sci. Technol. 110, 102–119. doi:10.1016/j.coldregions.2014.11.006

McFarlane, V., Loewen, M., Hicks, F., 2014. Laboratory measurements of the rise velocity of frazil ice particles. Cold Reg. Sci. Technol. 106–107, 120–130. doi:10.1016/j.coldregions.2014.06.009

McFarlane, V., Loewen, M., Hicks, F., 2015. Measurements of the evolution of frazil ice particle size distributions. Cold Reg. Sci. Technol. 120, 45–55. doi:10.1016/j.coldregions.2015.09.001

McFarlane, V., Loewen, M., Hicks, F., 2017. Measurements of the size distribution of frazil ice particles in three Alberta rivers. Cold Reg. Sci. Technol. 142, 100–117. doi:10.1016/j.coldregions.2017.08.001

McFarlane, V., Loewen, M., Hicks, F., 2018b. Field measurements of suspended frazil ice. Part I: A support vector machine learning algorithm to identify frazil ice particles. Submitted to Cold Reg. Sci. Technol.

Morse, B., Richard, M., 2009. A field study of suspended frazil ice particles. Cold Reg. Sci. Technol. 55, 86–102. doi:10.1016/j.coldregions.2008.03.004

Osterkamp, T.E., Gosink, J.P., 1983. Frazil ice formation and ice cover development in interior Alaska streams. Cold Reg. Sci. Technol. 8, 43–56. doi:10.1016/0165-232X(83)90016-2

QGIS Development Team, 2017. QGIS Geographic Information System. Open Source Geospatial Foundation Project. URL. http://qgis.osgeo.org.

Richard, M., Morse, B., Daly, S.F., Emond, J., 2011. Quantifying suspended frazil ice using multi-frequency underwater acoustic devices. River Res. Appl. 27, 1106–1117. doi:10.1002/rra.1446

Tsang, G., 1984. Concentration of frazil in flowing water as measured in laboratory and in the field, in: Proceedings of the 7th IAHR International Symposium on Ice. International Association for Hydraulic Research, Hamburg, Germany, pp. 99–111.

Tsang, G., 1985. An instrument for measuring frazil concentration. Cold Reg. Sci. Technol. 10, 235–249. doi:10.1016/0165-232X(85)90035-7

Tsang, G., 1986. Preliminary report on field study at Lachine Rapids on cooling of river and formation of frazil and anchor ice, in: Proceedings of the 4thWorkshop on the Hydraulics of Ice Covered Rivers. CGU HS Committee on River Ice Processes and the Environment, Montreal, Canada, p. F5.1–F5.51.

Ye, S.Q., Doering, J., Shen, H.T., 2004. A laboratory study of frazil evolution in a counter-rotating flume. Can. J. Civ. Eng. 31, 899–914. doi:10.1139/l04-056

6 SUMMARY AND CONCLUSIONS

Understanding how the properties of frazil ice particles vary with time and under different flow conditions has long been an area of interest in river ice engineering. Knowledge of these properties is essential for improving our ability to accurately model and predict river ice processes on northern rivers. Previous laboratory studies focussed on answering these questions have provided useful data but have been limited by the resolution of the digital images, meaning that the smallest frazil ice particles could not be measured (e.g. Clark and Doering, 2008, 2006, 2009; Ye et al., 2004). Field studies have primarily relied on indirect measurements using acoustic devices that have been calibrated in laboratory studies (e.g. Ghobrial et al., 2013a, 2013b, 2012; Marko et al., 2015; Marko and Jasek, 2010a, 2010b; Marko and Topham, 2015; Morse and Richard, 2009) while direct observations have been very limited and have not provided much quantitative data (Osterkamp and Gosink, 1983). This study addressed the gaps in the available data through a series of detailed laboratory and field measurements. The laboratory experiments improved on past studies through the use of a high-resolution DSLR camera that was able to resolve particles as small as 22 μm in diameter. Field measurements were obtained through the successful development and deployment of a digital imaging system called the FrazilCam, which was used to obtain accurate measurements of in-situ frazil ice particles in three rivers. These laboratory and field measurements led to the completion of three objectives.

6.1 Objective 1: Determine How the Size Distribution of Frazil Ice Particles Evolves Throughout a Supercooling Event and Under Varying Turbulence Conditions in a Controlled Environment

This objective was successfully completed through a series of laboratory experiments. The laboratory measurements conducted in this study were of a much higher resolution (spatially and temporally) than those previously conducted, making it possible to study the size of frazil particles throughout a supercooling event with much greater detail. Examining the moving average particle properties revealed how the number of particles and the mean and standard deviation of the particle diameter vary throughout the supercooling process. During the principal supercooling phase at the highest dissipation rate of TKE it was observed that the mean particle size was ~0.4 mm as the first particles were produced, then increased and reached a maximum of ~0.7 mm at approximately the same time as the maximum degree of supercooling was reached. As the water temperature began to increase again, the mean particle size decreased and reached a relatively stable particle size of ~0.6 mm during the residual supercooling phase. The number of suspended crystals was very small (i.e. fewer than 10 particles were observed in a 35 second period giving a concentration < 0.012×10^6 particles/m^3) in the early stages of supercooling, then rapidly increased reaching a maximum concentration of 1.8×10^6 particles/m^3 slightly after maximum supercooling had occurred. This increase in frazil ice particle formation released a large amount of latent heat and caused the water temperature to rise to the residual supercooling temperature. As the residual supercooling temperature approached, the number of suspended particles steadily declined as they began to flocculate and subsequently rise to the surface, removing them from the flow. These overall trends were also observed at the two lower levels of turbulence in the frazil ice tank.

The mean particle diameter and standard deviation averaged over the entire supercooling event were observed to vary with the TKE dissipation rate in the tank. At dissipation rates of 23.9, 85.5, and 336 cm^2/s^3 the mean particle diameters were 0.94, 0.66, and 0.59 mm and the standard deviations were 0.73, 0.51, and 0.45 mm, respectively. Particles were observed to range in size from 22 μm to 5.5 mm and in all cases the particle size distribution was well described by a lognormal distribution. These laboratory results indicate what might be expected in rivers under varying flow conditions. Rivers with more intense turbulence and higher TKE dissipation rates may be expected to produce frazil ice particles with a smaller mean diameters compared to rivers with less intense turbulence under the same conditions. However, the temporal evolution of the size distribution throughout a supercooling event could be expected to be the same in various rivers under similar meteorological conditions.

6.2 Objective 2: Develop a Digital Imaging System for Measuring Frazil Particles in Field Environments

The next step was to adapt the laboratory imaging system for use in real rivers. This was achieved with the development of the FrazilCam, successfully designed to be deployed on the riverbed and capture cross-polarised images of frazil ice particles suspended in the flow. The FrazilCam system was deployed in the Kananaskis, North Saskatchewan, and Peace Rivers during the freeze-up season in the winters of 2014-15, 2015-16, and 2016-17. While processing the images from the first of those winters it was discovered that suspended sediment particles with mean diameters on the order of ~0.1 mm appeared in the images and were indistinguishable from ice particles to the naked eye. However, images had also been captured when no ice was present in the Kananaskis and North Saskatchewan Rivers, and these images were analysed to determine the shape of the suspended sediment size distribution in each river. To minimise the impact of these

sediment particles on the estimated frazil ice particle size distributions, a portion of the size distribution corresponding to the sediment sizes observed was subtracted. This resulted in frazil ice particle size distributions with mean diameters of 0.73 to 1.20 mm during the principal supercooling phase and 0.32 to 0.61 mm during the residual supercooling phase. These were the first direct measurements of frazil ice particle size distributions in real rivers and each size distribution could be described reasonably well by a lognormal size distribution. Furthermore, this demonstrated the functionality of the FrazilCam system for photographing frazil ice particles in rivers, which was an essential milestone in the completion of Objective 2.

With the functionality of the FrazilCam demonstrated, it was desirable to further refine the accuracy of the image processing algorithm by classifying each individual particle as either ice or sediment. This would result in size distributions that were more complete, as frazil ice particles of all sizes could be identified and there would be no unrealistic gaps in the size distribution at diameters on the order of 0.1 mm. To achieve this accuracy SVM algorithms were trained to classify the ice and sediment particles in each river. The SVM algorithms were able to correctly identify and remove sediment particles with 98% accuracy, resulting in frazil ice size distributions that contained particles as small as 34 μm in diameter. However, there were practical limits to the accuracy of the SVM algorithms. Since only 98% of the sediment particles were removed during processing the ratio of sediment to frazil ice particles could not be too great or the resulting frazil ice properties would still be affected by the remaining 2% of the sediment particles. It was demonstrated that as long as the ratio of sediment to frazil ice particles was less than 14 the resulting frazil ice particle size distributions were acceptable. The FrazilCam deployments from 2014-15 were reanalysed using the SVM algorithm and the resulting mean particle diameters were reduced by 7 to 23% compared to the results obtained using

the sediment subtraction technique. The resulting size distributions were much improved as well and no longer had abnormal gaps in the 0.1 to 0.2 mm diameter range.

Completion of this objective demonstrated that it is possible to capture high-resolution images of suspended frazil crystals in field environments using imaging techniques that have been developed in the laboratory. The successful training of SVM algorithms to differentiate the ice crystals from other particles suspended in the flow provided a method that can easily be adapted for use at new study sites in other rivers, as the only data required to train an SVM for a new site is a series of ice-free images. The FrazilCam system can also be adapted for use in other marine environments where frazil ice is produced, including oceans. Therefore, this system is not only beneficial to the river ice engineering community, but the sea ice research community as well.

6.3 Objective 3: Investigate the Properties of Suspended Frazil Ice Particles Under Varying Meteorological and Flow Conditions in Rivers

Images of suspended frazil ice obtained from all three rivers under different meteorological and flow conditions and at various stages of the supercooling process were analysed using the SVM algorithms. The resulting frazil ice particle size distributions from the winters of 2014-15, 2015-16, and 2016-17 had mean diameters ranging from 0.63 to 1.32 mm during the principal supercooling phase and 0.32 to 0.93 mm during the residual supercooling phase. Frazil ice number concentrations were also directly measured for the first time in the field, and were observed to range from 1.48×10^4 to 1.81×10^6 particles/m^3. Using a constant particle aspect ratio of 37 the particle volume concentrations were calculated as well, and ranged from 1.0 to 18 $\times$ 10^{-6} m^3/m^3. In all cases where the FrazilCam deployment occurred during steady flow conditions the frazil ice size

distribution was well described by a lognormal distribution, and time-series analysis indicated that the frazil ice properties remain essentially constant during the residual supercooling phase. However, during one deployment the flow rate increased rapidly as a hydropeaking wave passed through the site. This resulted in a dramatic increase in the number concentration of particles from 5.8×10^4 to 1.2×10^6 particles/m^3 in only one minute, a significant drop in the mean particle diameter from 1.3 to 0.40 mm, and a bimodal frazil ice particle size distribution. This demonstrated that the frazil ice characteristics can very rapidly change in response to changing flow conditions.

One unique event was observed in which the maximum degree of supercooling was −0.145°C, which was greater than three times colder than any of the other supercooling events that were recorded. This event occurred on a day during which the conditions appeared unfavourable for supercooling, as the air temperature was +2.2°C when supercooling began and the average wind speed was only 0.2 m/s. However, the sky was clear which resulted in a net radiative heat loss after the sun had set and there was no snow or frost on the riverbanks or in the air to provide seed particles for frazil ice formation. As a result, the water steadily supercooled until shard-like anchor ice crystals began growing on all submerged surfaces. This unusual event indicates that, under the right circumstances, ice will predominantly grow as anchor ice in the form of large, shard-like crystals rather than small, disc-shaped suspended frazil ice particles.

These results provide valuable insight and answer important questions about the components of the river freeze-up process that occur beneath the water surface. The direct observations made using the FrazilCam provide a reliable range of frazil ice particle sizes in rivers, and demonstrate that a lognormal distribution represents the frazil particle size distribution well under steady flow conditions. Direct measurements of the number

concentration of suspended, disc-shaped frazil crystals have also been provided for the first time, and reasonable estimates of the volume concentration have been made. As previous field measurements of frazil ice have been made via indirect means it has been impossible to verify their accuracy. The FrazilCam system can now be used in conjunction with indirect methods (such as acoustic instruments) to verify and improve the results of both systems.

Reliable, in-situ frazil ice measurements are of great benefit to the river ice engineering community. Numerical models of the river ice freeze-up process such as CRISSP2D (Shen, 2005) and RIVICE (Environment Canada, 2013) rely on observational data for calibration and validation. At the present time observations of surface ice conditions (e.g. surface ice concentration and ice front location) are used and, as a result, the accuracy of these models in the early stages of freeze-up before the formation of frazil pans is unknown. The frazil ice particle sizes and concentrations measured in this study provide valuable data at the earliest stages of river freeze-up. These data can be used for calibration and validation of numerical models during different phases of the supercooling process and in rivers of different scales.

Many previous studies have attributed the growth of anchor ice primarily to the accretion of frazil ice particles to the bed material, with little emphasis being placed on the in-situ growth of these crystals. It was demonstrated in this study that, under the right conditions (i.e. net radiative heat loss and a lack of seed particles), an extreme supercooling event can occur leading to the heterogeneous nucleation of shard-like anchor ice crystals on all submerged objects including the substrate. The knowledge that this type of anchor ice growth and such extreme levels of supercooling can occur in rivers is something that should be taken into account in future developments to numerical freeze-up models.

6.4 RECOMMENDATIONS FOR FUTURE WORK

This study has demonstrated that it is possible to make accurate, direct measurements of frazil ice properties in real rivers, and the methodology could easily be adapted for use in other bodies of water. However, there are still modifications that can be made to improve the accuracy and quality of the measurements in future studies. The greatest challenge with deploying the FrazilCam is preventing ice from freezing onto or growing on the polarising lenses and obstructing the images. These crystals must be manually removed by flushing with warm water whenever possible throughout the deployment, and segments of the image series that are affected must be discarded. This was especially troublesome for deployments that occurred during the principal supercooling phase, making it extremely difficult to capture time-series data during that period. If this problem could be resolved, perhaps by heating the polarising lenses throughout the deployment to prevent ice from adhering to them, it would be possible to capture more reliable data with an unobstructed field of view.

It is also important to work to improve the accuracy of the SVM algorithms used for classifying the ice and sediment particles. Although these algorithms are 98% accurate at identifying sediment particles, the 2% of sediment particles that are misclassified as ice are enough to obscure the frazil ice distribution when the sediment to ice ratio is greater than 14. One way to improve the algorithm would be to acquire an ice dataset using the FrazilCam that is completely free of sediment or any other non-ice particles. This dataset could be collected in the laboratory under very carefully controlled conditions. The water used would have to be run through a very fine filter in order to remove any suspended particles larger than ~0.03 mm, which are the finest particles that can be observed by the FrazilCam. The FrazilCam itself and the tank used to generate the frazil ice particles would also have to be very carefully cleaned to ensure they did not introduce any foreign particles

to the clean, filtered water. It would also be necessary to cover the tank to prevent any airborne particles from entering the flow, meaning that ice crystals would have to be manually added to the water once supercooling had begun in order to provide seed crystals on which the first frazil particles could form. It is also possible that a different, more advanced type of machine learning algorithm could provide better results with the available data, which could be the focus of a future study.

Accurate measurements of the turbulence characteristics at field study sites would also be very beneficial in future field investigations. An ADV could be used to acquire high-resolution time-series velocity data at each study site, which could be analysed to calculate the turbulence intensity and TKE dissipation rate. This would make it possible to more directly compare the flow conditions in the field to those observed in laboratory studies, and determine a relationship between frazil ice characteristics and turbulence intensity in field environments.

The river ice forecasting community would also benefit from studies focussed on fully understanding the driving factors behind when a supercooling event will occur. In fact, one of the most difficult parts of this field study was predicting when and where on the river supercooling would begin. Although water temperature and meteorological data were measured during this study for the purpose of evaluating the conditions when the FrazilCam deployments took place, more detailed measurements are required. This would allow us to better understand the heat fluxes involved in causing the water to supercool and what conditions lead to the formation of disc-shaped frazil crystals rather than the shard-like anchor ice crystals observed during deployment NSR-5 in Chapter 5. Hannah et al. (2004) performed very detailed measurements of the energy budget in a small stream in Scotland, including the net radiation directly above the water surface, bed temperatures

at three depths below the stream bed, and heat flux through the stream bed. However, this study did not occur during the winter months and therefore no supercooling events were analysed. It would be extremely valuable for a future study to perform similar measurements throughout the freeze-up season in order to quantify all of the factors contributing to a supercooling event.

REFERENCES

AltaLIS [WWW Document], 2017. URL http://www.altalis.com/altalis/ (accessed 6.7.17).

Arakawa, K., 1954. Studies on the Freezing of Water (II) Formation of Disc Crystals. J. Fac. Sci. Hokkaido Univ. Japan 4, 311–349.

Brown, R.S., Hubert, W.A., Daly, S.F., 2011. A Primer on Winter, Ice, and Fish: What Fisheries Biologists Should Know about Winter Ice Processes and Stream-Dwelling Fish. Fisheries 36, 8–26. https://doi.org/10.1577/03632415.2011.10389052

Carstens, T., 1966. Experiments with supercooling and ice formation in flowing water. Geofys. Publ. 26, 1–18.

Clark, S., Doering, J., 2008. Experimental investigation of the effects of turbulence intensity on frazil ice characteristics. Can. J. Civ. Eng. 35, 67–79. https://doi.org/10.1139/L07-086

Clark, S., Doering, J., 2006. Laboratory Experiments on Frazil-Size Characteristics in a Counterrotating Flume. J. Hydraul. Eng. 132, 94–101. https://doi.org/10.1061/(ASCE)0733-9429(2006)132:1(94)

Clark, S., Doering, J.C., 2004. A laboratory study of frazil ice size distributions, in: Proceedings of the 17th International Symposium on Ice. International Association of Hydraulic Engineering and Research, Saint Petersburg, Russia, pp. 291–297.

Clark, S.P., Doering, J.C., 2009. Frazil flocculation and secondary nucleation in a counter-rotating flume. Cold Reg. Sci. Technol. 55, 221–229. https://doi.org/10.1016/j.coldregions.2008.04.002

Cortes, C., Vapnik, V., 1995. Support-vector networks. Mach. Learn. 20, 273–297. https://doi.org/10.1007/BF00994018

Cristianini, N., Shawe-Taylor, J., 2000. An Introduction to Support Vector Machines and Other Kernel-based Learning Methods. Cambridge University Press, Cambridge. https://doi.org/10.1017/CBO9780511801389

Daly, S.F., 2013. Frazil Ice, in: Beltaos, S. (Ed.), River Ice Formation. Committee on River Ice Processes and the Environment, CGU-HS, Edmonton, Alberta, pp. 107–134.

Daly, S.F., 1994. Report on frazil ice. U.S. Army Cold Regions Research and Engineering Laboratory, Hanover, N. H.

Daly, S.F., 1984. Frazil ice dynamics. U.S. Army Cold Regions Research and Engineering Laboratory, Hanover, N. H.

Daly, S.F., Colbeck, S.C., 1986. Frazil ice measurements in CRREL's flume facility, in: Proceedings of the IAHR Ice Symposium 1986. International Association for Hydraulic Research, Iowa City, Iowa, USA, pp. 427–438.

Doering, J.C., Morris, M.P., 2003. A digital image processing system to characterize frazil ice. Can. J. Civ. Eng. 30, 1–10.

Dubé, M., Turcotte, B., Morse, B., 2014. Inner structure of anchor ice and ice dams in steep channels. Cold Reg. Sci. Technol. 106–107, 194–206. https://doi.org/10.1016/j.coldregions.2014.06.013

Environment Canada, 2013. RIVICE Model - User's Manual.

Ettema, R., Chen, Z., Doering, J., 2003. Making Frazil Ice in a Large Ice Tank, in: Proceedings of the 12th Workshop on the Hydraulics of Ice Covered Rivers. CGU HS Committee on River Ice Processes and the Environment, Edmonton, Alberta, p. 13.

Ettema, R., Karim, M.F., Kennedy, J.F., 1984. Frazil ice formation. U.S. Army Cold Regions Research and Engineering Laboratory, Hanover, N. H.

Ettema, R., Karim, M.F., Kennedy, J.F., 1984. Laboratory experiments on frazil ice growth in supercooled water. Cold Reg. Sci. Technol. 10, 43–58. https://doi.org/10.1016/0165-232X(84)90032-6

Forest, T.W., 1986. Thermodynamic Stability of Frazil Ice Crystals, in: Proceedings of the Fifth International Offshore Mechanics and Arctic Engineering (OMAE) Symposium. The American Society of Mechanical Engineers, Tokyo, Japan, pp. 266–270.

Forest, T.W., Sharma, R., 1992. Growth Rates of Frazil Ice Discs, in: Proceedings of the 11th International Symposium on Ice. International Association for Hydraulic Research, Banff, Alberta, pp. 723–734.

Ghobrial, T.R., Loewen, M.R., Hicks, F., 2012. Laboratory calibration of upward looking sonars for measuring suspended frazil ice concentration. Cold Reg. Sci. Technol. 70, 19–31. https://doi.org/10.1016/j.coldregions.2011.08.010

Ghobrial, T.R., Loewen, M.R., Hicks, F.E., 2013a. Continuous monitoring of river surface ice during freeze-up using upward looking sonar. Cold Reg. Sci. Technol. 86, 69–85. https://doi.org/10.1016/j.coldregions.2012.10.009

Ghobrial, T.R., Loewen, M.R., Hicks, F.E., 2013b. Characterizing suspended frazil ice in rivers using upward looking sonars. Cold Reg. Sci. Technol. 86, 113–126. https://doi.org/10.1016/j.coldregions.2012.10.002

Gosink, J.P., Osterkamp, T.E., 1983. Measurements and Analyses of Velocity Profiles and Frazil Ice-Crystal Rise Velocities During Periods of Frazil-Ice Formation in Rivers.

Ann. Glaciol. 4, 79–84. https://doi.org/10.3189/S0260305500005279

Government of Alberta, 2017. Alberta Environment and Parks - Alberta River Basins flood alerting, advisories, reporting and water management [WWW Document]. URL https://rivers.alberta.ca/ (accessed 6.16.17).

Hammar, L., Shen, H.T., 1995. Frazil Evolution in Channels. J. Hydraul. Res. 33, 291–306. https://doi.org/10.1080/00221689509498572

Hannah, D.M., Malcolm, I.A., Soulsby, C., Youngson, A.F., 2004. Heat exchanges and temperatures within a salmon spawning stream in the Cairngorms, Scotland: Seasonal and sub-seasonal dynamics. River Res. Appl. 20, 635–652. https://doi.org/10.1002/rra.771

Hicks, F., 2016. An introduction to River Ice Engineering for Civil Engineers and Geoscientists. Charleston, SC, USA.

Islam, M.R., Zhu, D.Z., 2013. Kernel Density-Based Algorithm for Despiking ADV Data. J. Hydraul. Eng. 139, 785–793. https://doi.org/10.1061/(ASCE)HY.1943-7900-0000734

Jasek, M., 2016. Investigations of Anchor Ice Formation and Release Waves, in: Proceedings of the 23rd IAHR International Symposium on Ice. International Association of Hydro-Environment Engineering and Research, Ann Arbor, Michigan USA, p. 11.

Jasek, M., Ghobrial, T., Loewen, M., Hicks, F., 2011. Comparison of CRISSP modeled and SWIPS measured ice concentrations on the Peace River, in: Proceedings of the 16th Workshop on River Ice. CGU HS Committee on River Ice Processes and the Environment, Winnipeg, Manitoba, p. 25.

Kalke, H., Loewen, M., 2017. Predicting Surface Ice Concentration using Machine Learning, in: Proceedings of the 19. CGU HS Committee on River Ice Processes and the Environment, Whitehorse, YK, Canada, p. 17.

Kalke, H., McFarlane, V., Schneck, C., Loewen, M., 2017. The transport of sediments by released anchor ice. Cold Reg. Sci. Technol. 143, 70–80. https://doi.org/10.1016/j.coldregions.2017.09.003

Kellerhals, R., Neill, C.R., Bray, D.I., 1972. Hydraulic and Geomorphic Characteristics of Rivers in Alberta. Alberta Cooperative Research Program in Highway and River Engineering, Edmonton, Alberta.

Kempema, E.W., Ettema, R., 2016. Fish, Ice, and Wedge-Wire Screen Water Intakes. J. Cold Reg. Eng. 30, 19. https://doi.org/10.1061/(ASCE)CR.1943-5495.0000097

Kempema, E.W., Ettema, R., 2011. Anchor Ice Rafting: Observations from the Laramie River. River Res. Appl. 27, 1126–1135. https://doi.org/10.1002/rra.1450

Kempema, E.W., Reimnitz, E., Hunter, R.E., 1986. Flume studies and field observations of the interaction of frazil ice and anchor ice with sediment. U.S. Geological Survey, Menlo Park, California.

Kerr, D.J., Shen, H.T., Daly, S.F., 2002. Evolution and hydraulic resistance of anchor ice on gravel bed. Cold Reg. Sci. Technol. 35, 101–114. https://doi.org/10.1016/S0165-232X(02)00043-5

Kondolf, G.M., Adhikari, A., 2000. Weibull vs. Lognormal Distributions for Fluvial Gravels. J. Sediment. Res. 70, 456–460. https://doi.org/10.1306/2DC4091E-0E47-11D7-8643000102C1865D

Liang, Y., Xu, Q.-S., Li, H.-D., Cao, D.-S., 2011. Support vector machines and their application in chemistry and biotechnology. CRC Press, Boca Raton, FL.

Marko, J.R., Jasek, M., 2010a. Sonar detection and measurements of ice in a freezing river I: Methods and data characteristics. Cold Reg. Sci. Technol. 63, 121–134.

Marko, J.R., Jasek, M., 2010b. Sonar detection and measurement of ice in a freezing river II: Observations and results on frazil ice. Cold Reg. Sci. Technol. 63, 135–153. https://doi.org/10.1016/j.coldregions.2010.05.003

Marko, J.R., Jasek, M., 2010c. Frazil monitoring by multi-frequency Shallow Water Ice Profiling Sonar (SWIPS): present status, in: Proceedings of the 20th IAHR International Symposium on Ice. International Association of Hydro-Environment Engineering and Research, Lahti, Finland, p. 13.

Marko, J.R., Jasek, M., Topham, D.R., 2015. Multifrequency analyses of 2011–2012 Peace River SWIPS frazil backscattering data. Cold Reg. Sci. Technol. 110, 102–119. https://doi.org/10.1016/j.coldregions.2014.11.006

Marko, J.R., Topham, D.R., 2015. Laboratory measurements of acoustic backscattering from polystyrene pseudo-ice particles as a basis for quantitative characterization of frazil ice. Cold Reg. Sci. Technol. 112, 66–86. https://doi.org/10.1016/j.coldregions.2015.01.003

Mazumder, B.S., Ray, R.N., Dalal, D.C., 2005. Size distributions of suspended particles in open channel flow over bed materials. Environmetrics 16, 149–165. https://doi.org/10.1002/env.690

McFarlane, V., Loewen, M., Hicks, F., 2018a. Field measurements of suspended frazil ice. Part II: Observations and analyses of frazil ice properties during the principal and residual supercooling phases. Submitt. to Cold Reg. Sci. Technol.

McFarlane, V., Loewen, M., Hicks, F., 2018b. Field measurements of suspended frazil ice. Part I: A support vector machine learning algorithm to identify frazil ice particles. Submitt. to Cold Reg. Sci. Technol.

McFarlane, V., Loewen, M., Hicks, F., 2017. Measurements of the size distribution of frazil ice particles in three Alberta rivers. Cold Reg. Sci. Technol. 142, 100–117. https://doi.org/10.1016/j.coldregions.2017.08.001

McFarlane, V., Loewen, M., Hicks, F., 2015. Measurements of the evolution of frazil ice particle size distributions. Cold Reg. Sci. Technol. 120, 45–55. https://doi.org/10.1016/j.coldregions.2015.09.001

McFarlane, V., Loewen, M., Hicks, F., 2014. Laboratory measurements of the rise velocity of frazil ice particles. Cold Reg. Sci. Technol. 106–107, 120–130. https://doi.org/10.1016/j.coldregions.2014.06.009

McFarlane, V., Loewen, M., Hicks, F., 2012. Laboratory Experiments to Determine Frazil Ice Properties, in: Proceedings of the Annual Conference and General Meeting of the CSCE - 2012. Edmonton, Alberta, p. 10.

McFarlane, V.J., 2014. Laboratory Studies of Suspended Frazil Ice Particles. University of Alberta.

McLelland, S.J., Nicholas, A.P., 2000. A new method for evaluating errors in high-frequency ADV measurements. Hydrol. Process. 14, 351–366. https://doi.org/10.1002/(SICI)1099-1085(20000215)14:2<351::AID-HYP963>3.0.CO;2-K

Morse, B., Richard, M., 2009. A field study of suspended frazil ice particles. Cold Reg. Sci. Technol. 55, 86–102. https://doi.org/10.1016/j.coldregions.2008.03.004

Muller, A., 1978. Frazil ice formation in turbulent flow. Iowa City, Iowa, USA.

Osterkamp, T.E., 1978. Frazil Ice Formation: A Review. J. Hydraul. Div. 104, 1239–1255.

Osterkamp, T.E., Gosink, J.P., 1983. Frazil ice formation and ice cover development in interior Alaska streams. Cold Reg. Sci. Technol. 8, 43–56. https://doi.org/10.1016/0165-232X(83)90016-2

Pope, S.B., 2000. Turbulent Flows. Cambridge University Press, Cambridge, U.K.

Pratt, W.K., 2007. Digital Image Processing, 4th Editio. ed. John Wiley & Sons, Hoboken, NJ.

QGIS Development Team, 2017. QGIS Geographic Information System. Open Source Geospatial Foundation Project. URL http://qgis.osgeo.org.

Qu, Y.X., Doering, J., 2007. Laboratory study of anchor ice evolution around rocks and on gravel beds. Can. J. Civ. Eng. 34, 46–55. https://doi.org/10.1139/l06-094

Reimnitz, E., Clayton, J.R., Kempema, E.W., Payne, J.R., Weber, W.S., 1993. Interaction of rising frazil with suspended particles: tank experiments with applications to nature. Cold Reg. Sci. Technol. 21, 117–135.

Richard, M., Morse, B., 2008. Multiple frazil ice blockages at a water intake in the St. Lawrence River. Cold Reg. Sci. Technol. 53, 131–149. https://doi.org/10.1016/j.coldregions.2007.10.003

Richard, M., Morse, B., Daly, S.F., Emond, J., 2011. Quantifying suspended frazil ice using multi-frequency underwater acoustic devices. River Res. Appl. 27, 1106–1117. https://doi.org/10.1002/rra.1446

Romagnoli, M., García, C.M., Lopardo, R.A., 2012. Signal Postprocessing Technique and Uncertainty Analysis of ADV Turbulence Measurements on Free Hydraulic Jumps. J. Hydraul. Eng. 138, 353–357. https://doi.org/10.1061/(ASCE)HY.1943-7900.0000507

Schaefer, V.J., 1950. The formation of frazil and anchor ice in cold water. Trans. Am. Geophys. Union 31, 885–893.

Shen, H.T., 2005. CRISSP2D Programmer's Manual. CEA Technologies Inc., Montreal, Canada.

Stiansen, J.E., Sundby, S., 2001. Improved methods for generating and estimating turbulence in tanks suitable for fish larvae experiments. Sci. Mar. 65, 151–167. https://doi.org/10.3989/scimar.2001.65n2151

Stickler, M., Alfredsen, K.T., Linnansaari, T., Fjeldstad, H., 2010. The influence of dynamic ice formation on hydraulic heterogeneity in steep streams. River Res. Appl. 26, 1187–1197. https://doi.org/10.1002/rra.1331

Tennekes, H., Lumley, J.L., 1972. A first course in turbulence. MIT Press, Cambridge, Mass.

Tsang, G., 1986. Preliminary report on field study at Lachine Rapids on cooling of river and formation of frazil and anchor ice, in: Proceedings of the 4thWorkshop on the Hydraulics of Ice Covered Rivers. CGU HS Committee on River Ice Processes and the Environment, Montreal, Canada, p. F5.1–F5.51.

Tsang, G., 1985. An instrument for measuring frazil concentration. Cold Reg. Sci. Technol. 10, 235–249. https://doi.org/10.1016/0165-232X(85)90035-7

Tsang, G., 1984. Concentration of frazil in flowing water as measured in laboratory and in

the field, in: Proceedings of the 7th IAHR International Symposium on Ice. International Association for Hydraulic Research, Hamburg, Germany, pp. 99–111.

Tsang, G., Hanley, T.O., 1985. Frazil formation in water of different salinities and supercoolings. J. Glaciol. 31, 74–85.

Verma, P.K., 2010. Optical Mineralogy. CRC Press, Boca Raton, FL.

Wuebben, J.L., 1984. The Rise Pattern and Velocity of Frazil Ice, in: Proceedings of the 3rd Workshop on the Hydraulics of Ice Covered Rivers. Committee on River Ice Processes and the Environment, Fredericton, New Brunswick, Canada, pp. 297–316.

Ye, S.Q., Doering, J., 2004. Simulation of the Supercooling Process and Frazil Evolution in Turbulent Flows. Can. J. Civ. Eng. 31, 915–926. https://doi.org/10.1139/L04-055

Ye, S.Q., Doering, J., Shen, H.T., 2004. A laboratory study of frazil evolution in a counter-rotating flume. Can. J. Civ. Eng. 31, 899–914. https://doi.org/10.1139/l04-056

Yoshikawa, Y., Watanabe, Y., Abe, T., Ito, A., 2014. Study of Frazil Particle Distribution and Frazil Transport Capacity, in: Proceedings of the 22nd IAHR International Symposium on Ice. International Association of Hydro-Environment Engineering and Research, Singapore, SG, pp. 679–686. https://doi.org/10.3850/978-981-09-0750-1